

https://dspace.org/

An extension to classical lamination theory for buckling and vibration of functionally graded plates

Catanho, R.V.

2019-08

https://hdl.handle.net/10539/29151

Catanho, Roberto Vincent, (2019). An extension to classical lamination theory for buckling and vibration of functionally graded plates, University of the Witwatersrand, https://hdl.handle.net/10539/29151

Downloaded from a DSpace repository. https://dspace.org/



SCHOOL OF MECHANICAL,
INDUSTRIAL & AERONAUTICAL
ENGINEERING

An Extension to Classical Lamination Theory for Buckling and Vibration of Functionally Graded Plates

MECN7018 - Masters of Science in Engineering Research Project

R.V. Catanho

Supervisor: Professor R. Reid

A project report submitted to the Faculty of Engineering and the Built Environment, University of the Witwatersrand, Johannesburg, in partial fulfilment of the requirements for the degree of Master of Science in Engineering.

Johannesburg, August 2019



University of the Witwatersrand, Johannesburg

School of Mechanical, Industrial & Aeronautical Engineering



INDIVIDUAL DECLARATION WITH TASK SUBMITTED FOR ASSESSMENT

I, the undersigned, am registered for the course **MECN7018 - Masters of Science in Engineering Research Project** in the year 2019. I herewith submit the following task "**An Extension to Classical Lamination Theory for Buckling and Vibration of Functionally Graded Plates**" in partial fulfilment of the requirements of the above course.

I hereby declare the following:

- I am aware that plagiarism (the use of someone else's work without their permission and / or without acknowledging the original source) is wrong;
- I confirm that the work submitted herewith for assessment in the above course is my own unaided work except where I have explicitly stated otherwise;
- This task has not been submitted before. either individually or jointly, for any course requirement, examination or degree at this or any other tertiary educational institution;
- I have followed the required conventions in referencing the thoughts and ideas of others;
- I understand that the University of the Witwatersrand may take disciplinary action against me if it can be shown that this task is not my own unaided work or that I failed to acknowledge the sources of the ideas or words in my writing in this task.

Signed this 10th day of August 2019



R.V. Catanho

Acknowledgements

I would like to thank my supervisor, Professor Robert Reid of the School of Mechanical, Industrial and Aeronautical Engineering at the University of the Witwatersrand. The door to Professor Reid's office was always open when I needed to discuss any issue relating to my research. He consistently guided this thesis to be of a high quality and steered me in the right the direction whenever he thought I needed it. I would also like to acknowledge him for thoroughly proof reading the thesis and I am humbly indebted to him for his valuable contribution to my thesis.

Finally, I must express my very profound appreciation to my wife for providing me with ever lasting support, patience and continuous encouragement throughout my years of study and through the process producing my thesis. This accomplishment would not have been possible without her. Thank you.

Abstract

An extension to classical lamination theory (CLT) is presented to analyse the natural frequencies and critical buckling loads of simply supported functionally graded plates. The variation of the through-thickness properties of the plate is governed by a power law which is subsequently represented by a polynomial series of sufficient order and varies according to the law of mixtures or the Mori-Tanaka Homogenization method. The stiffness matrices are found, from which the position of the neutral plane is established which allows for the governing equations for the natural frequency and critical buckling load to be derived using the Rayleigh-Ritz method. The natural frequency and critical buckling loads are determined for various volume indices, aspect and span ratios and the accuracy thereof is validated against 2D, 3D and quasi-3D solutions found in literature. A comparison with CLT found that the present study produces natural frequencies and critical bucking loads which are more accurate and which converge faster than CLT.

Contents

Declaration i

Acknowledgements ii

Abstract iii

Contents iv

List of Figures vii

List of Tables viii

1 Introduction 1

2 Literature Survey 2

2.1 Load Cases In Literature 2

2.1.1 Free Vibration 2

2.1.2 Buckling 5

2.2 Volume Fraction 6

2.3 Through-Thickness Variation 7

2.3.1 Rule of Mixtures 7

2.3.2 Mori-Tanaka Homogenization Procedure 8

2.4 Classic Lamination Theory 9

2.5 Rayleigh-Ritz 14

3 Objectives 17

4 Theory Development **18**

4.1 Elastic Stress-Strain Relationships 18

4.2 Internal Strain Energy 21

4.3 External Work - Vibration Case 29

4.4 External Work - Buckling Case 35

4.5 Natural Frequency of Plate Subjected to Compressive Loads 38

5 Results **40**

5.1 Natural Frequency Results 40

5.2 Buckling Load Results 46

5.3 Variation of Natural Frequency with Compressive Load 52

5.4 Curve Fit Accuracy and Convergence 54

6 Discussion **59**

6.1 Natural Frequency 59

6.2 Buckling Load 63

6.3 Variation in Natural Frequency with Compressive Load 66

6.4 Convergence and Curve Fit Accuracy 67

7 Conclusions **69**

8 Recommendations **70**

References **71**

A Input Parameters and Constituent Properties **75**

B Bending Stiffness Matrix Investigation 76

C Input Code 79

D Polynomial Fit Code 82

E ABD Matrices Code 87

F Rayleigh Ritz Code 90

G Natural Frequency with Buckling Load Code 93

H Curve Fit Accuracy and Convergence Code 95

List of Figures

1 Variation of volume fraction of the ceramic material for various values of λ. . 7

2 Displacement of a plate [37]. 12

3 Total displacement in a plate [37]. 12

4 Configuration of laminate under consideration 18

5 Cross section of laminate under consideration 31

6 Comparison of uniaxial and biaxial compressive load (MN) with natural frequency of a SSSS square plate (Al/Al_2O_3) with an aspect ratio a/h = 20 and varying volume index λ using the present theory (a = b = 1). 52

7 Comparison of uniaxial and biaxial compressive load (MN) with natural frequency of a SSSS square plate (Al/Al_2O_3) with an aspect ratio a/h = 20 and varying volume index λ using the present theory (a = 1, b = 2). 53

8 Comparison of uniaxial and biaxial compressive load (MN) with natural frequency of a SSSS square plate ($SUS304/Si_3N_4$) with an aspect ratio a/h = 100 and varying volume index λ using the present theory (a = b = 1). 53

9 Variation of natural frequency using CLT with increasing discretization layers. 55

10 Variation of natural frequency using the present study with the polynomial fit error percentage. 56

11 Variation of critical buckling load using CLT with increasing discretization layers. 57

12 Variation of critical buckling load using the present study with increasing polynomial fit error percentage limits. 58

13 Variation of E, D matrix, $\overline{D}$ matrix with λ 76

14 Displacement of the neutral axis from mid-plane with λ 77

List of Tables

1 Comparison of non-dimensional fundamental frequency $\overline{\omega} = \omega h\sqrt{\frac{\rho_m}{E_m}}$ of a SSSS square plate (Al/ZrO_2) with a varying volume index λ and an aspect ratio a/h = 5 using the present theory (a = b = 1). 41

2 Comparison of non-dimensional fundamental frequency $\overline{\omega} = \omega h\sqrt{\frac{\rho_c}{E_c}}$ of a SSSS square plate (Al/Al_2O_3) with a varying volume index λ and an aspect ratio a/h = 10 using the present theory (a = b = 1). 41

3 Comparison of non-dimensional fundamental frequency $\overline{\omega} = \omega h\sqrt{\frac{\rho_c}{E_c}}$ of a SSSS square plate (Al/Al_2O_3) with a varying volume index λ and an aspect ratio a/h = 20 using the present theory (a = b = 1). 42

4 Comparison of non-dimensional fundamental frequencies $\overline{\omega} = \omega a^2\sqrt{\frac{12\rho_c h(1\text{-}\nu_c^2)}{E_c h^3}}$ of a SSSS square plate (Al/Al_2O_3) with a varying volume index λ and an aspect ratio a/h = 100 using the present theory (a = b = 1). 42

5 Comparison of first 4 non-dimensional frequencies $\overline{\omega} = \omega a^2/h\sqrt{\frac{\rho_c}{E_c}}$ of a SSSS square plate (Al/Al_2O_3) with a varying volume index λ and an aspect ratio a/h = 10 using the present theory (a = b = 1). 43

6 Comparison of first 5 non-dimensional frequencies $\overline{\omega} = \omega h\sqrt{\frac{\rho_m}{E_m}}$ of a SSSS square plate (Al/ZrO_2) with a volume fraction index λ = 1 and an aspect ratio a/h = 20 using the present theory (a = b = 1). 43

7 Comparison of non-dimensional fundamental frequency $\overline{\omega} = \omega h\sqrt{\frac{\rho_m}{E_m}}$ of a SSSS square plate (Al/ZrO_2) with a varying volume index λ and an aspect ratio a/h = 5, excluding in-plane displacements using the present theory (a = b = 1). 44

8 Comparison of non-dimensional fundamental frequency $\overline{\omega} = \omega h\sqrt{\frac{\rho_c}{E_c}}$ of a SSSS square plate (Al/Al_2O_3) with a varying volume index λ and an aspect ratio a/h = 10, excluding in-plane displacements using the present theory (a = b = 1). 44

9 Comparison of non-dimensional fundamental frequency $\overline{\omega} = \omega h\sqrt{\frac{\rho_c}{E_c}}$ of a SSSS square plate (Al/Al_2O_3) with a varying volume index λ and an aspect ratio a/h = 20, excluding in-plane displacements using the present theory (a = b = 1). 45

10 Comparison of uniaxial critical buckling load (MN) of a SSSS square plate (Al/Al_2O_3) with varying aspect ratio a/h and a volume index λ = 1 using the present theory (a = 1 ; b = 2) (ψ = 0). 46

11 Comparison of non-dimensional uniaxial critical buckling load $\overline{\mathrm{N}} = \mathrm{N}a^2/h^3E_m$ of a SSSS square plate (Al/Al_2O_3) with varying aspect ratio a/h and volume index λ using the present theory (a = 1 ; b = 1/2) (ψ = 0). 47

12 Comparison of non-dimensional uniaxial critical buckling load $\overline{\mathrm{N}} = \mathrm{N}a^2/h^3E_m$ of a SSSS square plate (Al/Al_2O_3) with varying aspect ratio a/h and volume index λ using the present theory (a = 1 ; b = 1/2) (ψ = 0). 48

13 Comparison of non-dimensional uniaxial critical buckling load $\overline{\mathrm{N}} = \mathrm{N}a^2 12(1\text{-}{\nu_c}^2)/h^3E_c$ of a SSSS square plate (Al/Al_2O_3) with an an aspect ratio a/h = 100 and volume index λ = 0 using the present theory (a = 1 ; b = 1/2) (ψ = 0). 48

14 Comparison of non-dimensional uniaxial critical buckling load $\overline{\mathrm{N}} = \mathrm{N}a^2 12(1\text{-}{\nu_c}^2)/\pi^2h^3E_c$ of a SSSS square plate ($SUS304/Si_3N_4$) with varying aspect ratio a/h and volume index λ using the present theory (a = b = 1) (ψ = 0). 49

15 Comparison of 4 non-dimensional uniaxial buckling loads $\overline{\mathrm{N}} = \mathrm{N}a^2 12(1\text{-}{\nu_c}^2)/\pi^2h^3E_c$ of a SSSS square plate ($SUS304/Si_3N_4$) with an aspect ratio a/h = 100 and volume fraction index λ = 0 using the present theory (a = b = 1) (ψ = 0). 49

16 Comparison of non-dimensional biaxial critical buckling load $\overline{\mathrm{N}} = \mathrm{N}a^2 12(1\text{-}{\nu_c}^2)/\pi^2h^3E_c$ of a SSSS square plate ($SUS304/Si_3N_4$) with varying aspect ratio a/h and volume index λ using the present theory (a = b = 1) (ψ = 1). 50

17 Comparison of biaxial critical buckling load (MN) of a SSSS square plate (Al/Al_2O_3) with varying aspect ratio a/h and a volume index λ = 1 using the present theory (a = 1 ; b = 2) (ψ = 1). 51

18 Natural frequency (Hz) results for various discretization layers of a SSSS square plate (Al/Al_2O_3) with an aspect ratio a/h = 20 and varying volume index λ using CLT (a = 1 ; b = 1). 54

19 Natural frequency (Hz) results for various polynomial fit error percentage limits of a SSSS square plate (Al/Al_2O_3) with an aspect ratio a/h = 20 and varying volume index λ using the present study (a = 1 ; b = 1). 55

20 Critical buckling loads (MN) results for various discretization layers of a SSSS square plate (Al/Al_2O_3) with an aspect ratio a/h = 20 and varying volume index λ using CLT (a = 1 ; b = 2). 56

21 Critical buckling load (MN) results for various polynomial fit error percentage limits of a SSSS square plate (Al/Al_2O_3) with an aspect ratio a/h = 20 and varying volume index λ using the present study (a = 1 ; b = 2). 57

22 Standard input parameters. 75

23 Material properties of plate constituents. 75

1 Introduction

The concept of Functionally Graded Materials (FGMs) was first introduced in 1987 during a project at the National Aerospace Laboratory of Japan. Researchers building a space plane which would be subject to extreme temperatures, required a material which had high thermal resistance that was capable of withstanding 2000K on the outer surface and reduce the inner surface to a temperature of 1000K over a 10 mm thick plate [1, 2]. These materials are composite materials, characterized by having two distinct materials on either side of a dimension, with a gradual change from one of these materials to the other between these two points [1]. The gradual material transformation of FGMs may occur via volume fraction gradient, shape gradient, orientation gradient or size gradient [3].

The original application of FGMs were for the aerospace industry and specifically for the thermal barrier required for space plane bodies. However, since then, applications for FGMs have increased significantly and include applications in medicine, defence, the energy industry, electronics and optoelectronics, automobiles, tooling and machining [1, 2, 4].

Functionally Graded Material Plates (FGMPs) are being increasingly used for various applications among a number of industries due to their superior thermal and mechanical properties, among others. There are properties and advantages to FGMs which are superior to traditional composites and stand alone materials. They can have high hardness, high thermal and corrosive resistance and can offer various desirable properties from each type of material used to form the material [2, 3, 4]. These properties, advantages and the ability to tailor make materials to suit applications renders FGMs versatile and uniquely superior to traditional composites and materials.

The increasing number of applications and the vast list of superior properties and advantages that FGMPs provide, infers that these new materials will be increasingly used in various applications among a number of industries. Given that these materials are relatively new and not widely used at present, there is complex theory relating to their practical mechanical analysis. These analyses involve significant complex mathematics which renders the analysis impractical for many typical engineering applications. As a result, engineers are unable to sufficiently and confidently design these materials without performing these complex analyses. This research report adapts a well known theory for composite materials to simply and practically calculate the critical buckling loads and natural frequencies of FGMPs.

2 Literature Survey

2.1 Load Cases In Literature

The following section briefly discusses literature of a similar nature to the present study, all of which will be used for comparison with the results of the present study.

A review of the range of methods used to study the vibration and buckling of FGMPs was conducted by Swaminthan et al.[5]. The research covers both numerical finite element methods and meshless methods for vibrational and buckling cases. In addition, 2D and 3D analytical methods are covered for vibrational load cases whereas only 2D methods are covered for the buckling cases. The majority of the methods used for the analysis are extensions of the approaches used in composite or isotropic plates including Classical Lamination Theory (CLT). Since FGMs have the potential for future use in engineering applications, Swaminathan et al.[5] have proposed five areas of study which may assist in improving the solution techniques and methodologies.

Birman and Byrd [6], conducted a review of the recent developments in FGMs since 2000. The research documents a number of aspects related to FGMs including a brief introduction, approaches to homogenization, mechanical response to static or dynamic loads, manufacturing, design and modelling related aspects, testing methods and results and applications. Birman and Byrd [6] list a number of observations or areas of study which need focus to achieve effective implementation of FGMs. Several of these areas include the interaction between the particles which should not be disregarded, irrespective of which homogenization method is adopted. In addition, FGMs are generally asymmetric and therefore, a coupling effect exists which needs to be accounted for.

2.1.1 Free Vibration

A three-dimensional (3D) exact solution for the natural frequency of SSSS (simply supported on all four sides) FGMPs was presented by Vel and Batra [7]. The authors used a set of suitable displacement functions which were reduced to ordinary differential equations and solved by the power series method. Exact solutions were found for thin and thick plates with an arbitrary variation of material properties which were found using the Mori-Tanaka Homogenization [8] or the self-consistent method. The results were obtained for a range of material property variations and aspect ratios. The results were compared with CLT, a First Order Shear Deformation Theory (FSDT) and a third order shear deformation theory. Neves

et al.[9] used a Higher-Order Shear Deformation Theory (HSDT) through the Unified Formulation proposed by Carrera (CUF) to model the natural frequency of SSSS FGMPs, with and without accounting for through thickness stretching. The authors used the Mori-Tanaka Homogenization [8] method to determine the elastic properties and obtained results for a range of material property variations and aspect ratios. Their approach achieved accurate results when compared to 3D results. Akavci and Tanrikulu [10] presented a two-dimensional (2D) and quasi 3D shear deformation analysis for the free vibration of FGMPs using a new hyperbolic shape function. The method accounted for transverse and normal shear strains. Hamilton's principle was used to obtain the governing equations and the Double Fourier series was used to solve the partial differential equations. The authors considered three different through thickness variations of material: power law, exponential and the Mori-Tanaka Homogenization [8] method. Results were compared to 2D, 3D and quasi 3D literature including Neves et al.[11] and Vel and Batra [7]. The results obtained illustrated agreement with 2D, 3D and quasi 3D literature, including for thick plates. Moghaddam and Baradaran [12] presented a 3D analysis using the meshless local Petrov-Galerkin (MLPG) method for FGMPs. The penalty method was used to impose the boundary conditions and the Mori-Tanaka Homogenization method [8] was used to determine the elastic properties through the thickness. Results were obtained for various through thickness variations in material properties, aspect ratios and boundary conditions. These results were compared to the results presented by Vel and Batra [7]. The comparison illustrated that Moghaddam and Baradaran [12] obtained results which were comparable to other 3D results. Matsunaga [13] analysed natural frequencies of plates, taking into account the transverse shear, normal deformations and rotatory inertia. Using the method of power series expansion, a set of equations of 2D higher order theory was derived using Hamilton's principle. Transverse stresses were obtained by integrating the 3D equations of motion through the plate thickness. The results of this theory accurately predicted the natural frequencies. Belabed et al.[14] used a new higher order shear and normal deformable plate theory (HOSNDPT) which has five unknowns and includes the stretching effect of the plate. The displacement field chosen was a hyperbolic variation of in plane and transverse displacements. The equations of motion and boundary conditions were solved using Hamiltons principle. The results were compared and were in agreement with 3D results even for the case of very thick plates with $a/h = 2$. Sheikholeslami and Saidi [15] analysed the natural frequency of plates using the HOSNDPT of Batra and Vidoli. All three displacement components are expanded in the thickness direction using the Legendre polynomials. Transverse shear and normal deformations were accounted for and the equations of motion are derived using the principle of virtual work. The natural frequencies were then established through the governing equations. Results were compared and considered to be close to 3D theory.

Qian et al. [16] used a HOSNDPT and a MLPG method to analyse the natural frequency of rectangular SSSS FGMPs. Plate theory equations were used to compute the equations of the stress tensor. The authors used the Mori-Tanaka Homogenization method [8] to determine the elastic properties and compared their results to that of Vel and Batra [7]. The results obtained by Qian et al. [16] agree well with those of Vel and Batra [7]. Neves at al.[11] presented a new application for Carrera's Unified Formulation (CUF) by utilising a meshless discretization for the analysis of FGMPs. The governing equations were established using a sinusoidal shear deformation theory (SDT). The Mori-Tanaka Homogenization method [8] was used to determine the elastic properties and results were obtained considering and neglecting through thickness stretching. The results were compared to Qian et al. [16] and Vel and Batra [7]. The results which accounted for through thickness stretching were significantly more accurate, especially for thicker plates. Hosseini et al.[17] presented exact closed form solutions for natural frequency of thick functionally graded plates based on Reddy's third order shear deformation plate theory. Five governing partial differential equations of motion were solved. The author compared results that vary with length ratio, aspect ratio and the volume index with various 3D literature and found that the theory accurately predicts the natural frequency of plates.

Zhu and Liew [18] used the local Kriging meshless method to establish the natural frequencies of moderately thick plates. The system equations for the eigenvalues were based on FSDT and the Petrov-Galerkin formulation. Comparison with other literature such as Matsunaga [13], showed that the results were accurate and robust for moderately thick plates. A four variable refined plate theory for natural frequency was presented by Benachour et al.[19]. Unlike other shear deformation theories, the four variable plate theory has four unknowns as opposed to five for other shear deformation theories. This results in a lower computational effort and has many similarities to CLT. The material properties vary according to the rule of mixtures and obey the power law variation. Equations of motion are established using the Hamilton's principle and the closed form solutions are obtained using the Navier technique. The natural frequencies are then found by solving the eigenvalue problems. Results were compared to other shear deformation theories and results were found to be in good agreement and sometimes identical.

Baferani et al.[20] presented an analysis of functionally graded thin plates based on classical lamination theory. Navier and Levy-type solutions were used to study the natural frequency of thin plates. Results were compared with an analysis of FSDT. Kumar et. al[21] used dynamic stiffness method based on classical lamination theory. The dynamic stiffness matrix was established using Wittrick-Williams algorithm, allowing the natural frequencies to be found. Results were compared with literature including Baferani et al.[20] and found to be in agreement. Li et al.[22] used classical lamination theory to obtain relations between

solutions for bending, buckling and free vibration for functionally graded plates and for a reference homogeneous plate with the same load condition and geometry. Establishing the neutral surface, the natural frequency of the functionally graded plates could be predicted using the relations and results of the reference homogeneous plate. Results were compared with available literature.

2.1.2 Buckling

Asemi et al.[23] presented a 3D approach to determine the buckling loads of functionally graded plates. The authors used a formulation that utilizes a full compatible 3D Hermitian element with 168 degrees of freedom. The buckling results were then established based on Galerkin type orthogonality. Results were presented for a range of load cases. Liu et al.[24] based their research on isogeometric analysis (IGA) and a simple quasi 3D hyperbolic shear deformation theory (S-Q3DHSDT) to study the critical buckling loads on functionally graded plates. The authors found that their results compared favourably with results from other literature including Neves et al.[9] and Thai and Choi [25]. Uymaz and Aydogdu [26] considered the buckling of functionally graded plates using a 3D linear elasticity theory and exponential shear deformation plate theory (ESDPT). Uymaz and Aydogdu [27] used small strain elasticity theory for the buckling of functionally graded plates. Both sets of results were obtained using the Ritz method with Chebyshev polynomials as displacement functions. Various load cases were considered with varying aspect ratio and volume indices.

Shariat and Eslami [28] derived the equilibrium and stability equations for buckling using the third order shear deformation plate theory (TSDT). Closed-form solutions were obtained for the critical buckling loads for each load case. Results were then compared with other literature including Javaheri and Eslami [29]. Thai and Choi [25] used a HSDT by accounting for a quadratic variation of the transverse shear strains through the thickness without using any shear correction factors. The governing equations were established using the principle of minimum potential energy. A comparison with other literature including Shariat and Eslami [28] and Asemi et al.[23] was done and results were shown to be accurate. Bodaghi and Saidi [30] established equilibrium and stability equations using a HSDT. The coupled governing equations were converted into two uncoupled partial differential equations. The Levy-type solution was used to solve for the buckling loads under various loading conditions. The results compared well with the results by Mohammadi et al.[31]. Kulkarni et al.[32] made use of a recently developed non-polynomial shear deformation theory called inverse trigonometric shear deformation theory (ITSDT). The governing differential equations were solved using the Navier-type technique. The results compared were found to be accurate for predicting the buckling loads of functionally graded SSSS plates. Nguyen [33] presented a HSDT where the

transverse shear stresses were accounted for using a hyperbolic variation through the plate thickness. The theory only had four unknowns and the equations of motion were established using Hamilton's principle. The Navier-type solutions were then used to find the critical buckling loads. The results obtained agreed compared well with HSDT and quasi 3D models.

Yin et al.[34] presented a S-FSDT for analysing the buckling of functionally graded plates. The non-uniform rational B-spline (NURBS) based isogeometric analysis was used to satisfy C^1-continuity required by FSDT. The results were found to compare well with other literature for both thin and thick plates.

Javaheri and Eslami [29] derived equations CLT and the variational approach was used to determine equilibrium and stability equations. Results were then derived for SSSS plates subjected to in-plane loading. Mohammadi et al.[31] presented a buckling analysis based on CLT and governing equations were obtained using the principle of minimum total potential energy. The boundary conditions were imposed using the Levy solution. Results were obtained for various volume indices and aspect ratios.

2.2 Volume Fraction

The material properties of the functionally graded plate vary through the thickness. This variation of material properties is governed by the two constituent materials, being a ceramic and metallic material. The volume fraction of the ceramic phase, V_c, is described according to the power law [35]:

$$V_c(z) = \left(\frac{1}{2} - \frac{z}{h}\right)^{\lambda} \tag{1}$$

where z is the through thickness coordinate, h is the thickness of the plate and λ is the volume index, a dimensionless constant that influences the extent of the variation in the profile of the volume fraction of the ceramic. Figure 1 is an illustration of the effects of the varying values of λ on the volume fraction of the ceramic.

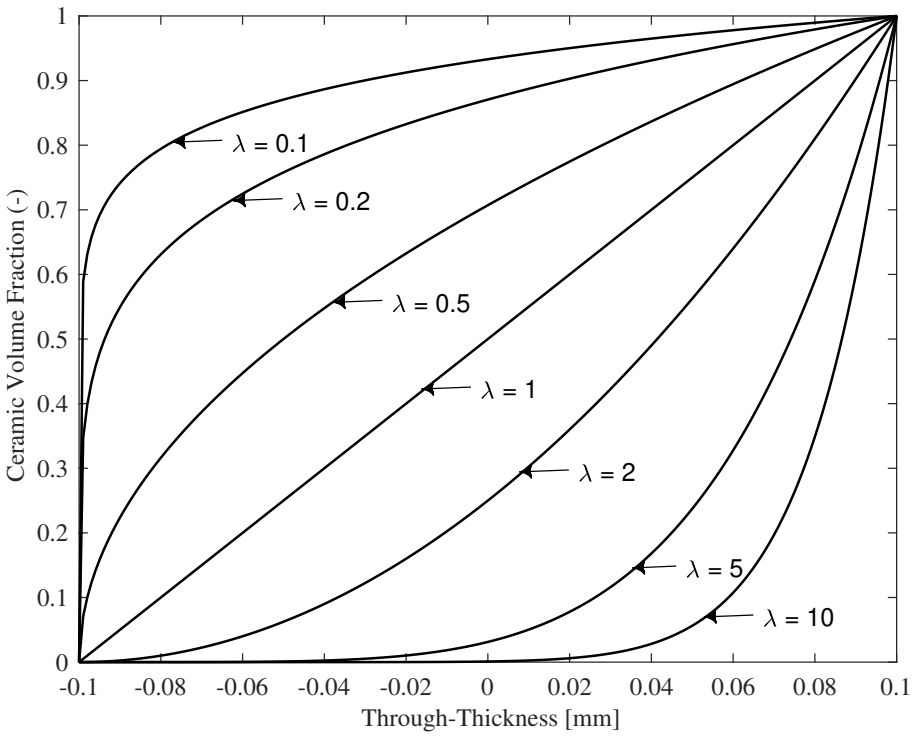


Figure 1: Variation of volume fraction of the ceramic material for various values of λ.

The power law equation for the volume fraction of the ceramic phase may be described using various other forms of equations, including simple higher order polynomials as follows:

$$V_c(Z_n) = a_n {Z_n}^n + a_{n-1} {Z_n}^{n-1} + ... + a_2 {Z_n}^2 + a_1 Z_n + a_0$$

Depending on the fit required, a greater order polynomial is required in order to achieve the required accuracy.

2.3 Through-Thickness Variation

The following section explores the two common methods of accounting for the through thickness variation of materials in functionally graded plates. There are two common methods for establishing these properties, the rule of mixtures method and the Mori-Tanaka Homogenization method [8][36].

2.3.1 Rule of Mixtures

The rule of mixtures method is based on micromechanics of composite materials and is the simplest method for establishing the variation of the local effective material properties of

functionally graded plates. The method entails the summation of the respective Young's modulus and Poisson's ratio based on the volume fraction of the respective metallic and ceramic materials, V_m and V_c respectively. The rule of mixtures method is given as follows:

$$E(z) = E_m V_m + E_c V_c \tag{2}$$

$$\nu(z) = \nu_m V_m + \nu_c V_c \tag{3}$$

Once the effective layer properties have been established using the rule of mixtures method, the elastic constants of the stress-strain relationships can be established.

2.3.2 Mori-Tanaka Homogenization Procedure

The Mori-Tanaka Homogenization method [8], later reformulated by Benveniste [36], establishes the locally effective material properties of composites. Perfect bonding is assumed between the two constituent materials which are also assumed to be of a random size and orientation. The two parameters required for the establishment of the effective material properties are the bulk modulus K, shear modulus G and Poisson's ratio, ν of each constituent material. However, literature shows that in many cases, only the Young's modulus E and Poisson's ratio ν, of a given constituent material is given and therefore, the bulk modulus and shear modulus of each material must be established as follows:

$$K = \frac{E}{3(1-2\nu)} \tag{4}$$

$$G = \frac{E}{3(1+\nu)} \tag{5}$$

Having established the bulk and shear moduli for each constituent material, the method entails the calculation of the modified bulk and shear moduli, $K$and G, which are then used to establish the effective Young's modulus and Poisson's ratio, E^k and ν^k respectively. The modified bulk and shear moduli are given as follows:

$$\frac{K(z) - K_m}{K_c - K_m} = \frac{V_c}{1 + (1 - V_c)\frac{K_c - K_m}{K_m + \frac{4}{3}G_m}} \tag{6}$$

$$\frac{G(z) - G_m}{G_c - G_m} = \frac{V_c}{1 + (1 - V_c)\frac{G_c - G_m}{G_m + \eta_m}} \tag{7}$$

where the subscripts for m and c refer to the metallic and ceramic components respectively and where the parameter η_m is given by equation 8 as follows:

$$\eta_m = \frac{G_m(9K_m + 8G_m)}{6(K_m + 2G_m)} \tag{8}$$

Using the modified bulk and shear moduli, $K$and G, the effective values for Young's modulus, E^k, and Poisson's ratio, ν^k, are then found using Equations 9 and 10 respectively, as follows:

$$E^k(z) = \frac{9KG}{3K+G} \tag{9}$$

$$\nu^k(z) = \frac{3K-2G}{2(3K+G)} \tag{10}$$

Once the effective layer properties have been established using the Mori-Tanaka Homogenization method, the elastic constants of the stress-strain relationships can be established.

2.4 Classic Lamination Theory

The present study is based on CLT which greatly simplifies the analysis of the natural frequencies and critical buckling loads of FG plates. CLT is a model which can be used to establish the stresses and strains in plates subjected to forces and moments. It is useful to establish the macromechanics of laminates before exploring CLT. The generalized Hooke's Law which relates the stresses and strains can be written as follows [37]:

$$\sigma_i = E_{ij}\epsilon_i \quad i,j \ = \ 1,2...6$$

where the first 3 stresses are normal stresses in the 1,2 and 3 directions and the last three are shear stresses acting on the 23, 31 and 12 planes respectively. These strains are specifically given as follows:

$$\epsilon_1 = \frac{\partial u}{\partial x}$$

$$\epsilon_2 = \frac{\partial v}{\partial y}$$

$$\epsilon_3 = \frac{\partial w}{\partial z}$$

$$\epsilon_4 = \ \gamma_{23} = \frac{\partial v}{\partial z} + \frac{\partial w}{\partial y}$$

$$\epsilon_5 = \ \gamma_{31} = \frac{\partial w}{\partial x} + \frac{\partial u}{\partial z}$$

$$\epsilon_6 = \ \gamma_{12} = \frac{\partial u}{\partial y} + \frac{\partial v}{\partial x}$$

where u, v and w are the displacements in the x, y and w directions respectively. CLT makes use of a number of assumptions which greatly reduces the complexity of the analysis and allows the problem to be easily solvable. The following assumptions underpin CLT [37]:

- The plate consists of orthotropic materials.
- The laminate thickness is very small in comparison with other dimensions.

- The lamina of the laminate are perfectly bonded.
- The laminate is macroscopically homogeneous and linearly elastic.
- Straight lines normal to the mid-plane remain normal to the mid-plane after deformation.
- The through-thickness strains are negligible.

These assumptions render the plate to be in a state of plane stress and significantly simplifies the analysis without sacrificing too much accuracy in most cases. These assumptions are not strictly true and may have an impact on the results. As a result of the assumptions, the following strains are eliminated:

$$\epsilon_3 = \frac{\partial w}{\partial z} = 0$$
$$\epsilon_4 = \gamma_{23} = \frac{\partial v}{\partial z} + \frac{\partial w}{\partial y} = 0$$
$$\epsilon_5 = \gamma_{31} = \frac{\partial w}{\partial x} + \frac{\partial u}{\partial z} = 0$$

As a result, the strain-stress relationship reduces to [37]:

$$\begin{bmatrix} \epsilon_1 \\ \epsilon_2 \\ \gamma_{12} \end{bmatrix} = \begin{bmatrix} S_{11} & S_{12} & 0 \\ S_{21} & S_{22} & 0 \\ 0 & 0 & S_{66} \end{bmatrix} \begin{bmatrix} \sigma_1 \\ \sigma_2 \\ \tau_{12} \end{bmatrix} \tag{11}$$

where Equation 11 is a 3x3 matrix known as the compliance matrix. In addition, each term is given as follows [37]:

$$S_{11} = \frac{1}{E_1}$$
$$S_{12} = -\frac{\nu_{12}}{E_1} = -\frac{\nu_{21}}{E_2}$$
$$S_{22} = \frac{1}{E_2}$$
$$S_{66} = \frac{1}{G_{12}}$$

where E_1 and ν_{12} is the Young's modulus and Poisson's ratio in the longitudinal or primary direction respectively and E_2 and ν_{21} is the Young's modulus and Poisson's ratio in the transverse or secondary direction respectively. G_{12} is the in-plane shear modulus which is given by:

$$G_{12} = \frac{E_1}{2(1-\nu_{12})} \tag{12}$$

Equation 12 for the calculation of the shear modulus is only applicable to isotropic materials. Inverting the compliance matrix, the stress as a function of strain can be established [37]:

$$\begin{bmatrix} \sigma_1 \\ \sigma_2 \\ \tau_{12} \end{bmatrix} = \begin{bmatrix} Q_{11} & Q_{12} & 0 \\ Q_{21} & Q_{22} & 0 \\ 0 & 0 & Q_{66} \end{bmatrix} \begin{bmatrix} \epsilon_1 \\ \epsilon_2 \\ \gamma_{12} \end{bmatrix} \tag{13}$$

where Equation 13 is a 3x3 matrix known as the reduced stiffness matrix, abbreviated as $[Q]$ and its terms are given in terms of the elastic constants by [37]:

$$\begin{aligned} Q_{11} &= \frac{E_1}{1 - \nu_{12}\nu_{21}} \\ Q_{12} &= \frac{E_2\nu_{12}}{1 - \nu_{12}\nu_{21}} \\ Q_{22} &= \frac{E_2}{1 - \nu_{12}\nu_{21}} \\ Q_{66} &= G_{12} \end{aligned}$$

The reduced stiffness matrix for σ_1, σ_2 and τ_{12} only allows for the normal stresses and strains to be established relative to the 1 and 2 direction and shear stress and strain in the 1-2 plane respectively. However, it is assumed that when the FG plate is transformed into the global coordinate system, the principle coordinate system is rotated relative to the global coordinate system and the stress-strain relationship is written as [35]:

$$\begin{bmatrix} \sigma_x \\ \sigma_y \\ \tau_{xy} \end{bmatrix} = \begin{bmatrix} \overline{Q}_{11} & \overline{Q}_{12} & 0 \\ \overline{Q}_{21} & \overline{Q}_{22} & 0 \\ 0 & 0 & \overline{Q}_{66} \end{bmatrix} \begin{bmatrix} \epsilon_x \\ \epsilon_y \\ \gamma_{xy} \end{bmatrix} \tag{14}$$

where the transformed reduced stiffness matrix is often referred to as $\overline{Q}$ and where σ_x, σ_y and τ_{xy} represent the normal stresses in the x and y directions and the shear stress in the xy plane respectively [35]. To establish the coordinate system for CLT, it is assumed that the laminate will lay in the x and y plane. Displacements will be defined as u, v and w in the x, y and z directions respectively. Figure 2 illustrates these displacements of the plate and the resulting strains are defined as [37]:

$$\begin{aligned} \epsilon_x &= \frac{\partial u}{\partial x} \\ \epsilon_y &= \frac{\partial v}{\partial y} \\ \gamma_{12} &= \frac{\partial u}{\partial y} + \frac{\partial v}{\partial x} \end{aligned} \tag{15}$$

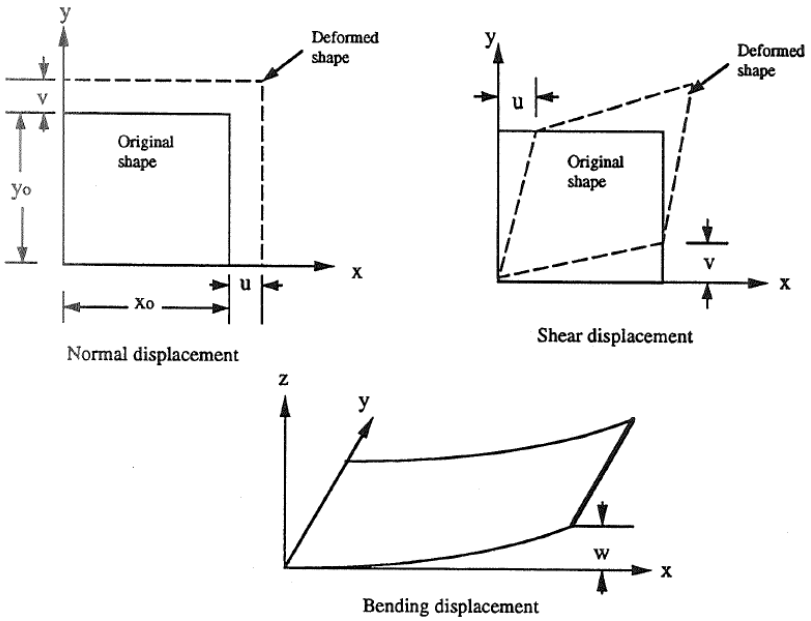


Figure 2: Displacement of a plate [37].

The total in-plane displacement of the plate at any point is the sum of the normal displacements plus the displacements due to bending. Figure 3 illustrates the total displacement at a point after loads have been applied to a plate.

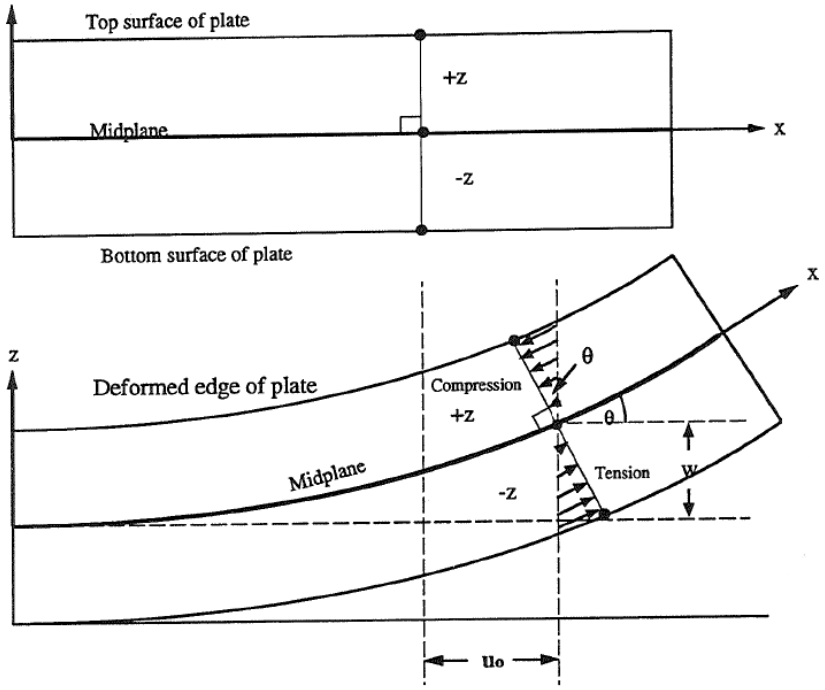


Figure 3: Total displacement in a plate [37].

The slope of the plate during bending is given as [37]:

$$\theta_x \approx \frac{\partial w}{\partial x}$$
$$\theta_y \approx \frac{\partial w}{\partial y} \tag{16}$$

since the slope θ is small. By combining the displacements of the plate at the mid-plane, together with the displacement due to bending, the total displacements are as follows:

$$u = u_0 - z\frac{\partial w}{\partial x}$$
$$v = v_0 - z\frac{\partial w}{\partial y} \tag{17}$$

where u_0 and v_0 are the displacements of the mid-plane of the plate in the x and y directions respectively. From Equations 16 and 17, it then follows [37]:

$$\begin{aligned}
\epsilon_x &= \frac{\partial u}{\partial x} = \frac{\partial u_0}{\partial x} - z\frac{\partial^2 w}{\partial x^2} \\
\epsilon_y &= \frac{\partial v}{\partial y} = \frac{\partial v_0}{\partial y} - z\frac{\partial^2 w}{\partial y^2} \\
\gamma_{xy} &= \frac{\partial u}{\partial y} + \frac{\partial v}{\partial x} = \frac{\partial u_0}{\partial y} + \frac{\partial v_0}{\partial x} - 2z\frac{\partial^2 w}{\partial x \partial y}
\end{aligned} \tag{18}$$

Equation 18 can the be simplified and rewritten in matrix form as [37]:

$$\begin{bmatrix} \epsilon_x \\ \epsilon_y \\ \gamma_{xy} \end{bmatrix} = \begin{bmatrix} \epsilon_x^0 \\ \epsilon_y^0 \\ \gamma_{xy}^0 \end{bmatrix} + z \begin{bmatrix} \kappa_x \\ \kappa_y \\ \kappa_{xy} \end{bmatrix} \tag{19}$$

where ϵ_x^0, ϵ_y^0 and γ_{xy}^0 are the mid-plane strains and κ_x, κ_y, and κ_{xy} are the plate curvatures. κ_x and κ_y is the rate of change of the slope of the bending plate in the x and y direction accordingly. κ_{xy} curvature term is the amount of bending in the x direction along the y axis (i.e., twisting). From Equation 14, the stress-strain relationship can now be expressed as [37]:

$$\begin{bmatrix} \sigma_x \\ \sigma_y \\ \tau_{xy} \end{bmatrix} = \begin{bmatrix} \overline{Q}_{11} & \overline{Q}_{12} & 0 \\ \overline{Q}_{21} & \overline{Q}_{22} & 0 \\ 0 & 0 & \overline{Q}_{66} \end{bmatrix} \begin{bmatrix} \epsilon_x^0 \\ \epsilon_y^0 \\ \gamma_{xy}^0 \end{bmatrix} + z \begin{bmatrix} \overline{Q}_{11} & \overline{Q}_{12} & 0 \\ \overline{Q}_{21} & \overline{Q}_{22} & 0 \\ 0 & 0 & \overline{Q}_{66} \end{bmatrix} \begin{bmatrix} \kappa_x \\ \kappa_y \\ \kappa_{xy} \end{bmatrix}$$

Since the stress in the laminate varies through the thickness due to the variation in material properties, the stresses are defined in terms of the equivalent forces acting at the mid-plane. The stresses acting at the end of the plate may be discretized and summed to produce an integral which is defined as the force resultant, N, which is a force per unit of width. The

force resultants are defined as follows [37].

$$N = \begin{bmatrix} N_x & N_y & N_{xy} \end{bmatrix}^{\mathrm{T}} = \int_{\frac{h}{2}}^{-\frac{h}{2}} \begin{bmatrix} \sigma_x & \sigma_y & \tau_{xy} \end{bmatrix}^{\mathrm{T}} \mathrm{d}z$$

The stresses acting within the plate produce moments about the mid-plane. The moment resultants, which are moments per unit of width, M, acting on a laminate are equal to the integral of stresses over the laminate thickness acting at a moment arm z.

$$M = \begin{bmatrix} M_x & M_y & M_{xy} \end{bmatrix}^{\mathrm{T}} = \int_{\frac{h}{2}}^{-\frac{h}{2}} \begin{bmatrix} \sigma_x & \sigma_y & \tau_{xy} \end{bmatrix}^{\mathrm{T}} z \mathrm{d}z$$

This section is a summary of CLT and will form the basis for all subsequent analysis.

2.5 Rayleigh-Ritz

To establish the natural frequencies and critical buckling loads, the use of an approximate method is required such as that of the Rayleigh-Ritz method. This method is based on the principle of stationary total potential energy, i.e. at equilibrium. Plates that are experiencing free vibration or buckling from it's initial unstrained position possess internal strain energy which is introduced through the external work being applied[38]. The principle of conservation of energy infers that the sum of the kinetic and strain energy must remain the same over time [39]. Therefore, the total potential energy, Π, remains constant and at equilibrium, is given as:

$$\frac{\partial \Pi}{\partial \Delta(x, y, z)} = 0 \tag{20}$$

where Π is the difference between the internal(or strain energy) and the external work and $\Delta(x, y, z)$ is a deflection function which represents the displacement at an arbitrary point within the plate described by the displacement function or trial function with deflection coefficients C. The method assumes that the displacement or trial function can be approximated by a combination of linear discrete vectors. Therefore, a reasonable displacement or trial function must be assumed which will approximate the form of the solution [38]. In the present theory, the following trial function has been assumed for the out of plane displacement specifically for the buckling case:

$$w = \sum_{m=1}^{M} \sum_{p=1}^{P} W_{mp} \sin\left(\frac{m\pi x}{a}\right) \sin\left(\frac{p\pi y}{b}\right)$$

where M and P are the total number of half waves in the x and y directions respectively, W_{mp} is a deflection coefficient, x and y are the positions on the x and y axes and a, b are the

length and width of the plate respectively. Since the natural frequency is a function of time, the trial function for the natural frequency case includes a time dependent variable:

$$w = \sum_{m=1}^{M} \sum_{p=1}^{P} W_{mp} \sin\left(\frac{m\pi x}{a}\right) \sin\left(\frac{p\pi y}{b}\right) \sin\left(\Omega t\right)$$

where Ω is the natural frequency of the plate. Using an expression with a finite number of degrees of freedom constrains the solution to a set number of deformations states which increases convergence, however, the accuracy thereof depends on the trial function chosen. Solutions generally underestimate plate deflections as a result of the assumed approximate displacement form which constrains the true shape of the plate and produces an artificial stiffening effect. No clear rules apply to the assumed trial function, only that it must satisfy the geometric boundary conditions [38]. It then follows that at equilibrium:

$$\frac{\partial \Pi}{\partial \Delta(x,y,z)} = \frac{\partial \Pi}{\partial C} \cdot \frac{\partial C}{\partial \Delta(x,y,z)}$$

where $\Delta(x,y,z) = \mathrm{d}(x,y,z) \cdot C$, $\mathrm{d}(x,y,z)$ is an array of deflection functions and C is an array of deflection coefficients. The partial derivative of the coefficient with respect to the deflection function results in:

$$\frac{\partial C}{\partial \Delta(x,y,z)} = \frac{1}{\mathrm{d}(x,y,z)}$$

but since $\mathrm{d}(x,y,z)$ is a constant at any position, it follows that:

$$\frac{\partial \Pi}{\partial \Delta(x,y,z)} = \frac{\partial \Pi}{\partial C} = 0 \tag{21}$$

Splitting the dividend of Equation 21 into the two forms of energy results in the following expression:

$$\frac{\mathrm{d}U}{\mathrm{d}C} - \frac{\mathrm{d}V}{\mathrm{d}C} = 0$$
$$\frac{\mathrm{d}U}{\mathrm{d}C} = \frac{\mathrm{d}V}{\mathrm{d}C}$$

which is the condition of equilibrium for the system, where U is the internal strain energy and V is the total external work. The internal strain energy may be expressed in a concise form, where the stress-strain relationship is represented by the generalized Hooke's Law:

$$U = \tfrac{1}{2} \int_{vol} \sigma^T(x,y,z)\epsilon(x,y,z)\ \mathrm{d}vol$$
$$U = \tfrac{1}{2} \int_{vol} \epsilon^T(x,y,z)Q\epsilon(x,y,z)\ \mathrm{d}vol \tag{22}$$

Furthermore, the strains may be expressed in terms of the displacement or trial function by appropriately differentiating the function:

$$\epsilon = \mathcal{D}\mathrm{d}(x, y, z)C \tag{23}$$

where $\mathcal{D}$ is the appropriate differential operator. By defining the matrix B as:

$$B = \mathcal{D}(\mathrm{d}(x, y, z))$$

Equation 23 may be rewritten as:

$$\epsilon = B(x, y, z)C \tag{24}$$

Substituting the above equation into Equation 22, Equation 22 can be rewritten as:

$$U = \tfrac{1}{2}\int_{vol} C^T B^T(x, y, z)QB(x, y, z)C \ \mathrm{d}vol \tag{25}$$

Subsequently, defining $K = \int_{vol} B^T(x, y, z)QB(x, y, z)$, the strain energy equation, Equation 25 is given by:

$$U = \tfrac{1}{2}W^T KW$$

The Rayleigh-Ritz method is used to establish the natural frequencies and critical buckling loads of the present theory.

3 Objectives

The work aims to achieve the following objectives:

- Develop the extension to CLT of Reid and Paskaramoorthy [35] to establish equations which describe the critical buckling loads and natural frequencies of vibration for FG-MPs.
- Using the developed theory, obtain the critical buckling loads and natural frequencies of vibration for load cases presented in the literature for which exact solutions exist.
- Compare and discuss the results obtained with those of the exact solutions.
- Determine the practicality of the use of the developed theory for basic engineering applications.

4 Theory Development

4.1 Elastic Stress-Strain Relationships

The laminate configuration illustrated in Figure 4 is under consideration. The laminate can be made up of any number of N layers of Functionally Graded Material (FGM) of orthotropic material properties with a layer thickness of h_n, total laminate thickness h, length of a and width of b. However, in the present study, it will be assumed that the laminate will only be made up of 1 layer. The z-axis is perpendicular to the plane and is taken positive downwards with it's origin at the mid-plane of the laminate. The layer properties vary through the thickness of the layer with the top surface of the layer being a pure ceramic material while at the bottom of the layer is a pure metallic material. The z-coordinate of the mid-plane of each layer is denoted by $\overline{z}_n$.

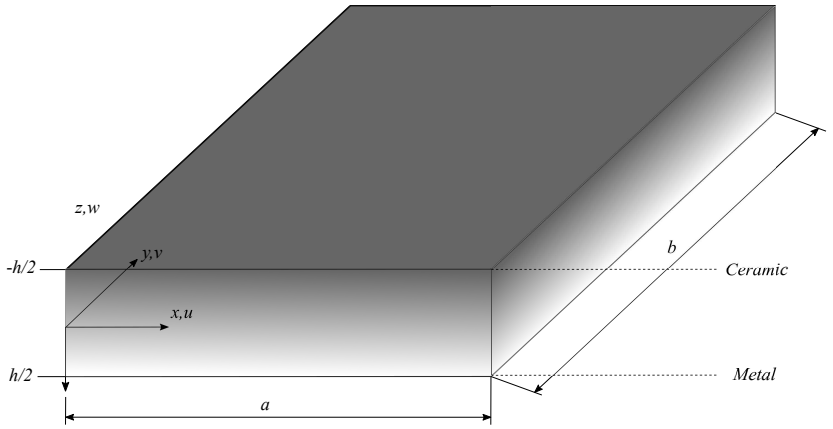


Figure 4: Configuration of laminate under consideration

A non-dimensional z-coordinate is introduced within each layer in Z_n which varies from -1 at the top surface to +1 at the bottom surface. The relationship between z and Z_n is defined as follows:

$$z = \overline{z}_n + \frac{h_n}{2} Z_n \tag{26}$$

The stress in the laminate varies through the thickness of the laminate so it is convenient to establish the force resultants, N, acting at the mid-plane. The force resultant, N, acting on a laminate must satisfy the conditions of equilibrium and is balanced by the integral of stresses over the laminate thickness.

$$N = \begin{bmatrix} N_x & N_y & N_{xy} \end{bmatrix}^{\mathrm{T}} = \int_{\frac{h_n}{2}}^{-\frac{h_n}{2}} \begin{bmatrix} \sigma_x & \sigma_y & \tau_{xy} \end{bmatrix}^{\mathrm{T}} \mathrm{d}z$$

The strain variation through the laminate is a function of both the mid-plane strain and the curvature and is continuous through the plate thickness. By substituting the geometric relationship for the total displacement in the laminate, it can be rewritten as:

$$N = \begin{bmatrix} N_x \\ N_y \\ N_{xy} \end{bmatrix} = \int_{-\frac{h_n}{2}}^{\frac{h_n}{2}} \overline{Q} \left\{ \begin{bmatrix} \epsilon_{0x} \\ \epsilon_{0y} \\ \gamma_{xy} \end{bmatrix} + z \begin{bmatrix} \kappa_x \\ \kappa_y \\ \kappa_{xy} \end{bmatrix} \right\} \mathrm{d}z$$

where $\overline{Q}$ is the laminate stiffness matrix, ϵ_0 is the mid-plane strains and κ the curvatures of the mid-plane. Should more than 1 layer be considered, the material properties in each layer are discontinuous, therefore, the resulting force, N, is found by summing the contributions for each layer:

$$N = \begin{bmatrix} N_x \\ N_y \\ N_{xy} \end{bmatrix} = \sum_{n=1}^{N} \int_{z_{n-1}}^{z_n} \overline{Q}_n \left\{ \begin{bmatrix} \epsilon_{0x} \\ \epsilon_{0y} \\ \gamma_{xy} \end{bmatrix} + z \begin{bmatrix} \kappa_x \\ \kappa_y \\ \kappa_{xy} \end{bmatrix} \right\} \mathrm{d}z \tag{27}$$

where $\overline{Q}_n$ is the transformed stiffness matrix of layer n. In the present study however, only 1 layer will be considered and therefore, $N = 1$. At this stage, it is clear that unless the z-variation of the terms within $\overline{Q}_n$ are simple functions, the integration of Equation 27 is complex. Therefore, each of the terms in $\overline{Q}_n$ may be represented in terms of the non-dimensional variable Z_n through a polynomial curve fit. As a result, the original function can be accurately represented by the polynomial series if sufficiently high order terms are used. Appendix D provides the software code used to establish the polynomial curves used to establish the elastic constants. The polynomial curve fit order is increased until each error percentage at a set number of locations within the plates through thickness is within a predetermined range. The polynomial representing the terms of $\overline{Q}_n$ can be rewritten in terms of the polynomial series of order P as follows:

$$\overline{Q}_n = \sum_{p=0}^{P} \begin{bmatrix} \overline{Q}_{11_{n_p}} & \overline{Q}_{21_{n_p}} & \overline{Q}_{31_{n_p}} \\ \overline{Q}_{12_{n_p}} & \overline{Q}_{22_{n_p}} & \overline{Q}_{32_{n_p}} \\ \overline{Q}_{13_{n_p}} & \overline{Q}_{23_{n_p}} & \overline{Q}_{33_{n_p}} \end{bmatrix} Z_n^p \tag{28}$$

where the square matrix on the right hand side of the equation represents the coefficients of the p^{th} terms in the series used to describe $\overline{Q}_n$. Let $\overline{Q}_{n_p}$ represent the p^{th} matrix on the right hand side of Equation 28:

$$\overline{Q}_{n_p} = \begin{bmatrix} \overline{Q}_{11_{n_p}} & \overline{Q}_{21_{n_p}} & \overline{Q}_{31_{n_p}} \\ \overline{Q}_{12_{n_p}} & \overline{Q}_{22_{n_p}} & \overline{Q}_{32_{n_p}} \\ \overline{Q}_{13_{n_p}} & \overline{Q}_{23_{n_p}} & \overline{Q}_{33_{n_p}} \end{bmatrix}$$

Equation 28 can accordingly be rewritten as:

$$\overline{Q}_n = \sum_{p=0}^{P} \overline{Q}_{n_p} Z_n^p$$

Substituting Equation 26 and changing the variable of integration within each layer to Z_n, the resulting equation can be written as:

$$N = \sum_{n=1}^{N} \int_{1}^{-1} \sum_{p=0}^{P} \overline{Q}_{n_p} Z_n^p \left(\epsilon_0 + \left(\overline{z}_n + \frac{h_n}{2} Z_n\right)\kappa\right) \frac{h_n}{2} \mathrm{d}Z_n$$

$$N = \sum_{n=1}^{N} \frac{h_n}{2} \int_{1}^{-1} \sum_{p=0}^{P} \overline{Q}_{n_p} \left(\epsilon_0 Z_n^p + \left(\overline{z}_n Z_n^p + \frac{h_n}{2} Z_n^{p+1}\right)\kappa\right) \mathrm{d}Z_n$$

The integral is evaluated as follows:

$$N = \sum_{n=1}^{N} h_n \left(\sum_{p=0,1,2\ldots}^{P} \frac{1-(-1)^{p+1}}{2(p+1)} \overline{Q}_{n_p} \right) \epsilon_0 + \sum_{n=1}^{N} h_n \left(\sum_{p=0,1,2\ldots}^{P} \frac{\overline{z}_n (1-(-1)^{p+1})}{2(p+1)} \overline{Q}_{n_p} + \sum_{p=0,1,2\ldots}^{P} \frac{h_n (1-(-1)^{p+2})}{4(p+2)} \overline{Q}_{n_p} \right) \kappa \tag{29}$$

In a similar manner, the moment resultants, M, acting on a laminate must satisfy the conditions of equilibrium and is balanced by the integral of stresses over the laminate thickness acting at a moment arm z.

$$M = \begin{bmatrix} M_x & M_y & M_{xy} \end{bmatrix}^{\mathrm{T}} = \int_{\frac{h_n}{2}}^{-\frac{h_n}{2}} \begin{bmatrix} \sigma_x & \sigma_y & \tau_{xy} \end{bmatrix}^{\mathrm{T}} z \mathrm{d}z$$

The integral is evaluated as follows:

$$M = \sum_{n=1}^{N} h_n \left(\sum_{p=0,1,2\ldots}^{P} \frac{\overline{z}_n (1-(-1)^{p+1})}{2(p+1)} \overline{Q}_{np} + \frac{h_{nn} (1-(-1)^{p+2})}{4(p+2)} \overline{Q}_{np} \right) \epsilon_0 + \sum_{n=1}^{N} h_n \left(\sum_{p=0,1,2\ldots}^{P} \frac{\overline{z}_n{}^2 (1-(-1)^{p+1})}{2(p+1)} \overline{Q}_{np} + \frac{\overline{z}_n h_n (1-(-1)^{p+2})}{2(p+2)} \overline{Q}_{np} + \frac{\overline{h_{nn}}{}^2 (1-(-1)^{p+3})}{8(p+3)} \overline{Q}_{np} \right) \kappa \tag{30}$$

The forces and moments acting on the laminate, Equation 29 and 30 respectively, can be expressed in matrix form as:

$$\begin{bmatrix} N \\ M \end{bmatrix} = \begin{bmatrix} A & B \\ B & D \end{bmatrix} \begin{bmatrix} \epsilon_0 \\ \kappa \end{bmatrix} \tag{31}$$

where each component of the square matrix on the right hand side has a distinct function and is termed:

A = extensional stiffness matrix
B = extension-bending coupling stiffness matrix
D = bending stiffness matrix

The A, B and D terms can then be found as:

$$A = \sum_{n=1}^{N} h_n \left(\sum_{p=0,1,2\ldots}^{P} \frac{1-(-1)^{p+1}}{2(p+1)} \overline{Q}_{np} \right) \tag{32}$$

$$B = \sum_{n=1}^{N} h_n \left(\sum_{p=0,1,2\ldots}^{P} \frac{\overline{z}_n (1-(-1)^{p+1})}{2(p+1)} \overline{Q}_{np} + \frac{h_n (1-(-1)^{p+2})}{4(p+2)} \overline{Q}_{np} \right) \tag{33}$$

$$D = \sum_{n=1}^{N} h_n \left(\sum_{p=0,1,2\ldots}^{P} \frac{\overline{z}_n{}^2 (1-(-1)^{p+1})}{2(p+1)} \overline{Q}_{np} + \frac{\overline{z}_n h_n (1-(-1)^{p+2})}{2(p+2)} \overline{Q}_{np} + \frac{\overline{h_{nn}}{}^2 (1-(-1)^{p+3})}{8(p+3)} \overline{Q}_{np} \right) \tag{34}$$

Appendix E provides the software code used to establish the stiffness matrix as described above.

4.2 Internal Strain Energy

The governing equations need to be formulated to establish the natural frequency and critical buckling load for any functionally graded plate. To establish the governing equations, the Rayleigh-Ritz method is used which requires a trial function which must be assumed and must satisfactorily model the expected displacements in the z direction as well as satisfy the geometric boundary conditions. The trial function used is as follows:

$$w = \sum_{m=1}^{M} \sum_{p=1}^{P} W_{mp} \sin\left(\frac{m\pi x}{a}\right) \sin\left(\frac{p\pi y}{b}\right) \sin\left(\Omega_{mp} t\right)$$

Let:

$$\alpha_m = \left(\frac{m\pi}{a}\right)$$

and

$$\beta_p = \left(\frac{p\pi}{b}\right)$$

The trial function can then be written as follows:

$$w = \sum_{m=1}^{M}\sum_{p=1}^{P} W_{mp}\sin(\alpha_m x)\sin(\beta_p y)\sin(\Omega_{mp}t) \tag{35}$$

The strain energy within the plate is given by the work done in deforming the plate which is therefore the product of all moments and their corresponding curvatures integrated over the entire surface of the plate. The strain energy equation in its basic form is given by:

$$U = \frac{1}{2}\int_0^A M\kappa \, \mathrm{d}A$$

Considering the contributions from all moments, the strain energy equation can be rewritten as follows:

$$U = \frac{1}{2}\int_0^a \int_0^b \begin{bmatrix} M_x & M_y & M_{xy} \end{bmatrix} \begin{bmatrix} -w_{xx} & -w_{yy} & -2w_{xy} \end{bmatrix}^{\mathrm{T}} \mathrm{d}x\mathrm{d}y \tag{36}$$

where w_{xx}, w_{yy} and w_{xy} are the plate curvatures as discussed in Section 2.4 and are defined as follows:

$$w_{xx} = \kappa_x = \frac{\partial^2 w}{\partial x^2}$$
$$w_{yy} = \kappa_y = \frac{\partial^2 w}{\partial y^2}$$
$$w_{xy} = \kappa_{xy} = \frac{\partial}{\partial y}\left(\frac{\partial w}{\partial x}\right)$$

w_{xx} and w_{yy} are the rates of change in the slope in the x or y directions, respectively, while w_{xy} is the rate of change of slope in the x direction with respect to changes in the y direction (i.e. twisting). The bending moments for an orthotropic plate are given by:

$$\begin{bmatrix} M_x \\ M_y \\ M_{xy} \end{bmatrix} = \begin{bmatrix} D_{11} & D_{12} & 0 \\ D_{21} & D_{22} & 0 \\ 0 & 0 & D_{66} \end{bmatrix} \begin{bmatrix} -w_{xx} \\ -w_{yy} \\ -2w_{xy} \end{bmatrix} \tag{37}$$

Therefore, the bending moments can be described by the following equations:

$$M_x = -D_{11}w_{xx} - D_{12}w_{yy}$$
$$M_y = -D_{21}w_{xx} - D_{22}w_{yy}$$
$$M_{xy} = -2D_{66}w_{xy}$$

Substituting the above bending moment equations into Equation 36 results in the following:

$$U = \frac{1}{2}\int_0^a \int_0^b \Big[D_{11}w_{xx} + D_{12}w_{yy}\Big]w_{xx} + \Big[D_{21}w_{xx} + D_{22}w_{yy}\Big]w_{yy} + \Big[2D_{66}w_{xy}\Big]2w_{xy}\ \mathrm{d}x\mathrm{d}y$$

Since D_{12} is equal to D_{21}, the above equation can simplified to:

$$U = \frac{1}{2}\int_0^a \int_0^b D_{11}{w_{xx}}^2 + 2D_{12}w_{xx}w_{yy} + D_{22}{w_{yy}}^2 + 4D_{66}{w_{xy}}^2\ \mathrm{d}x\mathrm{d}y \tag{38}$$

Equation 38 provides the strain energy for an orthotropic plate. CLT assumes that the moments are applied relative to the mid-plane, $\overline{z}_n$. However, FGMPs are usually unsymmetrical and therefore, the mid-plane and neutral axis, $\widehat{z}_n$, do not coincide. In the case of vibration, the simply supported plate infers that there is no moment at the edges and the in-plane displacements are assumed to be zero at the neutral axis. In the case of the buckling loads, the load is assumed to be applied on the neutral axis and not the mid-plane since this would induce a moment. This means that Equation 38 is based on the assumption that moments are calculated relative to the neutral axis, while the D terms of Equation 34 are calculated relative to the mid-plane. Therefore, they need to be reformulated so that they are calculated relative to the neutral axis to be used in Equation 38. As before, Equation 31 expresses the forces and moments acting on the laminate in matrix form as:

$$\begin{bmatrix} N \\ M \end{bmatrix} = \begin{bmatrix} A & B \\ B & D \end{bmatrix} \begin{bmatrix} \epsilon_0 \\ \kappa \end{bmatrix}$$

To make the mid-plane strains and curvatures the subject of the formula, Equation 31 is inverted:

$$\begin{bmatrix} \epsilon_0 \\ \kappa \end{bmatrix} = \begin{bmatrix} a & b \\ b & d \end{bmatrix} \begin{bmatrix} N \\ M \end{bmatrix} \tag{39}$$

From CLT, the strain variation through the laminate is expressed using the mid-plane strains and the mid-plane curvatures as follows:

$$\epsilon = \epsilon_0 + z\kappa \tag{40}$$

The strain variation through the laminate can then be expressed in terms of the inverted matrix of Equation 39:

$$\epsilon = [aN + bM] + z[bN + dM]$$

When only a moment M is applied, the tensile load N is zero and the strains within the laminate can be expressed as follows:

$$\epsilon = [\cancel{aN} + bM] + z[\cancel{bN} + dM]$$
$$\epsilon = bM + zdM$$
$$\epsilon = (b + zd)M$$

The components of strain variation through the laminate are split as follows:

$$\begin{bmatrix} \epsilon_x \\ \epsilon_y \\ \gamma_{xy} \end{bmatrix} = \left[\begin{bmatrix} b_{11} & b_{12} & \\ b_{12} & b_{22} & \\ & & b_{33} \end{bmatrix} + z \begin{bmatrix} d_{11} & d_{12} & \\ d_{12} & d_{22} & \\ & & d_{33} \end{bmatrix} \right] \begin{bmatrix} M_x \\ M_y \\ M_{xy} \end{bmatrix}$$

The simple support is located at the neutral axis, therefore, when only a moment M is applied, the neutral axis experiences no strain. At the neutral axis, $\widehat{z}_n$, the strain in the x direction is zero, $\epsilon_x = 0$, when only M_x is applied:

$$0 = \big(b_{11} + \widehat{z}_n d_{11}\big) M_x$$
$$0 = b_{11} + \widehat{z}_n d_{11}$$
$$\widehat{z}_n = -\, b_{11}/d_{11} \tag{41}$$

Similarly, in the y direction:

$$\widehat{z}_n = -\, b_{22}/d_{22}$$

The position of the neutral axis is then equal to $\widehat{z}_n = -b_{11}/d_{11}$. The z position of the neutral axis has now been established. The internal strain energy must be modified to account for the neutral axis position. Now, it is known from Equation 31 that:

$$M = B\epsilon_0 + D\kappa \tag{42}$$

So for pure bending about the neutral axis, $\epsilon = 0$ at the neutral axis. Using Equation 40 and making the strain equal to zero at the neutral axis results in the mid-plane strain equal to

the strain induced by the curvature at the neutral axis:

$$\begin{aligned}\epsilon &= \epsilon_0 + \widehat{z}_n\kappa \\ 0 &= \epsilon_0 + \widehat{z}_n\kappa \\ \epsilon_0 &= -\widehat{z}_n\kappa \end{aligned} \tag{43}$$

Substituting Equation 43 into Equation 42 results in:

$$\begin{aligned}M &= -B\widehat{z}_n\kappa + D\kappa \\ M &= (D - \widehat{z}_n B)\kappa\end{aligned}$$

Substituting Equation 41 in for $\widehat{z}_n$ results in:

$$M = (D + b_{11}/d_{11}B)\kappa \tag{44}$$

By comparing the moment matrix, Equation 37, with Equation 44, it is clear that the D matrix must now be replaced with the expression in Equation 44 which includes the extension-bending coupling stiffness matrix. The modified D matrix can now be redefined as:

$$\overline{D} = D + (b_{11}/d_{11})B$$

And as a result, the internal strain energy equation, Equation 38 can now be expressed as:

$$U = \frac{1}{2}\int_0^a \int_0^b \overline{D}_{11}{w_{xx}}^2 + 2\overline{D}_{12}w_{xx}w_{yy} + \overline{D}_{22}{w_{yy}}^2 + 4\overline{D}_{66}{w_{xy}}^2 \, \mathrm{d}x\mathrm{d}y \tag{45}$$

Now that the internal strain energy equation has been modified to include the D matrix terms calculated relative to the neutral axis, the simplified expression for the internal strain energy of a plate can now be found. To evaluate Equation 45, the first and second partial differential equation with respect to x must be established as required from Equation 35:

$$\begin{aligned}w_x &= \frac{\mathrm{d}w}{\mathrm{d}x} = \sum_{m=1}^{M}\sum_{p=1}^{P} W_{mp}\alpha_m \cos(\alpha_m x)\sin(\beta_p y)\sin(\Omega_{mp}t) \\ w_{xx} &= \frac{\mathrm{d}^2 w}{\mathrm{d}x^2} = \sum_{m=1}^{M}\sum_{p=1}^{P} -W_{mp}{\alpha_m}^2 \sin(\alpha_m x)\sin(\beta_p y)\sin(\Omega_{mp}t)\end{aligned} \tag{46}$$

In addition, the first and second partial differential equation with respect to y must be established as required from Equation 35:

$$w_y = \frac{\mathrm{d}w}{\mathrm{d}y} = \sum_{m=1}^{M}\sum_{p=1}^{P} W_{mp}\beta_p \sin(\alpha_m x)\cos(\beta_p y)\sin(\Omega_{mp}t)$$
$$w_{yy} = \frac{\mathrm{d}^2 w}{\mathrm{d}y^2} = \sum_{m=1}^{M}\sum_{p=1}^{P} -W_{mp}{\beta_p}^2 \sin(\alpha_m x)\sin(\beta_p y)\sin(\Omega_{mp}t) \tag{47}$$

Finally, the partial differential with respect to x and y as required from Equation 35 must be established:

$$w_x = \frac{\mathrm{d}w}{\mathrm{d}x} = \sum_{m=1}^{M}\sum_{p=1}^{P} W_{mp}\alpha_m \cos(\alpha_m x)\sin(\beta_p y)\sin(\Omega_{mp}t)$$
$$w_{xy} = \frac{\mathrm{d}w_x}{\mathrm{d}y} = \sum_{m=1}^{M}\sum_{p=1}^{P} W_{mp}\alpha_m\beta_p \cos(\alpha_m x)\cos(\beta_p y)\sin(\Omega_{mp}t) \tag{48}$$

Breaking the integral of Equation 45 into components and substituting in Equation 46. The first term is evaluated:

$$\int_0^a\int_0^b \overline{D}_{11}{w_{xx}}^2 \,\mathrm{d}x\mathrm{d}y$$
$$= \int_0^a\int_0^b \overline{D}_{11}\Big(\sum_{m=1}^{M}\sum_{p=1}^{P} -W_{mp}{\alpha_m}^2 \sin(\alpha_m x)\sin(\beta_p y)\sin(\Omega_{mp}t)\Big)^2 \,\mathrm{d}x\mathrm{d}y$$
$$= \overline{D}_{11}\sum_{m=1}^{M}\sum_{p=1}^{P}\sum_{s=1}^{M}\sum_{t=1}^{P} W_{mp}W_{st}{\alpha_m}^2{\alpha_s}^2 \sin^2(\Omega_{mp}t)\int_0^a\int_0^b \sin(\alpha_m x)\sin(\beta_p y)\sin(\alpha_s x)\sin(\beta_t y)\,\mathrm{d}x\mathrm{d}y$$
$$= \overline{D}_{11}\sum_{m=1}^{M}\sum_{p=1}^{P}\sum_{s=1}^{M}\sum_{t=1}^{P} W_{mp}W_{st}{\alpha_m}^2{\alpha_s}^2 \sin^2(\Omega_{mp}t)\int_0^a\int_0^b \frac{1}{2}\Big(\cos((\alpha_m-\alpha_s)x) - \cos((\alpha_m+\alpha_s)x)\Big)$$
$$\frac{1}{2}\Big(\cos((\beta_p-\beta_t)y) - \cos((\beta_p+\beta_t)y)\Big)\,\mathrm{d}x\mathrm{d}y$$
$$= \overline{D}_{11}\sum_{m=1}^{M}\sum_{p=1}^{P}\sum_{s=1}^{M}\sum_{t=1}^{P} W_{mp}W_{st}{\alpha_m}^2{\alpha_s}^2 \sin^2(\Omega_{mp}t)\frac{1}{4}\left[\frac{\sin((\alpha_m-\alpha_s)x)}{(\alpha_m-\alpha_s)} - \frac{\sin((\alpha_m+\alpha_s)x)}{(\alpha_m+\alpha_s)}\right]\Bigg|_0^a$$
$$\left[\frac{\sin((\beta_p-\beta_t)y)}{(\beta_p-\beta_t)} - \frac{\sin((\beta_p+\beta_t)y)}{(\beta_p-\beta_t)}\right]\Bigg|_0^b \quad \text{Note : Terms in brackets only have values if m = s and p = t}$$
$$= \overline{D}_{11}\sum_{m=1}^{M}\sum_{p=1}^{P} W_{mp}{}^2{\alpha_m}^4 \sin^2(\Omega_{mp}t)\frac{ab}{4} \qquad [\text{m = s}][\text{p = t}]$$

Similarly, the second term is evaluated as follows:

$$
\begin{aligned}
&\int_0^a \int_0^b 2\overline{D}_{12} w_{xx} w_{yy} \, \mathrm{d}x\mathrm{d}y \\
&= \int_0^a \int_0^b 2\overline{D}_{12} \Big(\sum_{m=1}^{M} \sum_{p=1}^{P} -W_{mp} {\alpha_m}^2 \sin(\alpha_m x) \sin(\beta_p y) \sin(\Omega_{mp} t) \Big) \\
&\quad \Big(\sum_{m=1}^{M} \sum_{p=1}^{P} -W_{mp} {\beta_p}^2 \sin(\alpha_m x) \sin(\beta_p y) \sin(\Omega_{mp} t) \Big) \, \mathrm{d}x\mathrm{d}y \\
&= 2\overline{D}_{12} \sum_{m=1}^{M} \sum_{p=1}^{P} \sum_{s=1}^{M} \sum_{t=1}^{P} W_{mp} W_{st} \alpha_m \beta_p \alpha_s \beta_t \sin^2(\Omega_{mp} t) \int_0^a \int_0^b \sin(\alpha_m x) \sin(\beta_p y) \sin(\alpha_s x) \sin(\beta_t y) \, \mathrm{d}x\mathrm{d}y \\
&= 2\overline{D}_{12} \sum_{m=1}^{M} \sum_{p=1}^{P} \sum_{s=1}^{M} \sum_{t=1}^{P} W_{mp} W_{st} \alpha_m \beta_p \alpha_s \beta_t \sin^2(\Omega_{mp} t) \int_0^a \int_0^b \frac{1}{2} \Big(\cos((\alpha_m - \alpha_s)x) - \cos((\alpha_m + \alpha_s)x) \Big) \\
&\quad \frac{1}{2} \Big(\cos((\beta_p - \beta_t)y) - \cos((\beta_p + \beta_t)y) \Big) \, \mathrm{d}x\mathrm{d}y \\
&= 2\overline{D}_{12} \sum_{m=1}^{M} \sum_{p=1}^{P} \sum_{s=1}^{M} \sum_{t=1}^{P} W_{mp} W_{st} \alpha_m \beta_p \alpha_s \beta_t \sin^2(\Omega_{mp} t) \frac{1}{4} \left[\frac{\sin((\alpha_m - \alpha_s)x)}{(\alpha_m - \alpha_s)} - \frac{\sin((\alpha_m + \alpha_s)x)}{(\alpha_m + \alpha_s)} \right] \Bigg|_0^a \\
&\quad \left[\frac{\sin((\beta_p - \beta_t)y)}{(\beta_p - \beta_t)} - \frac{\sin((\beta_p + \beta_t)y)}{(\beta_p - \beta_t)} \right] \Bigg|_0^b \qquad \text{Note : Terms in brackets only have values if m = s and p = t} \\
&= 2\overline{D}_{12} \sum_{m=1}^{M} \sum_{p=1}^{P} {W_{mp}}^2 {\alpha_m}^2 {\beta_p}^2 \sin^2(\Omega_{mp} t) \frac{ab}{4} \qquad \text{[m = s][p = t]}
\end{aligned}
$$

The third term is evaluated as follows:

$$
\begin{aligned}
&\int_0^a \int_0^b \overline{D}_{22} {w_{yy}}^2 \, \mathrm{d}x\mathrm{d}y \\
&= \int_0^a \int_0^b \overline{D}_{22} \Big(\sum_{m=1}^{M} \sum_{p=1}^{P} -W_{mp} {\beta_p}^2 \sin(\alpha_m x) \sin(\beta_p y) \sin(\Omega_{mp} t) \Big)^2 \, \mathrm{d}x\mathrm{d}y \\
&= \overline{D}_{22} \sum_{m=1}^{M} \sum_{p=1}^{P} \sum_{s=1}^{M} \sum_{t=1}^{P} W_{mp} W_{st} {\beta_p}^2 {\beta_t}^2 \sin^2(\Omega_{mp} t) \int_0^a \int_0^b \sin(\alpha_m x) \sin(\beta_p y) \sin(\alpha_s x) \sin(\beta_t y) \, \mathrm{d}x\mathrm{d}y \\
&= \overline{D}_{22} \sum_{m=1}^{M} \sum_{p=1}^{P} \sum_{s=1}^{M} \sum_{t=1}^{P} W_{mp} W_{st} {\beta_p}^2 {\beta_t}^2 \sin^2(\Omega_{mp} t) \int_0^a \int_0^b \frac{1}{2} \Big(\cos((\alpha_m - \alpha_s)x) - \cos((\alpha_m + \alpha_s)x) \Big) \\
&\quad \frac{1}{2} \Big(\cos((\beta_p - \beta_t)y) - \cos((\beta_p + \beta_t)y) \Big) \, \mathrm{d}x\mathrm{d}y \\
&= \overline{D}_{22} \sum_{m=1}^{M} \sum_{p=1}^{P} \sum_{s=1}^{M} \sum_{t=1}^{P} W_{mp} W_{st} {\beta_p}^2 {\beta_t}^2 \sin^2(\Omega_{mp} t) \frac{1}{4} \left[\frac{\sin((\alpha_m - \alpha_s)x)}{(\alpha_m - \alpha_s)} - \frac{\sin((\alpha_m + \alpha_s)x)}{(\alpha_m + \alpha_s)} \right] \Bigg|_0^a \\
&\quad \left[\frac{\sin((\beta_p - \beta_t)y)}{(\beta_p - \beta_t)} - \frac{\sin((\beta_p + \beta_t)y)}{(\beta_p - \beta_t)} \right] \Bigg|_0^b \qquad \text{Note : Terms in brackets only have values if m = s and p = t} \\
&= \overline{D}_{22} \sum_{m=1}^{M} \sum_{p=1}^{P} {W_{mp}}^2 {\beta_p}^4 \sin^2(\Omega_{mp} t) \frac{ab}{4} \qquad \text{[m = s][p = t]}
\end{aligned}
$$

The final term is evaluated as follows:

$$
\begin{aligned}
&\int_0^a \int_0^b 4\overline{D}_{66} {w_{xy}}^2 \, \mathrm{d}x\mathrm{d}y \\
&= \int_0^a \int_0^b 4\overline{D}_{66} \Big(\sum_{m=1}^{M} \sum_{p=1}^{P} W_{mp} \alpha_m \beta_p \cos(\alpha_m x) \cos(\beta_p y) \sin(\Omega_{mp} t) \Big)^2 \, \mathrm{d}x\mathrm{d}y \\
&= 4\overline{D}_{66} \sum_{m=1}^{M} \sum_{p=1}^{P} \sum_{s=1}^{M} \sum_{t=1}^{P} W_{mp} W_{st} \alpha_m \beta_p \alpha_s \beta_t \sin^2(\Omega_{mp} t) \int_0^a \int_0^b \cos(\alpha_m x) \cos(\beta_p y) \cos(\alpha_s x) \cos(\beta_t y) \, \mathrm{d}x\mathrm{d}y \\
&= 4\overline{D}_{66} \sum_{m=1}^{M} \sum_{p=1}^{P} \sum_{s=1}^{M} \sum_{t=1}^{P} W_{mp} W_{st} \alpha_m \beta_p \alpha_s \beta_t \sin^2(\Omega_{mp} t) \int_0^a \int_0^b \frac{1}{2} \Big(\cos((\alpha_m - \alpha_s)x) + \cos((\alpha_m + \alpha_s)x) \Big) \\
&\quad \frac{1}{2} \Big(\cos((\beta_p - \beta_t)y) + \cos((\beta_p + \beta_t)y) \Big) \, \mathrm{d}x\mathrm{d}y \\
&= 4\overline{D}_{66} \sum_{m=1}^{M} \sum_{p=1}^{P} \sum_{s=1}^{M} \sum_{t=1}^{P} W_{mp} W_{st} \alpha_m \beta_p \alpha_s \beta_t \sin^2(\Omega_{mp} t) \frac{1}{4} \left[\frac{\sin((\alpha_m - \alpha_s)x)}{(\alpha_m - \alpha_s)} + \frac{\sin((\alpha_m + \alpha_s)x)}{(\alpha_m + \alpha_s)} \right] \Bigg|_0^a \\
&\quad \left[\frac{\sin((\beta_p - \beta_t)y)}{(\beta_p - \beta_t)} + \frac{\sin((\beta_p + \beta_t)y)}{(\beta_p + \beta_t)} \right] \Bigg|_0^b \qquad \text{Note : Terms in brackets only have values if m = s and p = t} \\
&= 4\overline{D}_{66} \sum_{m=1}^{M} \sum_{p=1}^{P} {W_{mp}}^2 {\alpha_m}^2 {\beta_p}^2 \sin^2(\Omega_{mp} t) \frac{ab}{4} \qquad \text{[m = s][p = t]}
\end{aligned}
$$

Therefore, combining the components of the resulting integrals:

$$
U = \frac{1}{2} \Bigg[\sum_{m=1}^{M} \sum_{p=1}^{P} \frac{ab}{4} \Big(\overline{D}_{11} {\alpha_m}^4 + 2\overline{D}_{12} {\alpha_m}^2 {\beta_p}^2 + \overline{D}_{22} {\beta_p}^4 + 4\overline{D}_{66} {\alpha_m}^2 {\beta_p}^2 \Big) \Bigg] {W_{mp}}^2 \sin^2(\Omega_{mp} t)
$$

Simplifying the above equation results in:

$$
U = \frac{1}{2} \Bigg[\sum_{m=1}^{M} \sum_{p=1}^{P} \frac{ab}{4} \Big(\overline{D}_{11} {\alpha_m}^4 + (2\overline{D}_{12} + 4\overline{D}_{66}) {\alpha_m}^2 {\beta_p}^2 + \overline{D}_{22} {\beta_p}^4 \Big) \Bigg] {W_{mp}}^2 \sin^2(\Omega_{mp} t)
$$

The critical buckling case is independent of time and therefore, the trial function does not contain the $\sin(\Omega_{mp} t)$ term at the end. The trial function specific to the critical buckling load case is given as:

$$
w = \sum_{m=1}^{M} \sum_{p=1}^{P} W_{mp} \sin(\alpha_m x) \sin(\beta_p y)
$$

As a result of the independence with time, the internal strain energy equation for the critical bucking load case is given by:

$$
U = \frac{1}{2} \Bigg[\sum_{m=1}^{M} \sum_{p=1}^{P} \frac{ab}{4} \Big(\overline{D}_{11} {\alpha_m}^4 + (2\overline{D}_{12} + 4\overline{D}_{66}) {\alpha_m}^2 {\beta_p}^2 + \overline{D}_{22} {\beta_p}^4 \Big) \Bigg] {W_{mp}}^2
$$

From Section 2.5, it is known that:

$$\frac{\mathrm{d}U}{\mathrm{d}W_{mp}} = \frac{\mathrm{d}}{\mathrm{d}W_{mp}}\left(\tfrac{1}{2}W^T K W \sin^2(\Omega t)\right) = KW\sin^2(\Omega t) \tag{49}$$

Therefore, in order to find the stiffness matrix K:

$$K\sin^2(\Omega t) = \frac{\mathrm{d}}{\mathrm{d}W_{mp}}\left(KW\sin^2(\Omega t)\right)$$

Substituting for $KW\sin^2(\Omega t)$ from Equation 49 results in:

$$K\sin^2(\Omega t) = \frac{\mathrm{d}}{\mathrm{d}W_{mp}}\left(KW\sin^2(\Omega t)\right) = \frac{\mathrm{d}}{\mathrm{d}W_{mp}}\left(\frac{\mathrm{d}U}{\mathrm{d}W_{mp}}\right) = \frac{\mathrm{d}^2U}{\mathrm{d}{W_{mp}}^2}$$

Therefore, the stiffness matrix K is given by:

$$K\sin^2(\Omega t) = \frac{\mathrm{d}^2U}{\mathrm{d}{W_{mp}}^2} = \frac{\mathrm{d}^2}{\mathrm{d}{W_{mp}}^2}\left(\frac{1}{2}\left[\sum_{m=1}^{M}\sum_{p=1}^{P}\frac{ab}{4}\Big(\overline{D}_{11}{\alpha_m}^4 + (2\overline{D}_{12}+4\overline{D}_{66}){\alpha_m}^2{\beta_p}^2 + \overline{D}_{22}{\beta_p}^4\Big)\right]{W_{mp}}^2\sin^2(\Omega_{mp}t)\right)$$

$$K\sin^2(\Omega t) = \frac{\mathrm{d}^2U}{\mathrm{d}{W_{mp}}^2} = \frac{\mathrm{d}}{\mathrm{d}W_{mp}}\left[\frac{ab}{4}\Big(\overline{D}_{11}{\alpha_m}^4 + (2\overline{D}_{12}+4\overline{D}_{66}){\alpha_m}^2{\beta_p}^2 + \overline{D}_{22}{\beta_p}^4\Big)\right]W_{mp}\sin^2(\Omega_{mp}t)$$

$$K\sin^2(\Omega t) = \frac{\mathrm{d}^2U}{\mathrm{d}{W_{mp}}^2} = \frac{ab}{4}\Big(\overline{D}_{11}{\alpha_m}^4 + (2\overline{D}_{12}+4\overline{D}_{66}){\alpha_m}^2{\beta_p}^2 + \overline{D}_{22}{\beta_p}^4\Big)\sin^2(\Omega_{mp}t)$$

In both cases, the stiffness matrix K is:

$$K = \frac{ab}{4}\Big(\overline{D}_{11}{\alpha_m}^4 + (2\overline{D}_{12}+4\overline{D}_{66}){\alpha_m}^2{\beta_p}^2 + \overline{D}_{22}{\beta_p}^4\Big) \tag{50}$$

4.3 External Work - Vibration Case

The next matter of interest is the total external energy due to vibration, V_f. The total external energy of the system is comprised of the out of plane inertial energy, V_w, the in-plane inertial energy in the x direction, V_u and the in-plane inertial energy in the y direction, V_v:

$$V_f = V_w + V_u + V_v$$

This equation may be broken into parts and each considered separately. The work done by the inertial force moving through a displacement in the z direction is given by:

$$V_w = -\frac{1}{2}F_z\delta_z \tag{51}$$

Where F_z and δ_z are the inertial force and displacement in the z direction respectively. Equation 51 can be rewritten with familiar terms in addition to the differential mass $\mathrm{d}m$ and the acceleration in the z direction, a_z, as follows:

$$V_w = -\frac{1}{2} F_z \delta_z$$
$$V_w = -\frac{1}{2} \int_0^m a_z \delta_z \ \mathrm{d}m$$

Since Z_n is the non-dimensional z-coordinate introduced in Section 4.1 , Figure 4, $\rho(Z_n)$ is the density of the laminate which is a function of non-dimensional Z_n and may be represented by a polynomial curve fit in terms of Z_n directly, $\mathrm{d}m$ can be written as $\rho(Z_n)\ h_n\ \mathrm{d}x\mathrm{d}y\mathrm{d}Z_n$ and hence:

$$V_w = \frac{1}{2} \int_0^a \int_0^b \int_1^{-1} -\rho(Z_n) h_n a_z \delta_z \ \mathrm{d}x\mathrm{d}y\mathrm{d}Z_n$$
$$V_w = \frac{1}{2} \int_0^a \int_0^b \int_1^{-1} -\rho(Z_n) h_n w_{tt} w \ \mathrm{d}x\mathrm{d}y\mathrm{d}Z_n \tag{52}$$

The resulting Equation 52 forms the basis for establishing the out of plane inertial energy. To evaluate Equation 52, the first and second partial derivative with respect to t must be established as required, from the trial function, Equation 35:

$$w_t = \frac{\mathrm{d}w}{\mathrm{d}t} = \sum_{m=1}^{M} \sum_{p=1}^{P} W_{mp} \Omega_{mp} \sin(\alpha_m x) \sin(\beta_p y) \cos(\Omega_{mp} t)$$
$$w_{tt} = \frac{\mathrm{d}^2 w}{\mathrm{d}t^2} = \sum_{m=1}^{M} \sum_{p=1}^{P} -W_{mp} \Omega_{mp}^2 \sin(\alpha_m x) \sin(\beta_p y) \sin(\Omega_{mp} t) = a_z \tag{53}$$

Substituting the trial function, Equation 35 and 53 into Equation 52:

$$V_w = \frac{1}{2} \int_0^a \int_0^b \int_1^{-1} -\rho(Z_n) h_n \Big(\sum_{m=1}^{M} \sum_{p=1}^{P} -W_{mp} \Omega_{mp}^2 \sin(\alpha_m x) \sin(\beta_p y) \sin(\Omega_{mp} t) \Big)$$
$$\Big(\sum_{m=1}^{M} \sum_{p=1}^{P} W_{mp} \sin(\alpha_m x) \sin(\beta_p y) \sin(\Omega_{mp} t) \Big) \ \mathrm{d}x\mathrm{d}y\mathrm{d}Z_n$$
$$V_w = \frac{h_n \Omega_{mp}^2}{2} \sum_{m=1}^{M} \sum_{p=1}^{P} \sum_{s=1}^{M} \sum_{t=1}^{P} W_{mp} W_{st} \sin^2(\Omega_{mp} t) \int_0^a \int_0^b \int_1^{-1} \rho(Z_n) \sin(\alpha_m x) \sin(\beta_p y) \sin(\alpha_s x) \sin(\beta_t y) \ \mathrm{d}x ...$$
$$V_w = \frac{h_n \Omega_{mp}^2}{2} \sum_{m=1}^{M} \sum_{p=1}^{P} \sum_{s=1}^{M} \sum_{t=1}^{P} W_{mp} W_{st} \sin^2(\Omega_{mp} t) \int_0^a \int_0^b \int_1^{-1} \rho(Z_n) \frac{1}{2} \Big(\cos((\alpha_m - \alpha_s)x) - \cos((\alpha_m + \alpha_s)x) \Big)$$
$$\frac{1}{2} \Big(\cos((\beta_p - \beta_t)y) - \cos((\beta_p + \beta_t)y) \Big) \ \mathrm{d}x\mathrm{d}y\mathrm{d}Z_n$$

$$V_w = \frac{h_n \Omega_{mp}^2}{2} \sum_{m=1}^{M} \sum_{p=1}^{P} \sum_{s=1}^{M} \sum_{t=1}^{P} W_{mp} W_{st} \sin^2(\Omega_{mp} t) \int_1^{-1} \rho(Z_n) \frac{1}{4} \left[\frac{\sin((\alpha_m - \alpha_s)x)}{(\alpha_m - \alpha_s)} - \frac{\sin((\alpha_m + \alpha_s)x)}{(\alpha_m + \alpha_s)} \right] \Bigg|_0^a$$
$$\left[\frac{\sin((\beta_p - \beta_t)y)}{(\beta_p - \beta_t)} - \frac{\sin((\beta_p + \beta_t)y)}{(\beta_p + \beta_t)} \right] \Bigg|_0^b \mathrm{d}Z_n \qquad \text{Note : Terms in brackets only have values if m = s and p = t}$$

Now, let:

$$\Gamma_w = \int_1^{-1} \rho(Z_n) \, \mathrm{d}Z_n$$

The resulting equation is as follows:

$$V_w = \frac{h_n \Omega_{mp}^2}{2} \sum_{m=1}^{M} \sum_{p=1}^{P} \sum_{s=1}^{M} \sum_{t=1}^{P} W_{mp} W_{st} \sin^2(\Omega_{mp} t) \Gamma_w \frac{ab}{4} \qquad [\mathrm{m = s}][\mathrm{p = t}]$$

The resultant equation is then simplified to provide the governing equation for the out of plane inertial energy of the plate:

$$V_w = \frac{h_n \Omega_{mp}^2 \Gamma_w}{2} \frac{ab}{4} \sum_{m=1}^{M} \sum_{p=1}^{P} {W_{mp}}^2 \sin^2(\Omega_{mp} t) \tag{54}$$

Applying the same methodology developed before, the work done by the inertial force moving through a displacement in the x direction is thus:

$$V_u = \frac{1}{2} \int_0^a \int_0^b \int_1^{-1} -\rho(Z_n) h_n u_{tt} u \, \mathrm{d}x \mathrm{d}y \mathrm{d}Z_n$$

Figure 5 illustrates the displacements in an unsymmetrical plate with the indicative mid-plane and neutral axis.

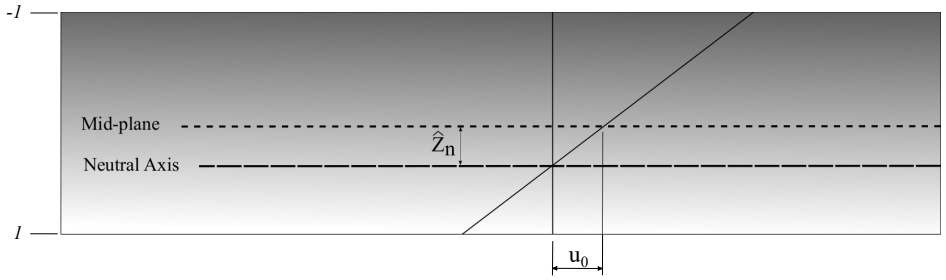


Figure 5: Cross section of laminate under consideration

Substituting in the relations for the curvature of the midplane:

$$V_u = \frac{1}{2} \int_0^a \int_0^b \int_1^{-1} -\rho(Z_n) h_n \left[\frac{\mathrm{d}^2}{\mathrm{d}t^2} \left(u_0 + Z_n \frac{h_n}{2} \frac{\mathrm{d}w}{\mathrm{d}x} \right) \right] \left(u_0 + Z_n \frac{h_n}{2} \frac{\mathrm{d}w}{\mathrm{d}x} \right) \mathrm{d}x \mathrm{d}y \mathrm{d}Z_n$$

u_0 is assumed to be fixed at the neutral axis and so:

$$u_0 = 0 - \widehat{z}_n \frac{\mathrm{d}w}{\mathrm{d}x}$$
$$u_0 = 0 - \widehat{Z}_n \frac{h_n}{2} \frac{\mathrm{d}w}{\mathrm{d}x}$$

where $\widehat{Z_n}$ is equal to b_{11}/d_{11}. Substituting in for u_0:

$$V_u = \frac{1}{2} \int_0^a \int_0^b \int_1^{-1} -\rho(Z_n) h_n \left[\frac{\mathrm{d}^2}{\mathrm{d}t^2} \Big(- \widehat{Z}_n \frac{h_n}{2} \frac{\mathrm{d}w}{\mathrm{d}x} + Z_n \frac{h_n}{2} \frac{\mathrm{d}w}{\mathrm{d}x} \Big) \right] \Big(- \widehat{Z}_n \frac{h_n}{2} \frac{\mathrm{d}w}{\mathrm{d}x} + Z_n \frac{h_n}{2} \frac{\mathrm{d}w}{\mathrm{d}x} \Big) \, \mathrm{d}x \mathrm{d}y \mathrm{d}Z_n$$
$$V_u = \frac{1}{2} \int_0^a \int_0^b \int_1^{-1} -\rho(Z_n) h_n \Big(\Omega_{mp}^2 \widehat{Z}_n \frac{h_n}{2} \frac{\mathrm{d}w}{\mathrm{d}x} - \Omega_{mp}^2 Z_n \frac{h_n}{2} \frac{\mathrm{d}w}{\mathrm{d}x} \Big) \Big(- \widehat{Z}_n \frac{h_n}{2} \frac{\mathrm{d}w}{\mathrm{d}x} + Z_n \frac{h_n}{2} \frac{\mathrm{d}w}{\mathrm{d}x} \Big) \, \mathrm{d}x \mathrm{d}y \mathrm{d}Z_n$$
$$V_u = \frac{1}{2} \int_0^a \int_0^b \int_1^{-1} \rho(Z_n) h_n \Omega_{mp}^2 \Big(\frac{h_n}{2} Z_n - \widehat{Z}_n \frac{h_n}{2} \Big)^2 \Big(\frac{\mathrm{d}w}{\mathrm{d}x} \Big)^2 \, \mathrm{d}x \mathrm{d}y \mathrm{d}Z_n$$
$$V_u = \frac{h_n \Omega_{mp}^2}{2} \int_0^a \int_0^b \int_1^{-1} \rho(Z_n) \Big(\frac{{h_n}^2}{4} Z_n^2 - \widehat{Z}_n \frac{2h^2}{4} Z_n + \frac{{h_n}^2}{4} \widehat{Z}_n^2 \Big) \Big(\frac{\mathrm{d}w}{\mathrm{d}x} \Big)^2 \, \mathrm{d}x \mathrm{d}y \mathrm{d}Z_n$$
$$V_u = \frac{{h_n}^3 \Omega_{mp}^2}{4} \int_0^a \int_0^b \int_1^{-1} \rho(Z_n) \Big(\frac{1}{2} Z_n^2 - \widehat{Z}_n Z_n + \frac{1}{2} \widehat{Z}_n^2 \Big) \Big(\sum_{m=1}^{M} \sum_{p=1}^{P} W_{mp} \alpha_m \cos(\alpha_m x) \sin(\beta_p y) \sin(\Omega_{mp} t) \Big)$$
$$\Big(\sum_{m=1}^{M} \sum_{p=1}^{P} W_{mp} \alpha_m \cos(\alpha_m x) \sin(\beta_p y) \sin(\Omega_{mp} t) \Big) \, \mathrm{d}x \mathrm{d}y \mathrm{d}Z_n$$
$$V_u = \frac{{h_n}^3 \Omega_{mp}^2}{4} \sum_{m=1}^{M} \sum_{p=1}^{P} \sum_{s=1}^{S} \sum_{t=1}^{T} \alpha_m \alpha_s W_{mp} W_{st} \sin^2(\Omega_{mp} t) \int_0^a \int_0^b \int_1^{-1} \rho(Z_n) \Big(\frac{1}{2} Z_n^2 - \widehat{Z}_n Z_n + \frac{1}{2} \widehat{Z}_n^2 \Big)$$
$$\Big(\cos(\alpha_m x) \sin(\beta_p y) \cos(\alpha_s x) \sin(\beta_t y) \Big) \, \mathrm{d}x \mathrm{d}y \mathrm{d}Z_n$$
$$V_u = \frac{{h_n}^3 \Omega_{mp}^2}{4} \sum_{m=1}^{M} \sum_{p=1}^{P} \sum_{s=1}^{S} \sum_{t=1}^{T} \alpha_m \alpha_s W_{mp} W_{st} \sin^2(\Omega_{mp} t) \int_0^a \int_0^b \int_1^{-1} \rho(Z_n) \Big(\frac{1}{2} Z_n^2 - \widehat{Z}_n Z_n + \frac{1}{2} \widehat{Z}_n^2 \Big)$$
$$\frac{1}{2} \Big(\cos((\alpha_m - \alpha_s)x) - \cos((\alpha_m + \alpha_s)x) \Big) \frac{1}{2} \Big(\cos((\beta_p - \beta_t)y) + \cos((\beta_p + \beta_t)y) \Big) \, \mathrm{d}x \mathrm{d}y \mathrm{d}Z_n$$

Now, let:

$$\Gamma_u = \int_1^{-1} \rho(Z_n) \Big(\frac{1}{2} Z_n^2 - \widehat{Z}_n Z_n + \frac{1}{2} \widehat{Z}_n^2 \Big) \, \mathrm{d}Z_n$$

The resulting equation is as follows:

$$V_u = \frac{{h_n}^3 \Omega_{mp}^2}{4} \sum_{m=1}^{M} \sum_{p=1}^{P} \sum_{s=1}^{M} \sum_{t=1}^{P} \alpha_m \alpha_s W_{mp} W_{st} \sin^2(\Omega_{mp} t) \int_0^a \int_0^b \Gamma_u \frac{1}{2} \Big(\cos((\alpha_m - \alpha_s)x) - \cos((\alpha_m + \alpha_s)x) \Big)$$
$$\frac{1}{2} \Big(\cos((\beta_p - \beta_t)y) + \cos((\beta_p + \beta_t)y) \Big) \, \mathrm{d}x \mathrm{d}y$$

$$V_u = \frac{{h_n}^3 \Omega_{mp}^2}{4} \sum_{m=1}^{M} \sum_{p=1}^{P} \sum_{s=1}^{M} \sum_{t=1}^{P} \alpha_m \alpha_s W_{mp} W_{st} \sin^2(\Omega_{mp} t) \Gamma_u \; \frac{1}{2} \left[\frac{\sin((\alpha_m - \alpha_s)x)}{(\alpha_m - \alpha_s)} - \frac{\sin((\alpha_m + \alpha_s)x)}{(\alpha_m + \alpha_s)} \right] \Bigg|_0^a$$

$$\frac{1}{2} \left[\frac{\sin((\beta_p - \beta_t)y)}{(\beta_p - \beta_t)} + \frac{\sin((\beta_p + \beta_t)y)}{(\beta_p + \beta_t)} \right] \Bigg|_0^b \qquad \text{Note : Terms in brackets only have values if m = s and p = t}$$

$$V_u = \frac{{h_n}^3 \Omega_{mp}^2}{4} \sum_{m=1}^{M} \sum_{p=1}^{P} \sum_{s=1}^{M} \sum_{t=1}^{P} \alpha_m \alpha_s W_{mp} W_{st} \sin^2(\Omega_{mp} t) \Gamma_u \frac{ab}{4}$$

The resultant equation is then simplified to provide the governing equation for the in plane inertial energy in the x direction of the plate:

$$V_u = \frac{{h_n}^3 \Omega_{mp}^2 \Gamma_u}{4} \frac{ab}{4} \sum_{m=1}^{M} \sum_{p=1}^{P} {W_{mp}}^2 {\alpha_m}^2 \sin^2(\Omega_{mp} t) \qquad \text{[m = s][p = t]}$$

Similarly, the work done by the inertial force moving through a displacement in the y direction is thus:

$$V_v = \frac{1}{2} \int_0^a \int_0^b \int_1^{-1} -\rho(Z_n) h_n v_{tt} v \; \mathrm{d}x \mathrm{d}y \mathrm{d}Z_n$$

The resultant equation is then simplified to provide the governing equation for the in plane inertial energy in the y direction of the plate:

$$V_v = \frac{{h_n}^3 \Omega_{mp}^2 \Gamma_v}{4} \frac{ab}{4} \sum_{m=1}^{M} \sum_{p=1}^{P} {W_{mp}}^2 {\beta_p}^2 \sin^2(\Omega_{mp} t) \qquad \text{[m = s][p = t]}$$

The resulting total external energy as before is as follows:

$$V_f = V_w + V_u + V_v$$

$$V_f = \Omega_{mp}^2 \frac{abh}{8} \left[\Gamma_w \sum_{m=1}^{M} \sum_{p=1}^{P} {W_{mp}}^2 + \frac{{h_n}^2 \Gamma_u}{2} \sum_{m=1}^{M} \sum_{p=1}^{P} {W_{mp}}^2 {\alpha_m}^2 + \frac{{h_n}^2 \Gamma_v}{2} \sum_{m=1}^{M} \sum_{p=1}^{P} {W_{mp}}^2 {\beta_p}^2 \right] \sin^2(\Omega_{mp} t)$$

Applying the same methodology as before for the internal strain energy, the inertial energy may be expressed as follows:

$$\frac{\mathrm{d}V}{\mathrm{d}W_{mp}} = \frac{\mathrm{d}}{\mathrm{d}W_{mp}} \left(\tfrac{1}{2} \Omega_{mp}^2 W^T M W \sin^2(\Omega_{mp} t) \right) = \Omega_{mp}^2 M W \sin^2(\Omega_{mp} t) \tag{55}$$

Therefore, in order to find the mass matrix M:

$$\Omega_{mp}^2 M \sin^2(\Omega_{mp} t) = \frac{\mathrm{d}}{\mathrm{d}W_{mp}} \left(\Omega_{mp}^2 M W \sin^2(\Omega_{mp} t) \right)$$

Substituting for $\Omega_{mp}^2 MW\sin^2(\Omega_{mp}t)$ from Equation 55 results in:

$$\Omega_{mp}^2 M\sin^2(\Omega_{mp}t)=\frac{\mathrm{d}}{\mathrm{d}W_{mp}}\left(\Omega_{mp}^2 MW\sin^2(\Omega_{mp}t)\right)=\frac{\mathrm{d}}{\mathrm{d}W_{mp}}\left(\frac{\mathrm{d}V}{\mathrm{d}W_{mp}}\right)=\frac{\mathrm{d}^2V}{\mathrm{d}{W_{mp}}^2}$$

Therefore, the mass matrix M is given by:

$$\Omega_{mp}^2 M\sin^2(\Omega_{mp}t)=\frac{\mathrm{d}^2V_f}{\mathrm{d}{W_{mp}}^2}=\frac{\mathrm{d}^2}{\mathrm{d}{W_{mp}}^2}\left[\Omega_{mp}^2\frac{abh}{8}\left(\Gamma_w\sum_{m=1}^{M}\sum_{p=1}^{P}{W_{mp}}^2+\frac{{h_n}^2\Gamma_u}{2}\sum_{m=1}^{M}\sum_{p=1}^{P}{W_{mp}}^2{\alpha_m}^2+\frac{{h_n}^2\Gamma_v}{2}\sum_{m=1}^{M}\sum_{p=1}^{P}{W_{mp}}^2{\beta_p}^2\right)\right]\sin^2(\Omega_{mp}t)$$

$$\Omega_{mp}^2 M\sin^2(\Omega_{mp}t)=\frac{\mathrm{d}^2V_f}{\mathrm{d}{W_{mp}}^2}=\frac{\mathrm{d}}{\mathrm{d}W_{mp}}\left[\Omega_{mp}^2\frac{abh}{4}\left(\Gamma_w W_{mp}+\frac{{h_n}^2\Gamma_u}{2}W_{mp}{\alpha_m}^2+\frac{{h_n}^2\Gamma_v}{2}W_{mp}{\beta_p}^2\right)\right]\sin^2(\Omega_{mp}t)$$

$$\Omega_{mp}^2 M\sin^2(\Omega_{mp}t)=\frac{\mathrm{d}^2V_f}{\mathrm{d}{W_{mp}}^2}=\Omega_{mp}^2\frac{abh}{4}\left(\Gamma_w+\frac{{h_n}^2\Gamma_u}{2}{\alpha_m}^2+\frac{{h_n}^2\Gamma_v}{2}{\beta_p}^2\right)\sin^2(\Omega_{mp}t)\qquad(56)$$

Therefore, the M matrix is as follows:

$$M=\frac{abh}{4}\left(\Gamma_w+\frac{{h_n}^2\Gamma_u}{2}{\alpha_m}^2+\frac{{h_n}^2\Gamma_v}{2}{\beta_p}^2\right)\qquad(57)$$

In terms of the Rayleigh Ritz method, for equilibrium we have the static total potential energy:

$$\frac{\mathrm{d}U}{\mathrm{d}W_{mp}}=\frac{\mathrm{d}V_f}{\mathrm{d}W_{mp}}$$

Which equates to the following:

$$K\cdot\cancel{W\sin^2(\Omega_{mp}t)}=\Omega_{mp}^2 M\cdot\cancel{W\sin^2(\Omega_{mp}t)}\qquad(58)$$

Equation 58 is an eigenvalue problem and therefore, the natural frequency can be found directly as:

$$\frac{\cancel{ab}}{\cancel{4}}\left(\overline{D}_{11}{\alpha_m}^4+(2\overline{D}_{12}+4\overline{D}_{66}){\alpha_m}^2{\beta_p}^2+\overline{D}_{22}{\beta_p}^4\right)=\Omega_{mp}^2 h_n\frac{\cancel{ab}}{\cancel{4}}\left(\Gamma_w+\frac{{h_n}^2\Gamma_u{\alpha_m}^2}{2}+\frac{{h_n}^2\Gamma_v{\beta_p}^2}{2}\right)$$

Solving for natural frequency Ω:

$$\Omega_{mp}^2=\frac{\left(\overline{D}_{11}{\alpha_m}^4+(2\overline{D}_{12}+4\overline{D}_{66}){\alpha_m}^2{\beta_p}^2+\overline{D}_{22}{\beta_p}^4\right)}{h_n\left(\Gamma_w+\frac{{h_n}^2\Gamma_u{\alpha_m}^2}{2}+\frac{{h_n}^2\Gamma_v{\beta_p}^2}{2}\right)}$$

The natural frequency Ω is given by:

$$\Omega_{mp} = \sqrt{\frac{\left(\overline{D}_{11}{\alpha_m}^4 + (2\overline{D}_{12} + 4\overline{D}_{66}){\alpha_m}^2{\beta_p}^2 + \overline{D}_{22}{\beta_p}^4\right)}{h_n\left(\Gamma_w + \frac{{h_n}^2\Gamma_u{\alpha_m}^2}{2} + \frac{{h_n}^2\Gamma_v{\beta_p}^2}{2}\right)}} \tag{59}$$

4.4 External Work - Buckling Case

The next matter of interest is the total external energy due to the buckling load, V_b. The total external work of the system is comprised of the in-plane work in the x direction, V_x, and the in-plane work in the y direction, V_y:

$$V_b = V_x + V_y$$

This equation may be broken into two parts and each considered separately, one for the in-plane work in the x direction and one for the in-plane work in the y direction. The in-plane work in the x direction is given as the critical buckling load multiplied by the shortening of the plate due to curvature:

$$V_x = \frac{1}{2}\int_0^a \int_0^b N_{crx}{w_x}^2 \, \mathrm{d}x\mathrm{d}y \tag{60}$$

To evaluate Equation 60, the partial derivative of the out of plane displacement, w, with respect to x must be established as required from the trial function, Equation 35:

$$w_x = \frac{\mathrm{d}w}{\mathrm{d}x} = \sum_{m=1}^{M}\sum_{p=1}^{P} W_{mp}\alpha_m \cos(\alpha_m x)\sin(\beta_p y) \tag{61}$$

Substituting Equation 61 into Equation 60 results in the following:

$$V_x = \frac{1}{2}\int_0^a \int_0^b N_{crx}\left(\sum_{m=1}^{M}\sum_{p=1}^{P} W_{mp}\alpha_m \cos(\alpha_m x)\sin(\beta_p y))\right)^2 \mathrm{d}x\mathrm{d}y$$

Simplifying the above equation before integration:

$$V_x = \frac{N_{crx}}{2}\sum_{m=1}^{M}\sum_{p=1}^{P}\sum_{s=1}^{M}\sum_{t=1}^{P} W_{mp}W_{st}\alpha_m\alpha_s \int_0^a \int_0^b \cos(\alpha_m x)\sin(\beta_p y)\cos(\alpha_s x)\sin(\beta_t y) \, \mathrm{d}x\mathrm{d}y$$

$$V_x = \frac{N_{crx}}{2}\sum_{m=1}^{M}\sum_{p=1}^{P}\sum_{s=1}^{M}\sum_{t=1}^{P} W_{mp}W_{st}\alpha_m\alpha_s \int_0^a \int_0^b \frac{1}{2}\Big(\cos((\alpha_m - \alpha_s)x) + \cos((\alpha_m + \alpha_s)x)\Big)$$
$$\frac{1}{2}\Big(\cos((\beta_p - \beta_t)y) - \cos((\beta_p + \beta_t)y)\Big) \, \mathrm{d}x\mathrm{d}y$$

Integrating the resulting simplified equation results in the following:

$$V_x = \frac{N_{crx}}{2}\sum_{m=1}^{M}\sum_{p=1}^{P}\sum_{s=1}^{M}\sum_{t=1}^{P} W_{mp}W_{st}\alpha_m\alpha_s \frac{1}{2}\left[\frac{\sin((\alpha_m-\alpha_s)x)}{(\alpha_m-\alpha_s)} + \frac{\sin((\alpha_m+\alpha_s)x)}{(\alpha_m+\alpha_s)}\right]\Bigg|_0^a$$
$$\frac{1}{2}\left[\frac{\sin((\beta_p-\beta_t)y)}{(\beta_p-\beta_t)} - \frac{\sin((\beta_p+\beta_t)y)}{(\beta_p+\beta_t)}\right]\Bigg|_0^b \quad \text{Note : Terms in brackets only have values if } m = s \text{ and } p = t$$

$$V_x = \frac{N_{crx}}{2}\sum_{m=1}^{M}\sum_{p=1}^{P}\sum_{s=1}^{M}\sum_{t=1}^{P} W_{mp}W_{st}\alpha_m\alpha_s \frac{ab}{4} \qquad [m = s][p = t]$$

The resultant equation is then simplified to provide the governing equation for the potential energy of the plate in the x direction:

$$V_x = \frac{N_{crx}}{2}\frac{ab}{4}\sum_{m=1}^{M}\sum_{p=1}^{P} W_{mp}{}^2\alpha_m{}^2 \tag{62}$$

Similarly, the in-plane potential energy in the y direction is given as follows:

$$V_y = \frac{1}{2}\int_0^a\int_0^b N_{cry}w_y{}^2 \,\mathrm{d}x\mathrm{d}y$$

The resultant equation is then simplified to provide the governing equation for the potential energy of the plate in the y direction:

$$V_y = \frac{N_{cry}}{2}\frac{ab}{4}\sum_{m=1}^{M}\sum_{p=1}^{P} W_{mp}{}^2\beta_p{}^2 \tag{63}$$

At this point it will be useful to introduce a new variable which determines the magnitude and direction of the load in the y direction relative to the load in the x direction.

$$\psi = \frac{N_{cry}}{N_{crx}}$$
$$N_{cry} = \psi N_{crx} \tag{64}$$

Therefore Equation 63 may be re-written as follows:

$$V_y = \psi\frac{N_{crx}}{2}\frac{ab}{4}\sum_{m=1}^{M}\sum_{p=1}^{P} W_{mp}{}^2\beta_p{}^2 \tag{65}$$

The resulting total external energy as before is as follows:

$$V_b = V_x + V_y$$
$$V_b = \left[\frac{N_{crx}ab}{8}\right]\sum_{m=1}^{M}\sum_{p=1}^{P} W_{mp}{}^2\left(\alpha_m{}^2 + \psi\beta_p{}^2\right)$$

Applying the same methodology as before for the vibration case, the inertial energy may be expressed as follows:

$$\frac{\mathrm{d}V}{\mathrm{d}W_{mp}} = \frac{\mathrm{d}}{\mathrm{d}W_{mp}}\left(\tfrac{1}{2}N_{crx}W^{T}SW\right) = N_{crx}SW \tag{66}$$

Therefore, in order to find matrix S:

$$N_{crx}S = \frac{\mathrm{d}}{\mathrm{d}W_{mp}}\left(N_{crx}SW\right)$$

Substituting for $N_{crx}SW$ from Equation 66 results in:

$$N_{crx}S = \frac{\mathrm{d}}{\mathrm{d}W_{mp}}\left(N_{crx}SW\right) = \frac{\mathrm{d}}{\mathrm{d}W_{mp}}\left(\frac{\mathrm{d}V}{\mathrm{d}W_{mp}}\right) = \frac{\mathrm{d}^2V}{\mathrm{d}{W_{mp}}^2}$$

Therefore, the matrix S is given by:

$$N_{crx}S = \frac{\mathrm{d}^2V}{\mathrm{d}{W_{mp}}^2} = \frac{\mathrm{d}^2}{\mathrm{d}{W_{mp}}^2}\left[N_{crx}\frac{ab}{8}\right]\sum_{m=1}^{M}\sum_{p=1}^{P}{W_{mp}}^2\left({\alpha_m}^2 + \psi{\beta_p}^2\right)$$

$$N_{crx}S = \frac{\mathrm{d}^2V}{\mathrm{d}{W_{mp}}^2} = \frac{\mathrm{d}}{\mathrm{d}W_{mp}}\left[N_{crx}\frac{ab}{4}\right]W_{mp}\left({\alpha_m}^2 + \psi{\beta_p}^2\right)$$

$$N_{crx}S = \frac{\mathrm{d}^2V}{\mathrm{d}{W_{mp}}^2} = N_{crx}\frac{ab}{4}\left({\alpha_m}^2 + \psi{\beta_p}^2\right) \tag{67}$$

Therefore, the S matrix is as follows:

$$S = \frac{ab}{4}\left({\alpha_m}^2 + \psi{\beta_p}^2\right) \tag{68}$$

In terms of the Rayleigh Ritz method and in the same manner as for the vibration case, for equilibrium we have the static total potential energy:

$$\frac{\mathrm{d}U}{\mathrm{d}W_{mp}} = \frac{\mathrm{d}V_b}{\mathrm{d}W_{mp}}$$

Which equates to the following:

$$K\cancel{W} = N_{crx}S\cancel{W} \tag{69}$$

In the same manner as the case of the natural frequency, Equation 69 is an eigenvalue problem and so the buckling loads can be found directly as:

$$\frac{a\cancel{b}}{\cancel{4}}\left(\overline{D}_{11}{\alpha_m}^4 + (2\overline{D}_{12} + 4\overline{D}_{66}){\alpha_m}^2{\beta_p}^2 + \overline{D}_{22}{\beta_p}^4\right) = N_{crx}\frac{a\cancel{b}}{\cancel{4}}\left({\alpha_m}^2 + \psi{\beta_p}^2\right)$$

The critical buckling load N_{crx} is given by:

$$N_{crx} = \frac{\left(\overline{D}_{11}{\alpha_m}^4 + (2\overline{D}_{12} + 4\overline{D}_{66}){\alpha_m}^2{\beta_p}^2 + \overline{D}_{22}{\beta_p}^4\right)}{\left({\alpha_m}^2 + \psi{\beta_p}^2\right)} \tag{70}$$

Equations 59 and 70 are the governing equations for establishing the natural frequencies and critical buckling loads for functionally graded plates given the input parameters. These two equations are used to establish the natural frequencies and critical buckling loads for functionally graded plates for a range of aspect ratios, a/h, and volume indices, λ, the results of which are detailed in section 5.

Appendix F provides the software code used to establish the natural frequency and buckling load as described above.

4.5 Natural Frequency of Plate Subjected to Compressive Loads

The variation of natural frequency with compressive load may be of interest and may be established using the present theory. To establish the governing equation for this relationship, the Rayleigh-Ritz method is employed. As before, at equilibrium we have:

$$\begin{aligned}\frac{\mathrm{d}U}{\mathrm{d}W_{mp}} &= \frac{\mathrm{d}V}{\mathrm{d}W_{mp}} \\ \frac{\mathrm{d}U}{\mathrm{d}W_{mp}} &= \frac{\mathrm{d}V_f}{\mathrm{d}W_{mp}} + \frac{\mathrm{d}V_b}{\mathrm{d}W_{mp}}\end{aligned} \tag{71}$$

where U is the internal strain energy and V is the sum of the external energy due to vibration as well as an in-plane loads as before. The partial derivative of the strain energy with respect to W_{mp} is given by:

$$\begin{aligned}U &= \frac{1}{2}\left[\sum_{m=1}^{M}\sum_{p=1}^{P}\frac{ab}{4}\left(\overline{D}_{11}{\alpha_m}^4 + (2\overline{D}_{12} + 4\overline{D}_{66}){\alpha_m}^2{\beta_p}^2 + \overline{D}_{22}{\beta_p}^4\right)\right]{W_{mp}}^2\sin^2(\Omega t) \\ \frac{\mathrm{d}U}{\mathrm{d}W_{mp}} &= \left[\frac{ab}{4}\left(\overline{D}_{11}{\alpha_m}^4 + (2\overline{D}_{12} + 4\overline{D}_{66}){\alpha_m}^2{\beta_p}^2 + \overline{D}_{22}{\beta_p}^4\right)\right]W_{mp}\sin^2(\Omega t)\end{aligned} \tag{72}$$

The partial derivative of the external work due to vibration with respect to W_{mp} is given by:

$$\begin{aligned}V_f &= \Omega_{mp}^2\frac{abh}{8}\left[\Gamma_w\sum_{m=1}^{M}\sum_{p=1}^{P}{W_{mp}}^2 + \frac{{h_n}^2\Gamma_u}{2}\sum_{m=1}^{M}\sum_{p=1}^{P}{W_{mp}}^2{\alpha_m}^2 + \frac{{h_n}^2\Gamma_v}{2}\sum_{m=1}^{M}\sum_{p=1}^{P}{W_{mp}}^2{\beta_p}^2\right]\sin^2(\Omega t) \\ \frac{\mathrm{d}V_f}{\mathrm{d}W_{mp}} &= \Omega_{mp}^2\frac{abh}{4}\left[\Gamma_w + \frac{{h_n}^2\Gamma_u}{2}{\alpha_m}^2 + \frac{{h_n}^2\Gamma_v}{2}{\beta_p}^2\right]W_{mp}\sin^2(\Omega t)\end{aligned} \tag{73}$$

In this instance, the application of the in-plane compressive load will vary with time and therefore, $\sin^2(\Omega t)$ forms part of the equation. The partial derivative of the external work due to in-plane loads with respect to W_{mp} is given by:

$$V_b = \left[\frac{N_{crx}ab}{8}\right] \sum_{m=1}^{M} \sum_{p=1}^{P} {W_{mp}}^2 \left({\alpha_m}^2 + \psi {\beta_p}^2\right) \sin^2(\Omega t)$$

$$\frac{\mathrm{d}V_b}{\mathrm{d}W_{mp}} = \left[\frac{N_{crx}ab}{4}\right] W_{mp} \left({\alpha_m}^2 + \psi {\beta_p}^2\right) \sin^2(\Omega t) \tag{74}$$

Substituting Equations 72, 73 and 74 into Equation 71 and removing the common terms results in the following:

$$\left(\overline{D}_{11}{\alpha_m}^4 + (2\overline{D}_{12} + 4\overline{D}_{66}){\alpha_m}^2{\beta_p}^2 + \overline{D}_{22}{\beta_p}^4\right) = h_n\Omega^2(\Gamma_w + \Gamma_u{\alpha_m}^2 + \Gamma_v{\beta_p}^2) + N_{crx}({\alpha_m}^2 + \psi{\beta_p}^2)$$

The governing equation for the variation of natural frequency with compressive load is given by:

$$\Omega = \sqrt{\frac{\left(\overline{D}_{11}{\alpha_m}^4 + (2\overline{D}_{12} + 4\overline{D}_{66}){\alpha_m}^2{\beta_p}^2 + \overline{D}_{22}{\beta_p}^4\right) - N_{crx}({\alpha_m}^2 + \psi{\beta_p}^2)}{h_n(\Gamma_w + \Gamma_u{\alpha_m}^2 + \Gamma_v{\beta_p}^2)}} \tag{75}$$

It is clear that when N_{crx} is zero, the natural frequency collapses to Equation 59. The critical buckling load is found by setting the natural frequency equal to zero:

$$\Omega = \sqrt{\frac{\left(\overline{D}_{11}{\alpha_m}^4 + (2\overline{D}_{12} + 4\overline{D}_{66}){\alpha_m}^2{\beta_p}^2 + \overline{D}_{22}{\beta_p}^4\right) - N_{crx}({\alpha_m}^2 + \psi{\beta_p}^2)}{h_n(\Gamma_w + \Gamma_u{\alpha_m}^2 + \Gamma_v{\beta_p}^2)}} = 0$$

The critical buckling load is found as follows, as before, in accordance with Equation 70:

$$N_{crx} = \frac{\left(\overline{D}_{11}{\alpha_m}^4 + (2\overline{D}_{12} + 4\overline{D}_{66}){\alpha_m}^2{\beta_p}^2 + \overline{D}_{22}{\beta_p}^4\right)}{({\alpha_m}^2 + \psi{\beta_p}^2)}$$

Appendix G provides the software code used to graphically present the variation in natural frequency with compressive load as described above.

5 Results

To demonstrate the accuracy and practicality of the present theory for predicting the natural frequency and buckling loads of simply supported functionally graded plates, various load cases are considered and compared to literature found and described in Section 2.1. All the results of the present theory have been established using a polynomial fit over 1000 points and an error percentage at each point of less than 0.1%.

5.1 Natural Frequency Results

Various numerical results of specific load cases for natural frequency are presented in the tables below. Tables 1, 2, 3 and 4 present the non-dimensional fundamental frequencies results for plates with a varying volume index λ and various aspect ratios a/h. To compare the results of various mode shapes, Table 5 and 6 present the non-dimensional frequency for various mode shapes with varying volume index λ and an aspect ratio $a/h = 20$ and $a/h = 10$ respectively. Finally, Table 7, 8 and 9 present the non-dimensional fundamental frequencies results for plates excluding in-plane inertial effects in x and y directions. With the exception of Table 4, all the results of the present theory have been presented with at least one set of three-dimensional results which are used for comparison. The results were obtained using software, the code of which is presented in Appendix C to Appendix F.

Tables 1, 2 and 3 display the non-dimensional fundamental frequencies of a simply supported square plate made from Al/ZrO_2 or Al/Al_2O_3 with varying volume index λ and aspect ratios $a/h = 5$, $a/h = 10$ and $a/h = 20$ respectively. The resulting error percentage for each set of results was established by comparing the results of the present study to the 3D results obtained by Neves et al.[9] and Akavci and Tanrikulu [10] accordingly.

Table 1: Comparison of non-dimensional fundamental frequency $\overline{\omega} = \omega h\sqrt{\frac{\rho_m}{E_m}}$ of a SSSS square plate (Al/ZrO_2) with a varying volume index λ and an aspect ratio a/h = 5 using the present theory (a = b = 1).

Source	λ = 0	λ = 0.5	λ = 1	λ = 3	λ = 10
Neves et al.[9][1]	0.2469	0.2228	0.2193	0.2215	0.2229
Neves et al.[9][2]	0.2459	0.2219	0.2184	0.2206	0.2219
Vel and Batra [7][1]			0.2192	0.2211	
Qian et al.[16] [3]			0.2152	0.2172	
Neves et al.[11][1]			0.2193	0.2212	
Neves et al.[11][4]			0.2184	0.2202	
Moghaddam and Baradaran [12][1]	0.2474		0.2251	0.2188	
Akavci and Tanrikulu [10][1]			0.2193	0.2216	
Present	0.2693	0.2419	0.2386	0.2437	0.2453
Error % relative to Neves et al.[9][1]	9.07%	8.57%	8.80%	10.02%	10.04%

Note : Material properties vary according to the Mori-Tanaka Homogenization procedure.

[1] Work done by Neves et al.[9] (Quasi 3D), Vel and Batra [7], Neves et al.[11] (Quasi 3D), Moghaddam and Baradaran [12] and Akavci and Tanrikulu [10] (Quasi 3D) based on 3D theory.

[2] Work done by Neves et al.[9] based on HSDT.

[3] Work done by Qian et al.[16] based on HOSNDPT and MLPG.

[4] Work done by Neves et al.[11] based on Sinusoidal SDT.

Table 2 displays the non-dimensional fundamental frequencies of a simply supported square plate made from Al/Al_2O_3 with a varying volume index λ and an aspect ratio a/h = 10.

Table 2: Comparison of non-dimensional fundamental frequency $\overline{\omega} = \omega h\sqrt{\frac{\rho_c}{E_c}}$ of a SSSS square plate (Al/Al_2O_3) with a varying volume index λ and an aspect ratio a/h = 10 using the present theory (a = b = 1).

Source	λ = 0	λ = 0.5	λ = 1	λ = 4	λ = 10
Akavci and Tanrikulu [10][1]	0.0578	0.0494	0.0449	0.0389	0.0368
Zhu and Liew [18][2]	0.0576	0.0489	0.0441	0.0381	0.0365
Benachour et al.[19][3]	0.0576	0.0490	0.0441	0.0380	0.0363
Hosseini et al.[17][4]	0.0577	0.0490	0.0442	0.0381	0.0364
Matsunaga [13][1]	0.0577	0.0491	0.0442	0.0381	0.0364
Sheikholeslami and Saidi [15][1]	0.0577	0.0491	0.0442	0.0381	0.0364
Belabed et al.[14][1]	0.0578	0.0494	0.0449	0.0389	0.0368
Present	0.0592	0.0502	0.0452	0.0393	0.0378
Error % relative to Akavci and Tanrikulu [10][1]	2.42%	1.61%	0.66%	1.02%	2.71%

Note : Material properties vary according to the rule of mixtures.

[1] Work done by Akavci and Tanrikulu [10] (Quasi 3D), Matsunaga [13] (Quasi 3D), Sheikholeslami and Saidi [15] and Belabed et al.[14] based on 3D theory.

[2] Work done by Zhu and Liew [18] based on Kriging meshless method (FSDT).

[3] Work done by Benachour et al.[19] based on four variable SDT.

[4] Work done by Hosseini et al.[17] based on Reddy's TSDT.

Table 3 displays the non-dimensional fundamental frequencies of a simply supported square plate made from Al/Al_2O_3 with a varying volume index λ and an aspect ratio a/h = 20.

Table 3: Comparison of non-dimensional fundamental frequency $\overline{\omega} = \omega h\sqrt{\frac{\rho_c}{E_c}}$ of a SSSS square plate (Al/Al_2O_3) with a varying volume index λ and an aspect ratio a/h = 20 using the present theory (a = b = 1).

Source	λ = 0	λ = 0.5	λ = 1	λ = 4	λ = 10
Akavci and Tanrikulu [10][1]	0.0148	0.0126	0.0115	0.0100	0.0095
Benachour et al.[19][2]	0.0148	0.0125	0.0113	0.0098	0.0094
Hosseini et al.[17][3]	0.0148	0.0125	0.0113	0.0098	0.0094
Sheikholeslami and Saidi [15][1]	0.0148	0.0125	0.0113	0.0098	0.0094
Belabed et al.[14][1]	0.0148	0.0126	0.0115	0.0100	0.0095
Present	0.0149	0.0126	0.0114	0.0099	0.0095
Error % relative to Akavci and Tanrikulu [10][1]	0.67%	0.00%	-0.86%	-1.00%	0.00%

Note : Material properties vary according to the rule of mixtures.

[1] Work done by Akavci and Tanrikulu [10] (Quasi 3D), Sheikholeslami and Saidi [15] and Belabed et al.[14] based on 3D theory.

[2] Work done by Benachour et al.[19] based on four variable SDT.

[3] Work done by Hosseini et al.[17] based on Reddy's TSDT.

Table 4 displays the non-dimensional fundamental frequencies of a simply supported square plate made from Al/Al_2O_3 with a varying volume index λ and an aspect ratio a/h = 100. The resulting error percentage was established by comparing the results of the present study to the 3D results obtained by Baferani et al.[20]. The macroscopic material properties vary according to the rule of mixtures. Importantly, various other CLT results were also included for comparison with the present study.

Table 4: Comparison of non-dimensional fundamental frequencies $\overline{\omega} = \omega a^2\sqrt{\frac{12\rho_c h(1\text{-}\nu_c^2)}{E_c h^3}}$ of a SSSS square plate (Al/Al_2O_3) with a varying volume index λ and an aspect ratio a/h = 100 using the present theory (a = b = 1).

Source	λ = 0	λ = 0.5	λ = 1	λ = 2
Baferani et al.[20][1]	19.7281	16.6879	15.0357	13.6808
Kumar et. al[21][1]	19.7392	16.7142	15.0610	13.6931
Li et. al[22][1]	19.7398	16.7141	15.0609	13.6930
Present	19.7376	16.7167	15.0655	13.6993
Error % relative to Baferani et al.[20][1]	0.04%	0.17%	0.19%	0.13%

Note : Material properties vary according to the rule of mixtures.

[1] Work done by Baferani et al.[20], Kumar et al.[21] and Li et al.[22] based on CLT.

Tables 5 and 6 display the first 4 and 5 non-dimensional fundamental frequencies of a simply supported square plate made from Al/Al_2O_3 and Al/ZrO_2 with a varying volume index λ and a volume index λ = 1 respectively. Table 5 illustrates results for an aspect ratio a/h = 10 and Table 6 for an aspect ratio a/h = 20. The resulting error percentages were established by comparing the results of the present study to the 3D results obtained by Neves et al.[9] and Akavci and Tanrikulu [10]. The macroscopic material properties vary according to the Mori-Tanaka Homogenization procedure [8] and the rule of mixtures.

Table 5: Comparison of first 4 non-dimensional frequencies $\overline{\omega} = \omega a^2/h\sqrt{\frac{\rho_c}{E_c}}$ of a SSSS square plate (Al/Al_2O_3) with a varying volume index λ and an aspect ratio a/h = 10 using the present theory (a = b = 1).

Source	(m;n)	λ = 0	λ = 0.5	λ = 1	λ = 10
Akavci and Tanrikulu [10][1]	(1;1)	5.7807	4.9410	4.4907	3.6827
Benachour et al.[19][2]		5.7690	4.9000	4.4160	3.6350
Matsunaga [13][1]		5.7777	4.9170	4.4270	3.6420
Belabed et al.[14][1]		5.7800	4.9400	4.4900	3.6800
Present		5.9248	5.0186	4.5225	3.7755
Error % relative to Akavci and Tanrikulu[10][1]		2.49%	1.57%	0.70%	2.51%
Akavci and Tanrikulu [10][1]	(1;2)	13.817	11.851	10.773	8.6768
Benachour et al.[19][2]		13.760	11.731	10.576	8.5570
Matsunaga [13][1]		13.810	11.800	10.630	8.5880
Belabed et al.[14][1]		13.800	11.840	10.770	8.6800
Present		14.635	12.398	11.171	9.3220
Error % relative to Akavci and Tanrikulu[10][1]		5.92%	4.61%	3.72%	7.43%
Akavci and Tanrikulu [10][1]	(2;2)	21.237	18.268	16.609	13.002
Benachour et al.[19][2]		21.125	18.055	16.282	12.995
Matsunaga [13][1]		21.210	18.190	16.400	13.060
Belabed et al.[14][1]		21.210	18.250	16.590	13.180
Present		23.144	19.610	17.667	14.735
Error % relative to Akavci and Tanrikulu [10][1]		8.97%	7.34%	6.37%	13.32%

Material properties vary according to the rule of mixtures.

[1] Work done by Akavci and Tanrikulu [10] (Quasi 3D), Matsunaga[13] (Quasi 3D) and Belabed et al.[14] based on 3D theory.

[2] Work done by Benachour et al.[19] based on four variable SDT.

Table 6 displays the first 5 non-dimensional fundamental frequencies of a simply supported square plate made from Al/ZrO_2 with varying volume index λ and an aspect ratio a/h = 20.

Table 6: Comparison of first 5 non-dimensional frequencies $\overline{\omega} = \omega h\sqrt{\frac{\rho_m}{E_m}}$ of a SSSS square plate (Al/ZrO_2) with a volume fraction index λ = 1 and an aspect ratio a/h = 20 using the present theory (a = b = 1).

Source	1(1;1)	2(1;2)	3(2;1)	4(2;2)	5(3;1)
Neves et al.[9][1]	0.0153	0.0377	0.0377	0.0596	0.0739
Qian et al.[16][2]	0.0149	0.0377	0.0377	0.0593	0.0747
Neves et al.[11][3]	0.0153	0.0377	0.0377	0.0596	0.0739
Present	0.0154	0.0383	0.0383	0.0611	0.0762
Error % relative to Neves et al.[9][1]	0.65%	1.59%	1.59%	2.51%	3.11%

Note : Material properties vary according to the Mori-Tanaka Homogenization procedure.

[1] Work done by Neves et al.[9] (Quasi 3D) based on 3D theory.

[2] Work done by Qian et al.[16] based on HOSNDPT and MLPG.

[3] Work done by Neves et al.[11] based on Sinusoidal SDT.

To demonstrate the significance of accounting for the in-plane displacements and the resulting strain energy on the accuracy of the natural frequency, the following results were established. These results exclude any inertial energy in the x and y directions. Tables 7, Table 8 and

Table 9 display the non-dimensional fundamental frequencies of a simply supported square plate made from Al/ZrO_2 and Al/Al_2O_3 with a varying volume index λ and an aspect ratio a/h = 5, a/h = 10 and a/h = 20 respectively. The resulting error percentage was established by comparing the results of the present study to the 3D results obtained by Neves et al.[9] and Akavci and Tanrikulu [10]. The macroscopic material properties vary according to the Mori-Tanaka Homogenization procedure[8] or the rule of mixtures. The newly presented results all exclude all in-plane inertial effects in the x and y directions and the resulting external work.

Table 7: Comparison of non-dimensional fundamental frequency $\overline{\omega} = \omega h\sqrt{\frac{\rho_m}{E_m}}$ of a SSSS square plate (Al/ZrO_2) with a varying volume index λ and an aspect ratio a/h = 5, excluding in-plane displacements using the present theory (a = b = 1).

Source	λ = 0	λ = 0.5	λ = 1	λ = 3	λ = 10
Neves et al.[9][1]	0.2469	0.2228	0.2193	0.2215	0.2229
Neves et al.[9][2]	0.2459	0.2219	0.2184	0.2206	0.2219
Present	0.2693	0.2419	0.2386	0.2437	0.2453
Present[3]	0.2781	0.2495	0.2462	0.2522	0.2541
Error % relative to Neves et al.[9][1]	9.07%	8.61%	8.89%	10.15%	10.09%
Error % relative to Neves et al.[9][2] [3]	12.63%	11.98%	12.26%	13.86%	13.99%

Note : Material properties vary according to the Mori-Tanaka Homogenization procedure.

[1] Work done by Neves et al.[9] (Quasi 3D) based on 3D theory.

[2] Work done by Neves et al.[9] based on HSDT.

[3] Result excludes in-plane inertial effects in x and y directions.

Table 8 displays the non-dimensional fundamental frequencies of a simply supported square plate made from Al/Al_2O_3 with a varying volume index λ and an aspect ratio a/h = 10.

Table 8: Comparison of non-dimensional fundamental frequency $\overline{\omega} = \omega h\sqrt{\frac{\rho_c}{E_c}}$ of a SSSS square plate (Al/Al_2O_3) with a varying volume index λ and an aspect ratio a/h = 10, excluding in-plane displacements using the present theory (a = b = 1).

Source	λ = 0	λ = 0.5	λ = 1	λ = 4	λ = 10
Akavci and Tanrikulu[10][1]	0.0578	0.0494	0.0449	0.0389	0.0368
Present	0.0592	0.0502	0.0452	0.0393	0.0378
Present[2]	0.0597	0.0506	0.0456	0.0396	0.0381
Error % relative to Akavci and Tanrikulu[10][1]	2.42%	1.61%	0.66%	0.77%	2.44%
Error % relative to Akavci and Tanrikulu[10][1] [2]	3.28%	2.42%	1.55%	1.79%	3.53%

Material properties vary according to the rule of mixtures.

[1] Work done by Akavci and Tanrikulu[10] (Quasi 3D) based on 3D theory.

[2] Result excludes in-plane inertial effects in x and y directions.

Table 9 displays the non-dimensional fundamental frequencies of a simply supported square plate made from Al/Al_2O_3 with a varying volume index λ and an aspect ratio a/h = 20.

Table 9: Comparison of non-dimensional fundamental frequency $\overline{\omega} = \omega h\sqrt{\frac{\rho_c}{E_c}}$ of a SSSS square plate (Al/Al_2O_3) with a varying volume index λ and an aspect ratio a/h = 20, excluding in-plane displacements using the present theory (a = b = 1).

Source	λ = 0	λ = 0.5	λ = 1	λ = 4	λ = 10
Akavci and Tanrikulu[10][1]	0.0148	0.0126	0.0115	0.0100	0.0095
Present	0.0149	0.0126	0.0114	0.0099	0.0095
Present [2]	0.0149	0.0126	0.0114	0.0099	0.0095
Error % relative to Akavci and Tanrikulu[10][1]	0.67%	0.00%	-0.86%	-1.00%	0.00%
Error % relative to Akavci and Tanrikulu[10][1] [2]	0.67%	0.00%	-0.86%	-1.00%	0.00%

Note : Material properties vary according to the rule of mixtures.

[1] Work done by Akavci and Tanrikulu[10] (Quasi 3D) based on 3D theory.

[2] Result excludes in-plane inertial effects in x and y directions.

5.2 Buckling Load Results

Various numerical results of specific load cases for buckling load are presented in the tables below. Tables 10, 11, 12, 13 and 14 present the uniaxial buckling load results for simply supported square plate made from Al/Al_2O_3 and $SUS304/Si_3N_4$ accordingly, with a volume index λ, varying aspect ratio a/h and varying span ratio a/b. Table 15 displays 4 non-dimensional uniaxial critical buckling loads of an in-plane compressive load on a simply supported square plate with a volume index $\lambda = 0$ and an aspect ratio $a/h = 100$. Finally, Tables 16 and 17 display the biaxial critical buckling loads on a simply supported plate with varying aspect ratio a/h and a volume index $\lambda = 1$. The results are all based on the material properties varying according to the rule of mixtures. Most of the results of the present theory have been presented with at least one set of three-dimensional results which are used for comparison, however, Tables 11 and 12 contain only a comparison to 2DT. The results were obtained using software,the coding of which is presented in Appendies C to F.

Table 10 displays the uniaxial critical buckling load (MN) of an in-plane compressive load on a simply supported square plate made from Al/Al_2O_3 with a volume index $\lambda = 1$ and varying aspect ratio a/h . The resulting error percentage was established by comparing the results of the present study to the 3D results obtained by Asemi et al.[23].

Table 10: Comparison of uniaxial critical buckling load (MN) of a SSSS square plate (Al/Al_2O_3) with varying aspect ratio a/h and a volume index $\lambda = 1$ using the present theory ($a = 1$; $b = 2$) ($\psi = 0$).

		$\lambda = 1$					
Source	a/b	$a/h = 5$	$a/h = 10$	$a/h = 20$	$a/h = 30$	$a/h = 40$	$a/h = 50$
Asemi et al.[23][1]	0.5	237.9880	32.3325	4.1289	1.2289	0.5195	0.2664
Javaheri and Eslami [29][2]	0.5	267.4800	33.4350	4.1794	1.2383	0.5224	0.2675
Shariat and Eslami [28][3]	0.5	239.1500	32.4720	4.1486	1.2343	0.5215	0.2672
Thai and Choi [25][4]	0.5	239.1450	32.4721	4.1486	1.2343	0.5215	0.2672
Bodaghi and Saidi [30][4]	0.5	239.1500	32.4720	4.1486	1.2343	0.5215	0.2672
Kulkarni et al.[32][5]	0.5	239.6600	32.4900	4.1492	1.2343	0.5215	0.2672
Present	0.5	267.4817	33.4352	4.1794	1.2383	0.5224	0.2674
Error % relative to Asemi et al.[23][1]		12.39%	3.41%	1.22%	0.76%	0.55%	0.37%

Note : Material properties vary according to the rule of mixtures.

[1] Work done by Asemi et al.[23] based on 3D theory.

[2] Work done by Javaheri and Eslami [29] based on CLT.

[3] Work done by Shariat and Eslami [28] based on TSDT.

[4] Work done by Thai and Choi [25] and Bodaghi and Saidi [30] based on HSDT.

[5] Work done by Kulkarni et al.[32] based on ITSDT.

Tables 11, 12, 13 and 14 display the non-dimensional uniaxial critical buckling load of an in-plane compressive load on a simply supported square plate made from Al/Al_2O_3 or $SUS304/Si_3N_4$ with varying aspect ratio a/h, volume indices λ and span ratios a/b. Table

11 displays the error percentages established by using the 2D SDT results by Thai and Choi [25].

Table 11: Comparison of non-dimensional uniaxial critical buckling load $\overline{\mathrm{N}} = \mathrm{N}a^2/h^3E_m$ of a SSSS square plate (Al/Al_2O_3) with varying aspect ratio a/h and volume index λ using the present theory (a = 1 ; b = 1/2) (ψ = 0).

Source	a/b	a/h	λ = 0	λ = 0.5	λ = 1	λ = 2	λ = 5	λ = 10
Thai and Choi[25][1]	0.5	5	6.7203	4.4235	3.4164	2.6451	2.1484	1.9213
Nguyen [33][1]	0.5	5	6.7417	4.4343	3.4257	2.6503	2.1459	1.9260
Kulkarni et al.[32][2]	0.5	5	6.7372	4.4334	3.4237	2.6489	2.1451	1.9242
Present	0.5	5	7.6662	4.9695	3.8212	2.9817	2.5216	2.2968
Error % relative to Thai and Choi [25][1]			14.07%	12.34%	11.84%	12.72%	17.37%	19.54%
Thai and Choi [25][1]	1	5	16.0211	10.6254	8.2245	6.3432	5.0531	4.4807
Nguyen [33][1]	1	5	16.1003	10.6670	8.2597	6.3631	5.0459	4.4981
Kulkarni et al.[32][2]	1	5	16.0837	10.6624	8.2524	6.3578	5.0432	4.4919
Present	1	5	19.6256	12.7217	9.7822	7.6332	6.4552	5.8798
Error % relative to Thai and Choi [25][1]			22.49%	19.72%	18.93%	20.33%	27.74%	31.22%
Thai and Choi [25][1]	0.5	10	7.4053	4.8206	3.7111	2.8897	2.4165	2.1896
Nguyen [33][1]	0.5	10	7.4115	4.8225	3.7137	2.8911	2.4155	2.1911
Kulkarni et al.[32][2]	0.5	10	7.4102	4.8234	3.7131	2.8907	2.4152	2.1904
Present	0.5	10	7.6662	4.9695	3.8212	2.9817	2.5216	2.2968
Error % relative to Thai and Choi [25][1]			3.52%	3.08%	2.96%	3.18%	4.34%	4.89%
Thai and Choi [25][1]	1	10	18.5785	12.1229	9.3391	7.2631	6.0353	5.4528
Nguyen [33][1]	1	10	18.6030	12.1317	9.3496	7.2687	6.0316	5.4587
Kulkarni et al.[32][2]	1	10	18.5977	12.1340	9.3473	7.2671	6.0307	5.4560
Present	1	10	19.6256	12.7217	9.7822	7.6332	6.4552	5.8798
Error % relative to Thai and Choi [25][1]			5.63%	4.93%	4.74%	5.09%	6.95%	7.83%
Thai and Choi [25][1]	0.5	20	7.5993	4.9315	3.7930	2.9582	2.4944	2.2690
Nguyen [33][1]	0.5	20	7.6009	4.9307	3.7937	2.9585	2.4942	2.2695
Kulkarni et al.[32][2]	0.5	20	7.6005	4.9322	3.7936	2.9584	2.4941	2.2692
Present	0.5	20	7.6662	4.9695	3.8212	2.9817	2.5216	2.2968
Error % relative to Thai and Choi [25][1]			0.88%	0.77%	0.74%	0.79%	1.09%	1.22%
Thai and Choi [25][1]	1	20	19.3528	12.5668	9.6675	7.5371	6.3448	5.7668
Nguyen [33][1]	1	20	19.3593	12.5652	9.6702	7.5386	6.3437	5.7689
Kulkarni et al.[32][2]	1	20	19.3579	12.5697	9.6696	7.5382	6.3434	5.7676
Present	1	20	19.6256	12.7217	9.7822	7.6332	6.4552	5.8798
Error % relative to Thai and Choi [25][1]			1.40%	1.23%	1.18%	1.27%	1.74%	1.95%

Note : Material properties vary according to the rule of mixtures.

[1] Work done by Thai and Choi [25] and Nguyen [33] based on HSDT.

[2] Work done by Kulkarni et al.[32] based on ITSDT.

Table 12 displays the non-dimensional uniaxial critical buckling load of an in-plane compressive load on plate made from Al/Al_2O_3 with a varying volume index λ and aspect ratio a/h.

Table 12: Comparison of non-dimensional uniaxial critical buckling load $\overline{\mathrm{N}} = \mathrm{N}a^2/h^3E_m$ of a SSSS square plate (Al/Al_2O_3) with varying aspect ratio a/h and volume index λ using the present theory (a = 1 ; b = 1/2) (ψ = 0).

Source	a/b	a/h	λ = 0	λ = 0.5	λ = 1	λ = 5	λ = 10	λ = 20	λ = 100
Thai and Choi[25][1]	0.5	20	7.5993	4.9315	3.7930	2.4944	2.2690	2.0054	1.5683
Present	0.5	20	7.6662	4.9695	3.8212	2.5216	2.2968	2.0287	1.5833
Error % relative to Thai and Choi [25][1]			0.82%	0.77%	0.74%	1.09%	1.22%	1.16%	0.95%
Thai and Choi [25][1]	1	20	19.3528	12.5668	9.6675	6.3448	5.7668	5.0988	3.9923
Present	1	20	19.6256	12.7217	9.7822	6.4552	5.8798	5.1935	4.0534
Error % relative to Thai and Choi [25][1]			1.40%	1.23%	1.18%	1.74%	1.95%	1.85%	1.53%
Thai and Choi [25][1]	0.5	50	7.6555	4.9634	3.8166	2.5172	2.2923	2.0250	1.5809
Present	0.5	50	7.6662	4.9695	3.8212	2.5216	2.2968	2.0287	1.5833
Error % relative to Thai and Choi [25][1]			0.13%	0.12%	0.12%	0.17%	0.19%	0.18%	0.15%
Thai and Choi [25][1]	1	50	19.5814	12.6970	9.7636	6.4373	5.8614	5.1782	4.0434
Present	1	50	19.6256	12.7217	9.7822	6.4552	5.8798	5.1935	4.0534
Error % relative to Thai and Choi[25][1]			0.22%	0.19%	0.19%	0.27%	0.31%	0.29%	0.24%
Thai and Choi [25][1]	0.5	100	7.6635	4.9680	3.8200	2.5205	2.2957	2.0278	1.5827
Present	0.5	100	7.6662	4.9695	3.8212	2.5216	2.2968	2.0287	1.5833
Error % relative to Thai and Choi [25][1]			-0.01%	0.03%	0.03%	0.04%	0.04%	0.04%	0.03%
Thai and Choi [25][1]	1	100	19.6145	12.7158	9.7775	6.4507	5.8752	5.1897	4.0508
Present	1	100	19.6256	12.7217	9.7822	6.4552	5.8798	5.1935	4.0534
Error % relative to Thai and Choi [25][1]			0.05%	0.04%	0.04%	0.06%	0.07%	0.07%	0.06%

Note : Material properties vary according to the rule of mixtures.

[1] Work done by Thai and Choi [25] based on HSDT.

Table 13 displays the non-dimensional uniaxial critical buckling load of a in-plane compressive load on a plate made from Al/Al_2O_3 with a varying span ratio a/b. The error percentage was established using the 3D results obtained by Liu et al.[24].

Table 13: Comparison of non-dimensional uniaxial critical buckling load $\overline{\mathrm{N}} = \mathrm{N}a^2 12(1\text{-}\nu_c{}^2)/h^3E_c$ of a SSSS square plate (Al/Al_2O_3) with an an aspect ratio a/h = 100 and volume index λ = 0 using the present theory (a = 1 ; b = 1/2) (ψ = 0).

Source	a/b = 0.5	a/b = 1
Liu et al.[24][1]	15.4065	39.4640
Yin et al.[34][2]	15.4200	39.4720
Mohammadi et al.[31][3]	15.4212	39.4784
Present	15.4213	39.4784
Error % relative to Liu et al.[24][1]	0.09%	0.03%

Note : Material properties vary according to the rule of mixtures.

[1] Work done by Liu et al.[24] (S-Q3DHSDT) based on 3D theory.

[2] Work done by Yin et al.[34] based on S-FSDT.

[3] Work done by Mohammadi et al.[31] based on CLT.

Table 14 displays the non-dimensional uniaxial critical buckling load of a in-plane compressive load on a simply supported square plate made from $SUS304/Si_3N_4$. The error percentage was established using the 3D results obtained by Uymaz and Aydogdu [26].

Table 14: Comparison of non-dimensional uniaxial critical buckling load $\overline{\mathrm{N}} = \mathrm{N}a^2 12(1\text{-}\nu_c{}^2)/\pi^2 h^3 E_c$ of a SSSS square plate (SUS304/Si_3N_4) with varying aspect ratio a/h and volume index λ using the present theory (a = b = 1) (ψ = 0).

Source	a/h	λ = 0	λ = 0.5	λ = 1	λ = 5	λ = 10
Uymaz and Aydogdu [26][1]	5	-	-	-	-	-
Uymaz and Aydogdu [26][2]	5	-	-	-	-	-
Present	5	4.0000	3.3849	3.1528	2.8423	2.7262
Error % relative to Uymaz and Aydogdu [26][1]		-%	-%	-%	-%	-%
Uymaz and Aydogdu [26][1]	10	3.8099	3.2299	2.9899	2.6699	2.5699
Uymaz and Aydogdu [26][2]	10	3.8009	3.2609	3.0609	2.7709	2.6609
Present	10	4.0000	3.3849	3.1528	2.8423	2.7262
Error % relative to Uymaz and Aydogdu [26][1]		4.98%	4.79%	5.44%	6.45%	6.08%
Uymaz and Aydogdu [26][1]	20	3.9499	3.3299	3.1099	2.7899	2.6699
Uymaz and Aydogdu [26][2]	20	3.9709	3.3709	3.1409	2.8309	2.7109
Present	20	4.0000	3.3849	3.1528	2.8423	2.7262
Error % relative to Uymaz and Aydogdu [26][1]		1.26%	1.70%	1.37%	1.87%	2.10%
Uymaz and Aydogdu [26][1]	50	3.9899	3.3699	3.1499	2.8299	2.7099
Uymaz and Aydogdu [26][2]	50	3.9909	3.3809	3.1509	2.8409	2.7209
Present	50	4.0000	3.3849	3.1528	2.8423	2.7262
Error % relative to Uymaz and Aydogdu [26][1]		0.25%	0.44%	0.09%	0.43%	0.60%
Uymaz and Aydogdu [26][1]	100	3.9899	3.3699	3.1499	2.8299	2.7099
Uymaz and Aydogdu [26][2]	100	3.9909	3.3809	3.1509	2.8499	2.7209
Present	100	4.0000	3.3849	3.1528	2.8423	2.7262
Error % relative to Uymaz and Aydogdu [26][1]		0.25%	0.44%	0.09%	0.43%	0.60%

Note : Material properties vary according to the rule of mixtures.

[1] Work done by Uymaz and Aydogdu [26] based on 3D theory.

[2] Work done by Uymaz and Aydogdu [26] based on ESDPT.

Table 15 displays 4 non-dimensional uniaxial buckling loads of an in-plane compressive load on a plate made from SUS304/Si_3N_4 with an aspect ratio a/h = 100 and a volume index λ = 0. The error percentage was established using the 3D results obtained by Uymaz and Aydogdu [27].

Table 15: Comparison of 4 non-dimensional uniaxial buckling loads $\overline{\mathrm{N}} = \mathrm{N}a^2 12(1\text{-}\nu_c{}^2)/\pi^2 h^3 E_c$ of a SSSS square plate (SUS304/Si_3N_4) with an aspect ratio a/h = 100 and volume fraction index λ = 0 using the present theory (a = b = 1) (ψ = 0).

Source	mode (1;1)	mode (2;1)	mode (2;2)	mode (4;1)
Uymaz and Aydogdu [27][1]	3.9899	6.2099	16.010	19.610
Present	4.0000	6.2500	16.000	18.062
Error % relative to Uymaz and Aydogdu [27][1]	0.25%	0.64%	-0.06%	-7.86%

Note : Material properties vary according to the rule of mixtures.

[1] Work done by Uymaz and Aydogdu [27] based on 3D theory.

Tables 16 and 17 display the results of biaxial critical buckling loads. Table 16 displays the non-dimensional biaxial critical buckling load of plate made from SUS304/Si_3N_4 with a

volume index λ and a varying aspect ratio a/h. Table 17 displays biaxial critical buckling load (MN) of plate made from Al/Al_2O_3 with a volume index λ = 1 and a varying aspect ratio a/h. The resulting error percentages were established using the 3D results obtained by Uymaz and Aydogdu [26] and Asemi et al.[23] accordingly.

Table 16: Comparison of non-dimensional biaxial critical buckling load $\overline{N} = Na^2 12(1\text{-}\nu_c{}^2)/\pi^2 h^3 E_c$ of a SSSS square plate ($SUS304/Si_3N_4$) with varying aspect ratio a/h and volume index λ using the present theory (a = b = 1) (ψ = 1).

Source	a/h	λ = 0	λ = 0.5	λ = 1	λ = 5	λ = 10
Uymaz and Aydogdu [26][1]	5	-	-	-	-	-
Uymaz and Aydogdu [26][2]	5	-	-	-	-	-
Present	5	2.0000	1.6925	1.5764	1.4212	1.3631
Error % relative to Uymaz and Aydogdu [26][1]		-%	-%	-%	-%	-%
Uymaz and Aydogdu [26][1]	10	1.8999	1.6099	1.4999	1.3399	1.2799
Uymaz and Aydogdu [26][2]	10	1.9009	1.6309	1.5309	1.3809	1.3309
Present	10	2.0000	1.6925	1.5764	1.4212	1.3631
Error % relative to Uymaz and Aydogdu [26][1]		5.26%	5.13%	5.10%	6.06%	6.50%
Uymaz and Aydogdu [26][1]	20	1.9699	1.6699	1.5599	1.3999	1.3399
Uymaz and Aydogdu [26][2]	20	1.9809	1.6809	1.5709	1.4109	1.3509
Present	20	2.0000	1.6925	1.5764	1.4212	1.3631
Error % relative to Uymaz and Aydogdu [26][1]		1.52%	1.35%	1.05%	1.52%	1.73%
Uymaz and Aydogdu [26][1]	50	1.9899	1.6899	1.5699	1.4199	1.3599
Uymaz and Aydogdu [26][2]	50	1.9909	1.6909	1.5709	1.4299	1.3609
Present	50	2.0000	1.6925	1.5764	1.4212	1.3631
Error % relative to Uymaz and Aydogdu [26][1]		0.50%	0.15%	0.41%	0.09%	0.23%
Uymaz and Aydogdu [26][1]	100	1.9899	1.6899	1.5699	1.4199	1.3599
Uymaz and Aydogdu [26][2]	100	1.9909	1.6909	1.5709	1.4209	1.3609
Present	100	2.0000	1.6925	1.5764	1.4212	1.3631
Error % relative to Uymaz and Aydogdu [26][1]		0.50%	0.15%	0.41%	0.09%	0.23%

Note : Material properties vary according to the rule of mixtures.

[1] Work done by Uymaz and Aydogdu [26] based on 3D theory.

[2] Work done by Uymaz and Aydogdu [26] based on ESDPT.

Table 17 displays the non-dimensional critical buckling load of a biaxial in-plane compressive load on a simply supported square plate made from Al/Al_2O_3.

Table 17: Comparison of biaxial critical buckling load (MN) of a SSSS square plate (Al/Al_2O_3) with varying aspect ratio a/h and a volume index $\lambda = 1$ using the present theory ($a = 1$; $b = 2$) ($\psi = 1$).

		$\lambda = 1$					
Source	a/b	$a/h = 5$	$a/h = 10$	$a/h = 20$	$a/h = 30$	$a/h = 40$	$a/h = 50$
Asemi et al.[23][1]	0.5	190.386	25.868	3.3071	0.9839	0.4162	0.2131
Javaheri and Eslami [29][2]	0.5	213.99	26.748	3.4353	0.9907	0.4179	0.2140
Shariat and Eslami [28][3]	0.5	191.32	25978	3.3189	0.9879	0.4172	0.2137
Thai and Choi [25][4]	0.5	191.3160	25.9777	3.3189	0.9874	0.4172	0.2137
Bodaghi and Saidi [30][4]	0.5	191.3200	25.9780	3.3189	0.9879	0.4172	0.2137
Kulkarni et al.[32][5]	0.5	191.7300	25.9920	3.3194	0.9875	0.4172	0.2137
Present	0.5	213.9853	26.7481	3.3435	0.9906	0.4179	0.2139
Error % relative to Asemi et al.[23][1]		12.39%	3.40%	1.10%	0.68%	0.40%	0.37%

Note : Material properties vary according to the rule of mixtures.

[1] Work done by Asemi et al.[23] based on 3D theory.

[2] Work done by Javaheri and Eslami [29] based on CLT.

[3] Work done by Shariat and Eslami [28] based on TSDT.

[4] Work done by Thai and Choi [25] and Bodaghi and Saidi[30] based on HSDT.

[5] Work done by Kulkarni et al.[32] based on ITSDT.

5.3 Variation of Natural Frequency with Compressive Load

The graphical representations of the variations of natural frequency with buckling load are presented in Figures 6, 7 and 8. They illustrate the variation of natural frequency for both the uniaxial and biaxial buckling loads (MN) of in-plane compressive loads on a simply supported square plate made from Al/Al_2O_3 and $SUS304/Si_3N_4$ with an aspect ratio $a/h = 20$ and $a/h = 100$ with various volume indices λ accordingly. The natural frequency is observed on the y axis and the compressive load on the x axis. Material properties vary according to the rule of mixtures as before.

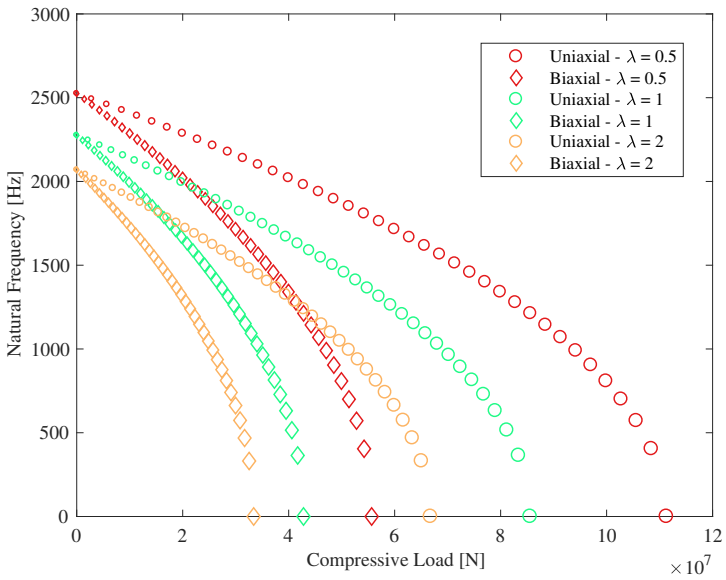


Figure 6: Comparison of uniaxial and biaxial compressive load (MN) with natural frequency of a SSSS square plate (Al/Al_2O_3) with an aspect ratio $a/h = 20$ and varying volume index λ using the present theory ($a = b = 1$).

Figure 7 illustrates the variation of natural frequency for both uniaxial and biaxial compressive loading (MN) of a simply supported square plate made from Al/Al_2O_3 with an aspect ratio $a/h = 20$.

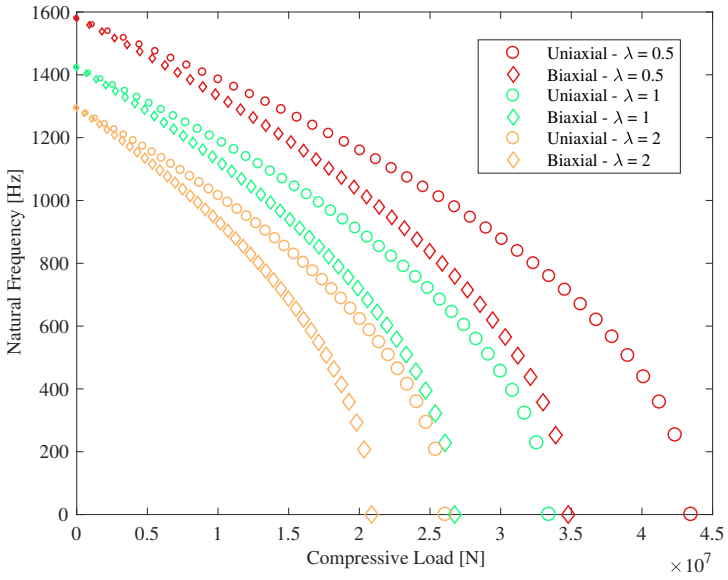


Figure 7: Comparison of uniaxial and biaxial compressive load (MN) with natural frequency of a SSSS square plate (Al/Al_2O_3) with an aspect ratio $a/h = 20$ and varying volume index λ using the present theory ($a = 1$, $b = 2$).

Figure 8 illustrates the variation of natural frequency for both the uniaxial and biaxial buckling loads (MN) of in-plane compressive loads on a simply supported square plate made from $SUS304/Si_3N_4$ with an aspect ratio $a/h = 100$.

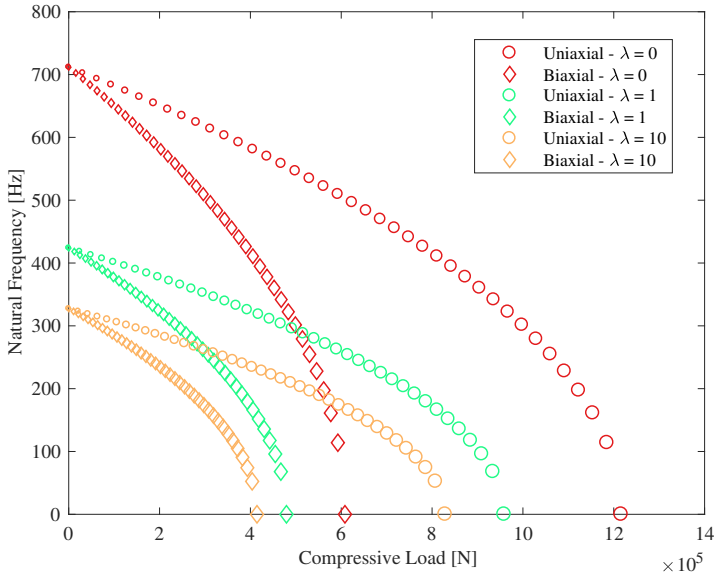


Figure 8: Comparison of uniaxial and biaxial compressive load (MN) with natural frequency of a SSSS square plate ($SUS304/Si_3N_4$) with an aspect ratio $a/h = 100$ and varying volume index λ using the present theory ($a = b = 1$).

5.4 Curve Fit Accuracy and Convergence

Since the present theory is an extension to CLT, the solutions to the natural frequency and critical buckling load using CLT may be of interest for comparison with the present study. In addition, it is worth noting that the polynomial fit error percentage limit has an effect on the results of the present study and therefore, confirming convergence may also be of interest. As such, results are displayed for CLT and the present study for both natural frequency, as well as for critical buckling loads for a particular load case.

To compare results of the CLT and the present study and confirm convergence of the present study, the following particular load case is considered: the results of CLT and the present study for the fundamental natural frequency (Hz) of a SSSS square plate (Al/Al_2O_3) with an aspect ratio $a/h = 20$ and varying volume index λ ($a = 1$; $b = 1$) are presented in Table 18 and 19 respectively. The natural frequencies for CLT vary with the degree of discretization, while for the present study, they vary with polynomial fit error percentage limit. For both set of results, the macroscopic material properties vary according to the Mori-Tanaka Homogenization procedure[8].

Table 18: Natural frequency (Hz) results for various discretization layers of a SSSS square plate (Al/Al_2O_3) with an aspect ratio $a/h = 20$ and varying volume index λ using CLT ($a = 1$; $b = 1$).

	Number of Layers						
λ	1000	2000	5000	10000	20000	50000	100000
$\lambda = 0$	2980.5559	2980.5559	2980.5559	2980.5559	2980.5559	2980.5559	2980.5559
$\lambda = 0.1$	2658.8279	2658.3461	2658.0438	2657.9390	2657.8850	2657.8518	2657.8404
$\lambda = 0.2$	2480.4940	2479.9737	2479.6531	2479.5437	2479.4882	2479.4543	2479.4429
$\lambda = 0.5$	2207.9311	2207.4727	2207.1959	2207.1033	2207.0568	2207.0289	2207.0196
$\lambda = 1$	2031.8483	2031.4790	2031.2574	2031.1835	2031.1466	2031.1244	2031.1170
$\lambda = 2$	1927.0706	1926.6996	1926.4770	1926.4028	1926.3656	1926.3434	1926.3359
$\lambda = 5$	1851.0377	1850.3598	1849.9531	1849.8176	1849.7498	1849.7092	1849.6956
$\lambda = 10$	1776.6197	1775.5132	1774.8506	1774.6300	1774.5197	1774.4536	1774.4315
$\lambda = 12$	1754.1866	1752.9565	1752.2206	1751.9756	1751.8532	1751.7797	1751.7553
$\lambda = 15$	1726.5609	1725.1804	1724.3554	1724.0809	1723.9438	1723.8616	1723.8342
$\lambda = 20$	1692.1814	1690.6137	1689.6787	1689.3680	1689.2129	1689.1198	1689.0888
$\lambda = 50$	1605.8980	1603.8286	1602.6097	1602.2071	1602.0066	1601.8865	1601.8465
$\lambda = 100$	1567.4539	1565.0863	1563.7185	1563.2716	1563.0498	1562.9173	1562.8732

The graphical representation of the results of Table 18 is displayed in Figure 9.

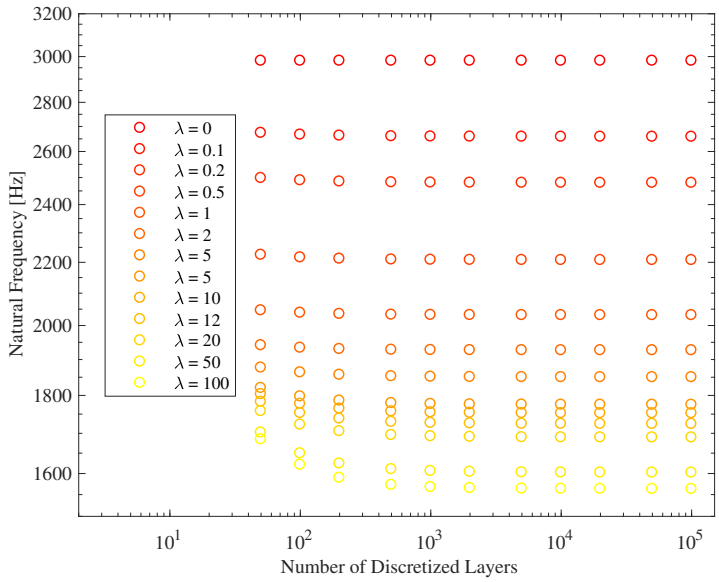


Figure 9: Variation of natural frequency using CLT with increasing discretization layers.

Table 19 lists the natural frequencies of the present study which vary with polynomial fit error percentage limits. The error percentage between a polynomial fit error percentage limit of 0.05% and the equivalent results for CLT using 100000 layers is listed in the final column.

Table 19: Natural frequency (Hz) results for various polynomial fit error percentage limits of a SSSS square plate (Al/Al_2O_3) with an aspect ratio $a/h = 20$ and varying volume index λ using the present study ($a = 1$; $b = 1$).

	Polynomial Fit Error Percentage							Error
λ	5%	2%	1%	0.5%	0.2%	0.1%	0.05%	
$\lambda = 0$	2980.5559	2980.5559	2980.5559	2980.5559	2980.5559	2980.5559	2980.5559	-0.00%
$\lambda = 0.1$	2657.3975	2657.8248	2657.7507	2657.7429	2657.7429	2657.7429	2657.7429	-0.00%
$\lambda = 0.2$	2479.1627	2479.2731	2479.4122	2479.4315	2479.4462	2479.4462	2479.4462	0.00%
$\lambda = 0.5$	2207.0259	2207.0482	2207.0559	2207.0528	2207.0572	2207.0631	2207.0726	0.00%
$\lambda = 1$	2031.1113	2031.1113	2031.1311	2031.1183	2031.1183	2031.1202	2031.1202	0.00%
$\lambda = 2$	1926.3299	1926.2414	1926.2617	1926.2439	1926.2478	1926.2444	1926.2444	-0.00%
$\lambda = 5$	1849.6707	1849.5658	1849.5256	1849.5197	1849.5245	1849.5193	1849.5168	-0.00%
$\lambda = 10$	1774.3545	1774.3040	1774.2790	1774.2738	1774.2679	1774.2650	1774.2636	-0.00%
$\lambda = 12$	1751.7399	1751.6881	1751.6496	1751.6231	1751.6007	1751.5990	1751.5975	-0.00%
$\lambda = 15$	1723.8109	1723.7813	1723.7383	1723.7143	1723.6953	1723.6919	1723.6901	-0.00%
$\lambda = 20$	1689.2263	1689.0616	1689.0250	1688.9793	1688.9723	1688.9680	1688.9624	-0.00%
$\lambda = 50$	1602.0568	1601.8649	1601.8413	1601.8020	1601.7748	1601.7655	1601.7695	-0.00%
$\lambda = 100$	1563.1273	1562.9593	1562.9000	1562.8815	1562.8253	1562.8111	1562.8040	-0.00%

The graphical representation of the results of Table 19 is displayed in Figure 10.

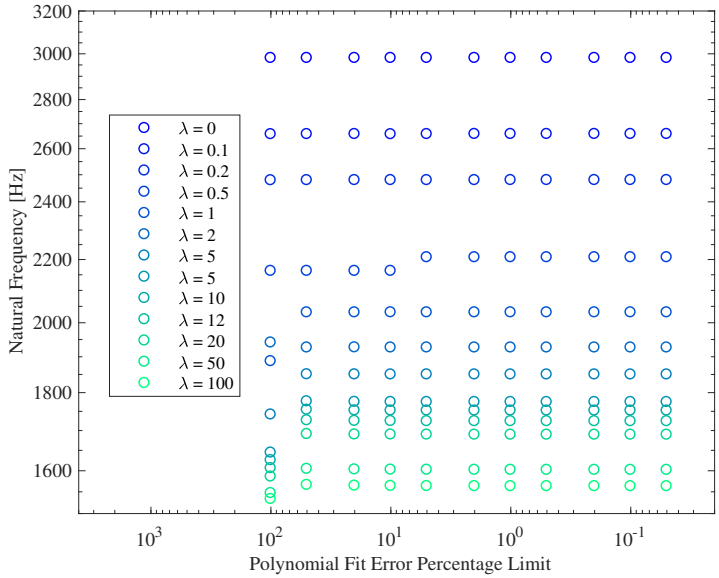


Figure 10: Variation of natural frequency using the present study with the polynomial fit error percentage.

Similarly for the critical buckling load, the results of CLT and the present study for a uniaxial critical buckling load (MN) of a SSSS square plate (Al/Al_2O_3) with an aspect ratio a/h = 20 and varying volume index λ (a = 1 ; b = 2) (ψ = 0) are presented in Table 20 and 21 respectively. The critical buckling loads for the CLT analysis vary with the degree of discretization, while for the present study, they vary with polynomial fit error percentage limit. For both set of results, the macroscopic material properties vary according to the rule of mixtures.

Table 20: Critical buckling loads (MN) results for various discretization layers of a SSSS square plate (Al/Al_2O_3) with an aspect ratio a/h = 20 and varying volume index λ using CLT (a = 1 ; b = 2).

	Number of Layers						
λ	1000	2000	5000	10000	20000	50000	100000
λ = 0	8384.9553	8384.9553	8384.9553	8384.9553	8384.9553	8384.9553	8384.9553
λ = 0.1	7561.7978	7559.6917	7558.3189	7557.8249	7557.5639	7557.3986	7557.3405
λ = 0.2	6880.7117	6877.7846	6875.9294	6875.2803	6874.9449	6874.7373	6874.6662
λ = 0.5	5441.3443	5438.4356	5436.6697	5436.0759	5435.7776	5435.5979	5435.5378
λ = 1	4183.3641	4181.3826	4180.1940	4179.7978	4179.5997	4179.4809	4179.4413
λ = 2	3263.5579	3262.4106	3261.7225	3261.4931	3261.3785	3261.3097	3261.2868
λ = 5	2760.1285	2759.0460	2758.3959	2758.1791	2758.0706	2758.0056	2757.9839
λ = 10	2515.8237	2513.9652	2512.8492	2512.4771	2512.2910	2512.1794	2512.1422
λ = 12	2441.8304	2439.7028	2438.4256	2437.9998	2437.7868	2437.6590	2437.6164
λ = 15	2347.3855	2344.9172	2343.4360	2342.9422	2342.6954	2342.5472	2342.4978
λ = 20	2224.7249	2221.8216	2220.0804	2219.5001	2219.2100	2219.0360	2218.9780
λ = 50	1895.5408	1891.4915	1889.0724	1888.2678	1887.8659	1887.6248	1887.5445
λ = 100	1740.9351	1736.3164	1733.5749	1732.6660	1732.2125	1731.9407	1731.8502

The results of Table 20 are plotted for illustrative purposes in Figure 11.

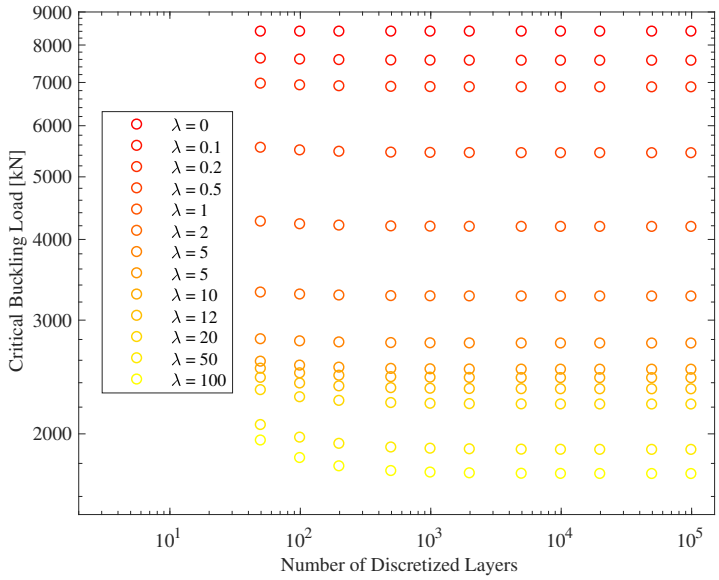


Figure 11: Variation of critical buckling load using CLT with increasing discretization layers.

Table 21 lists the critical buckling loads of the present study which vary with polynomial fit error percentage limits. The error percentage between a polynomial fit error percentage limit of 0.05% and the equivalent results for CLT using 100000 layers is again, listed in the final column.

Table 21: Critical buckling load (MN) results for various polynomial fit error percentage limits of a SSSS square plate (Al/Al_2O_3) with an aspect ratio a/h = 20 and varying volume index λ using the present study (a = 1 ; b = 2).

	Polynomial Fit Error Percentage							Error
λ	5%	2%	1%	0.5%	0.2%	0.1%	0.05%	
λ = 0	8384.9553	8384.9553	8384.9553	8384.9553	8384.9553	8384.9553	8384.9553	-0.00%
λ = 0.1	7555.6341	7555.5658	7555.5658	7555.5658	7555.5658	7555.5658	7555.5658	-0.02%
λ = 0.2	6872.3790	6873.7008	6873.9313	6873.9313	6873.9313	6873.9313	6873.9313	-0.01%
λ = 0.5	5435.1938	5435.3158	5435.3479	5435.4560	5435.4462	5435.2569	5435.4454	-0.00%
λ = 1	4179.4017	4179.4017	4179.4017	4179.4017	4179.4017	4179.4017	4179.4017	-0.00%
λ = 2	3261.2638	3261.2638	3261.2638	3261.2638	3261.2638	3261.2638	3261.2638	-0.00%
λ = 5	2757.9130	2757.9130	2757.9622	2757.9622	2757.9622	2757.9622	2757.9622	-0.00%
λ = 10	2512.0738	2512.0738	2512.1237	2512.1237	2512.1041	2512.1041	2512.1041	-0.00%
λ = 12	2437.5332	2437.6374	2437.5701	2437.5701	2437.5757	2437.5757	2437.5757	-0.00%
λ = 15	2342.6358	2342.4408	2342.4408	2342.4632	2342.4478	2342.4478	2342.4489	-0.00%
λ = 20	2218.9371	2219.0049	2218.9193	2218.9193	2218.9283	2218.9197	2218.9197	-0.00%
λ = 50	1887.6457	1887.5164	1887.5316	1887.4766	1887.4810	1887.4666	1887.4676	-0.00%
λ = 100	1732.1718	1731.9506	1731.8409	1731.7886	1731.7699	1731.7710	1731.7634	-0.00%

The results of Table 21 are plotted for illustrative purposes in Figure 12.

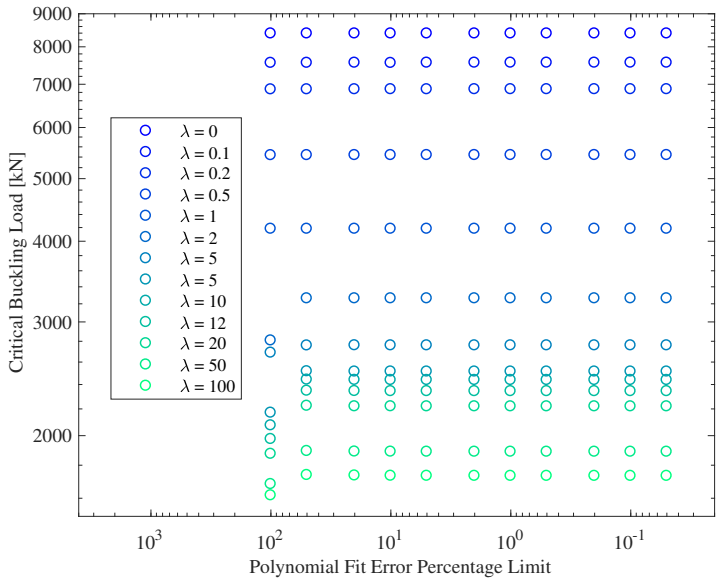


Figure 12: Variation of critical buckling load using the present study with increasing polynomial fit error percentage limits.

6 Discussion

The discussion of results is presented in the same order as was presented in Section 5.

6.1 Natural Frequency

The non-dimensional fundamental natural frequencies of plates with varying volume index λ and an aspect ratio $a/h = 5$, $a/h = 10$ and $a/h = 20$ are displayed in Tables 1, 2 and 3 respectively. The results show that for relatively thick plates, $a/h = 5$, the error percentage compared to the three dimensional results produced by Neves et al.[9] vary between 8.61% and 10.15% depending on the extent of the variation of material properties through the thickness which is given by the volume index λ. The results illustrate that the error percentage for an aspect ratio $a/h = 10$ compared to the three dimensional results produced by Akavci and Tanrikulu[10] improve to between 0.66% and 2.44%. These results are improved even further for an aspect ratio $a/h = 20$ where the error percentage improves to between 0.00% and 1.00% absolute. The negative errors and magnitude of the errors observed in Table 3 is a result of the difference in the last significant figure which has a significant impact on the error percentage, given the low value of the non-dimensional natural frequency for the load case. It may also be attributed to rounding off errors and the number of decimal places displayed. It is clear however, that the accuracy of the results compared to three dimensional results increase significantly as the aspect ratio a/h is increased. Consequently, for plates with an aspect ratio $a/h = 20$, the results compare very well with three dimensional results by Akavci and Tanrikulu[10]. By way of comparison, the average error percentage for the results of Table 1 for an aspect ratio $a/h = 5$ is 9.36%. The average error percentage for the results of Table 2 for an aspect ratio of $a/h = 10$ is 1.58%. The average error percentage for the results of Table 2 for an aspect ratio $a/h = 10$ is 1.58%. The average error percentage for the results of Table 3 for an aspect ratio of $a/h = 20$ is 0.50% (using all error percentages as absolute values). This confirms the sharp decrease in the significance of the through-thickness strains and their associated energy with increasing aspect ratio. The natural frequencies established using the present theory are in most cases, greater than the three-dimensional results. This observation is expected, given that the present theory has neglected the through thickness strains. In thicker plates the through-thickness strain energy is proportionately more significant than in thinner plates, and hence, neglecting this energy has a greater impact in thicker plates. Comparing Tables 1, 2 and 3, it is clear that the non-dimensional natural frequencies are greater for thicker plates and decrease with increasing aspect ratio a/h.

Tables 2 and 3 illustrate that the non-dimensional frequencies are at their greatest when the volume index $\lambda = 0$, and decrease with increasing volume index λ. This trend can be attributed

to the plate being made completely of the stiff ceramic material at $\lambda = 0$ which becomes increasing less stiff as more metallic material is introduced with increasing volume index λ. The difference in the specific stiffness (Young's modulus to density ratio) for aluminium and aluminium oxide is relatively high so, with the addition of the ceramic material, it is expected that the plate's natural frequency will increase. Contrary to Tables 2 and 3, Table 1 does not follow the same trend, the non-dimensional natural frequency is at a minimum at a volume index $\lambda = 1$ and then increases marginally as the metallic material is introduced with increasing λ. It is worth noting that the materials for the load case of Table 1 is made from aluminium and zirconium oxide whose difference in specific stiffness is relatively small. Appendix B details an investigation conducted to explain the reason for better results at volume indices of around $\lambda = 1$. The plate's neutral axis moves away from the mid-plane when there is a difference in stiffness between the top and bottom surfaces of the plate. Appendix B illustrates that at and around $\lambda = 1$, the difference between $D(1,1)$ and $\overline{D}(1,1)$ is greatest while the displacement between the mid-plane and the neutral axis also appears to peak at this point. The result of this displacement of the neutral axis from the mid-plane is that the $\overline{D}$ matrix has lower values at around $\lambda = 1$ and $\lambda = 2$. As a result, a lower bending stiffness matrix is calculated and therefore, greater curvature is experienced by the plate. This would imply that the plate experiences a greater bending strain which means that the bending strain will be a significantly greater proportion of the total internal strain energy in the plate, while the through-thickness strains diminish in significance. Considering the effect of the D matrix and the relatively small difference in specific stiffness for aluminium and zirconium oxide, it is reasonable to assume that this D effect dominates the material properties at $\lambda = 1$, in plates where the specific stiffnesss are relatively constant. This would explain why the results in Table 1 increase after $\lambda = 1$. Conversely, since there is a relatively large difference in the specific stiffnesss in Tables 2 and 3, the effects of the reversion of the neutral axis to the mid-plane after $\lambda = 1$ is not large enough to counter the effects of the introduction of the less stiff metallic materials.

The non-dimensional fundamental natural frequencies of plates with varying volume index λ, aspect ratio $a/h = 100$ and varying span ratio a/b are displayed in Table 4. The error percentages compared with the three dimensional results by Baferani et al.[20] are relatively small, given that the aspect ratio $a/h = 100$. This is consistent with the insignificant effects of the through thickness strains on thin plates. The natural frequencies of the present study compare well with the natural frequencies of the results of all the other authors used as a comparison and particularly with the CLT results as expected. However, the results of the present study should be exactly the same as the results for the CLT results, given that all the methods including the present study is based on CLT. The difference in the natural frequencies may perhaps be due to the insufficient polynomial accuracy fit of the present

study or that the CLT results have not reached convergence of results to the last significant figure. Further discussions on these issues are discussed in Section 6.4.

Tables 5 and 6 display the non-dimensional natural frequencies at various mode shapes. The first four (4) non-dimensional frequencies for a plate with an aspect ratio a/h = 10 and varying volume index λ is displayed in Table 5. The first five (5) non-dimensional frequencies for a plate with an aspect ratio a/h = 20 and volume index λ = 1 is displayed in Table 6. The results of both tables confirm that the fundamental natural frequency (mode 1;1) compares very well with their respective three-dimensional results as before. The results in Table 5 illustrate that for the fundamental frequency, the average error percentage compared to the three dimensional results by Akavci and Tanrikulu[10] may be established as 1.76% and varies between 0.65% and 3.11%. The next mode shape, (1;2) or (2;1), has an average error percentage compared to the three dimensional results of 5.28% and varies between 3.52% and 7.16%. Similarly, for the mode shape (2;2), the average error percentage is 8.79%. By comparison of the various mode shapes and average error percentages, it is evident that the error percentages increase significantly with higher mode shapes. Investigation of the strain displacement relationships from other 3D literature illustrates that the through-thickness strains, γ_{yz} and γ_{xz}, are a function of the out-of-plane trial function and given by $\frac{\partial u}{\partial dz} + \frac{\partial dw}{\partial dx}$ and $\frac{\partial dv}{\partial dz} + \frac{\partial dw}{\partial dy}$ respectively. As such, increasing the mode shape parameter would increase the $\frac{\partial dw}{\partial dx}$ and $\frac{\partial dw}{\partial dy}$ components. Accordingly, it is expected that the through-thickness strains would become increasingly more significant and would explain the increase in the error percentages with increasing mode shapes in the present study. It is also worth noting that at higher mode shapes, the natural frequency increases as expected.

To compare the effect of the aspect ratio a/h at different mode shapes, a comparison of the error percentages must be investigated. The error percentage for natural frequencies of Table 5 and 6 for a volume index λ = 1, is 0.63% and 0.65% respectively. Similarly, the next mode shape, (2;1 or 1;2) is 3.52% and 1.59%. Finally, for the mode shape (2;2), the error percentages are 6.09% and 2.51% respectively. It is important to note the reduced magnitude of there errors between the two tables is due to the difference in the aspect ratios a/h, where Table 5 has an aspect ratio a/h = 10, while Table 6 has an aspect ratio a/h = 20. It is clear that the greater aspect ratios derive smaller errors as before.

The non-dimensional fundamental natural frequencies of plates of aspect ratio a/h = 5, a/h = 10 and a/h = 20, including and excluding in-plane inertial energy are displayed in Table 7, 8, and 9 respectively. The results show that for plates with an aspect ratio a/h = 5 and neglecting in-plane inertial energy, the error percentage compared to the three dimensional results vary between 11.98% and 13.99% depending the volume index λ. For an aspect ratio a/h = 10, the error percentage compared to the three dimensional results vary between 1.55% and 3.53% and for an aspect ratio a/h = 20, the error percentage varies between 0.00% and 1.00%

absolute. When comparing the error percentages of Table 7 for the results including and excluding in-plane inertial energy for an aspect ratio $a/h = 5$, the difference in the error percentages of the two results vary between 3.9% and 3.37%, with an average difference of 3.58%. The difference indicates that for relatively thick plates, the in-plane inertial energy should be considered. The error percentages of Table 8 for the results including and excluding in-plane inertial energy for an aspect ratio $a/h = 10$ vary between 1.09% and 0.81%. The average error percentage is 0.93% which is an improvement of 2.65% when compared to the average error percentage of plates with an aspect ratio $a/h = 5$. This illustrates that the significance of the in-plane inertial energy decrease sharply as the aspect ratio increases. This is confirmed when considering the error percentages of Table 9 for the results including and excluding in-plane inertial energy for an aspect ratio $a/h = 10$ which show no difference and are identical. The results indicate that plates with an aspect ratio $a/h = 20$ are not influenced by in-plane inertial energy and therefore, there is no need to consider the in-plane inertial energy for plates with greater aspect ratios $a/h = 20$.

6.2 Buckling Load

Tables 10, 11, 12, 13 and 14 display the uniaxial critical buckling load of plates as a function of volume index λ, aspect ratio a/h and span ratio a/b accordingly. Table 10 displays the critical buckling load (MN) with a volume index $\lambda = 1$. The error percentage compared to the three dimensional results, which vary between 0.37% and 12.39% depending on the aspect ratio a/h. As expected, plates with an aspect ratio $a/h = 5$ have greater critical buckling loads since thicker plates can withstand greater loads and therefore, the critical buckling load decreases with increasing aspect ratio a/h. In addition, the error percentage decreases sharply with increasing aspect ratio a/h, given that the through thickness shear strains are increasingly less significant. It is also clear that the results of the present study produce results which over estimate the buckling load for a particular load case. It is worth noting that the results obtained in Table 10 for the present study compare very well with the CLT results found by Javaheri and Eslami[29] and at larger aspect ratios, the results compare well with the three dimensional results found by Asemi et al.[23]. The non-dimensional critical buckling load of plates with varying volume index λ and span ratio a/b are displayed in Table 11 and 12. These results could not be compared to 3DT but they have been compared to 2D results which include some forms of simple or complex shear deformation theories. The average error percentage of critical buckling loads for an aspect ratio $a/h = 5$ is 14.64% and 23.40% depending on the span ratio a/b. Consistent with previous observations, these error percentages decrease significantly with increasing aspect ratio a/h. The results illustrate that the critical buckling load varies with volume index λ, with the greatest values at volume index $\lambda = 0$, decreasing with increasing volume index λ. This is due to the ceramic material having a greater Young's modulus than the metallic material. Interestingly though, the critical buckling load established by other authors increase with increasing aspect ratio a/h, while the critical buckling loads of the present study remain the same for a particular load case and therefore are independent of aspect ratio a/h. This is a result of the fact that CLT does not consider through-thickness shear strains and associated energy which is dominant for thick plates, so therefore, the resulting energy which would produce the variation with thickness is non-existent and critical buckling loads are produced independent of thickness. Similarly to the results for natural frequency, the error percentages for critical buckling loads are at their minima at around $\lambda = 1$. This observation can be attributed to the displacement of the neutral access from the mid-plane, resulting in greater curvature and the dominance of bending energy which renders the through-thickness strains less significant. Details presented in Appendix B. Table 11, 12 and 13 illustrate the effect that the span ratio a/b has on the critical buckling loads for a particular load case. As expected, the results of the present theory compare well with comparative results at large aspect ratios. The span ratio a/b has a significant effect on the non-dimensional buckling load. An increase in the span ratio a/b results in an increase in the non-dimensional buckling load. This is as a result of the plate

having a greater length along is loaded side (the side measuring a length a) which will allow it to withstand a greater load. A smaller span ratio a/b would imply that it's effective length (the side measuring a length b) relative to it's loaded side would be significantly greater, thereby rendering the plate to act similar to a column. A simple caparison between each particular load case reveals that plates with a span ratio $a/b = 1$ buckle at 2.56 times more load than plates with a span ratio $a/b = 0.5$ according to the present theory. This factor arises from a purely geometric relation between the span ratios. Another important observation is the increased error percentage between load cases with different span ratios a/b. Span ratios $a/b = 1$ have significantly higher error percentages than the same load case with a span ratio of $a/b = 0.5$. In fact, load cases with lower aspect ratios a/h and a span ratio $a/b = 1$ have a consistent error percentage which is approximately 60% (for the load case in Table 11 for volume index $\lambda = 0$ and aspect ratio $a/h = 5$: (22.49 - 14.07)/14.07) greater than their corresponding load case with a span ratio of $a/b = 0.5$. The reason for the increased error percentage is unknown at this stage, however, the author suspects that it may be a result of the difference in curvature which is due to the difference in the geometric properties of the plates. The critical buckling loads of the present theory in Table 12 compare well with results found by Thai and Choi[25]. The non-dimensional critical buckling load of plates with varying span ratio a/b, volume index $\lambda = 0$ and aspect ratios $a/h = 100$ are displayed in Table 13. The error percentage compared to the three dimensional results produced by Liu et al. [24] vary between 0.03% and 0.09%. The critical buckling loads compare well with three dimensional results produced by Liu et al. [24], as well as the other 2 authors, Yin et al. [34] and Mohammadi and Saidi [31], given that the aspect ratio $a/h = 100$. The error percentage compared to the three dimensional results produced by Uymaz and Aydogdu [26] in Table 14 vary between 0.09% and 6.45%. It is again clear that at increasing aspect ratios, the results compare very well to three dimensional results. At an aspect ratio $a/h = 10$, the error percentage varies between 6.45% and 4.78% with an average percentage error of 5.54%. At an aspect ratio $a/h = 20$, the error percentage varies between 2.10% and 1.26% with an average error percentage of 1.64%. This translates into an average improvement of 3.90% (5.54% - 1.64%) from an aspect ratio $a/h = 10$ to an aspect ratio $a/h = 20$. A further average improvement of 1.28% is realised at an aspect ratio $a/h = 50$. At an aspect ratio $a/h = 50$, the authors results appear to converge and remain constant for an aspect ratio $a/h = 100$. It is again evident that the present theory produces results which over estimate the buckling loads, as before. In addition, the results illustrate the effect of the displacement of the neutral axis and resulting increased curvature as detailed in Appendix B, in which the error percentages are at their minima between a volume index $\lambda = 0.5$ and $\lambda = 1$.

The non-dimensional critical buckling load of four (4) modes shapes for a plate with an aspect ratio $a/h = 100$ and volume index $\lambda = 0$ is displayed in Table 15. The error percentage compared to the three dimensional results produced by Uymaz and Aydogdu [26] vary

between 0.25% and -7.86%. The results illustrate that the non-dimensional critical buckling load increases with increasing mode shapes. The error percentage compares very well with the three dimensional results by Uymaz and Aydogdu [26] except for the (4;1) mode shape load case. The results of the present study compare very well, given that the aspect ratio a/h = 100 and therefore, through-thickness shear strain and the associated energy contributes insignificantly to the total internal strain energy. Interestingly, the error percentage for the mode shape (4;1) is -7.86% which indicates a lower non-dimensional buckling load. This however, is contrary to the expectation that the present study should over approximate the non-dimensional buckling load at higher mode shapes, given the additional shear strain energy induced by the four (4) half waves. There is no obvious reason for this discrepancy at this stage.

Tables 16 and 17 display the biaxial critical buckling load of plates with varying volume index λ. Much of the observations for the uniaxial critical buckling load in Table 14 for similar load cases apply to the biaxial critical buckling load results. The error percentages compared to the three dimensional results produced by Uymaz and Aydogdu [26] in Table 16 vary between 0.09% and 6.50%, with results comparing very well at greater aspect ratios. It is once again clear that the present theory produces results which over estimate the buckling loads, as before, and the results of the present theory remain constant with varying aspect ratio a/h as a result of neglecting the through-thickness shear strains. The biaxial critical buckling load is again, greatest at a volume index λ = 0 and decreases with increasing volume index λ, similarly with uniaxial critical buckling load. Table 17 displays the biaxial critical buckling load (MN) with a volume index λ = 1. The error percentage compared to the three dimensional results by Asemi et al.[23] vary between 0.37% and 12.39%, closely related to similar figures achieved in Table 10 for similar load cases. It is worth pointing out that the results obtained in Table 17 for the present study compare very well with the CLT results found by Javaheri and Eslami[29]. The results compare well with the three dimensional results found by Asemi et al.[23] at an aspect ratio a/h = 10 and greater. The results of Table 16 and 17 confirm that the present theory is able to establish the biaxial critical buckling load with similar accuracy to that of uniaxial critical buckling load.

6.3 Variation in Natural Frequency with Compressive Load

The natural frequency of a simply supported plate is a function of the end load applied to the plate through Equation 75. The natural frequency of a plate is effected by the end load applied to the plates which reduces its frequency. Figures 6, 7 and 8 graphically represent the variation of the natural frequency as a function of the end load applied to the plates. When no end load is applied, the natural frequency collapses to the fundamental natural frequency for the specific load case. The figures confirm that with increasing volume index λ, the fundamental natural frequency decreases, consistent with previous observations that the plate composition is increasingly metallic which is less stiff than the ceramic material. The variation of natural frequency for both a uniaxial and biaxial end load is displayed in the figures which clearly illustrate the critical buckling loads when the natural frequency is zero. Figures 6 and 8 display a plate with a span ratio $a/b = 1$. The biaxial critical buckling load is half of the uniaxial critical buckling load. However, plates with a span ratio $a/b = 0.5$ do not illustrate the same behaviour, which is confirmed in Figure 7. It can be seen that the biaxial critical buckling load is not half of the uniaxial load, as before. This is because these relationships are effected by changes in the geometric properties and critical buckling modes. Comparison of the natural frequencies for a particular load case with a span ratio $a/b = 0.5$ and $a/b = 1$ reveals a consistent 37.4% decrease in value from $a/b = 1$ to $a/b = 0.5$. This inherently infers a geometric relationship which exists for different geometric properties of the plate. Interestingly, the variation in natural frequency with compressive load is not linear and the natural frequency of the plates reduce significantly as the end load approaches the critical buckling load. Finally, comparing the natural frequencies and critical buckling loads of Figures 6 and 7 for a particular load case, the values for the natural frequency and critical buckling loads for Figure 7 are significantly lower given the span ratio $a/b = 0.5$. This observation is consistent with the results found in Tables 11, 12 and 13.

6.4 Convergence and Curve Fit Accuracy

The results for the natural frequency calculated using CLT are displayed in Table 18. Careful observation shows that for 100000 layers, 1 natural frequency converges to 8 significant figures, 11 of the natural frequencies converge to 5 significant figures, while 1 natural frequency converges to 4 significant figures. Convergence to 5 significant figures for all listed value of λ is only achieved at 100000 layers. At 5000 layers, convergence of about half the results is achieved to 4 significant figures, while the other half of the results show that 100000 layers are needed to get convergence to 5 significant figures. Similarly for the critical buckling load results of CLT displayed in Table 20, after careful analysis, it can be shown that 1 natural frequency converges to 8 significant figures, 11 of the natural frequencies converge to 5 significant figures, while 1 natural frequencies converge to 4 significant figures. There is no apparent trend with volume index λ which would result in convergence to greater significant figures. In addition, by analysing the rate at which the results differ from 50000 layers to 100000 layers, it is reasonable to expect that not all results have converged to the said number of significant figures and that convergence may only occur for a greater number of discretization layers. The results for natural frequency using the present study for the same load case are displayed in Table 19. By contrast, the results illustrate that at a polynomial fit error percentage of 0.05%, 5 of the natural frequencies converge to 8 significant figures, 2 of the natural frequencies converge to 7 significant figures and 6 natural frequencies converge to 6 significant figures. In addition, it is clear that at least 6 results have fully converged at a polynomial fit error percentage of 0.05%, and possibly more since the rate of change of various of the results vary by only slightly at the 7th significant figure. Finally, careful consideration of the critical buckling load results of the present study displayed in Table 21 clearly illustrates 9 of the critical buckling loads converge to 8 significant figures, while 3 natural frequencies converge to 6 significant figures and 1 to 4 significant figures. Most of these results have clearly converged between a polynomial fit error percentage of between 1% and 0.2%. In addition and similarly to the natural frequency results for the present study, there is a possibility that some results have already converged which only possess 6 significant figures, given the rate of change of various of the results that vary only slightly at the 7th significant figure. Taking into consideration the results, it is clear that the present study obtains results which converge faster than CLT albeit, using greater computational effort in terms of time. To enable the comparison of the results to be truly comparable, there needs to be a method by which the number of discretization layers is equivalent to the polynomial fit error percentage. If the number of layers is considered and assuming a discretization of 100 layers is used by way of an example, then the error may be estimated as 1/100 which would equate to 0.01. However, this error would then need to be halved since the error would be the difference between the mid-point of the two layers and therefore, 0.005. Conversion of the decimal to a percentage translates to 0.5%. Thus, for a polynomial fit error percentage

of 0.05%, the equivalent number of layers for the results of CLT would equate to 2000 layers. Should this argument be valid as an approximation, then the present theory is by far superior with regards to the convergence of the results.

The results of Table 19 and 21 contain the error percentages between a polynomial fit error percentage limit of 0.05% and the equivalent results for CLT using 100000 layers for the natural frequency and critical buckling load respectively. The critical buckling load results of the present study illustrate lower loads, and thus better results for all values of volume index λ. However, for the natural frequency case, this does not hold true. Interestingly, for a volume index $\lambda = 0.2$ to $\lambda = 1$, the results illustrate that CLT produces better results than the present study. This observation would imply that for a linear and moderately smooth variation of through-thickness properties, CLT produces better results. On further analysis, it is clear that the discrepancy lies within the x and y in-plane accelerations which contain Γ_u and Γ_v of Equation 59 respectively. Using the CLT analysis reveals that the second term in the integral degenerates to zero whereas for the present study, this term is a small negative value. As a result of CLT having a zero value for the analysis of natural frequencies, the divisor of Equation 59 is increased in comparison to the present study, which then leads to a smaller value for natural frequency. However, for aggressive changes in the through-thickness properties of the plate governed by the very large or small values for volume index λ, the present study appears to model these in-plane affects better and although the second term in the integral degenerates to zero when using CLT, the other two terms in the integral appear to increase to a greater extent, offsetting the disappearance of the negative value contribution by the second term. This ultimately leads to the present study producing lower, and therefore better results for volume indices which induce rapid changes in through-thickness properties when compared to CLT. The exact reason for the second terms of Γ_u and Γ_v of Equation 59 degenerating to zero is not clear. This observation is not applicable to the critical buckling load results since the analysis of the critical buckling load does not contain these terms and as a result, the critical buckling load results for the present study are better than for CLT irrespective of the value of volume index λ. Finally, should the comparability argument between discretization layers being equivalent to the polynomial fit error percentage, then the results achieved by the present study are more accurate and therefore, superior to the results achieved by CLT. This would indicate that the present study produces natural frequency and critical bucking load results which are more accurate and which converge faster than CLT.

7 Conclusions

An extension to CLT has been presented to analyse the natural frequencies and critical buckling loads of simply supported functionally graded material plates. The governing equations for the natural frequency and critical buckling load consider the variation of properties through either the rule of mixtures or the Mori-Tanaka Homogenization method and are derived using Classical Lamination Theory and consequently solved with the Rayleigh-Ritz method. The natural frequency and critical buckling loads are determined for various load cases by exploring the effects of the volume index λ and aspect ratio a/h for various materials, modes and directional loadings respectively. The accuracy thereof is validated against 2D, 3D and quasi-3D solutions found in literature and found to compare well with 3D and quasi-3D results when the aspect ratio is greater than or equal to $a/h = 20$. In addition, the results indicate that plates with an aspect ratio $a/h = 20$ are not influenced by in-plane inertial energy. A comparison with CLT found that the present study produces natural frequency and critical bucking load results which are more accurate and which converge faster than CLT. Validation results demonstrate that the present method has sufficient accuracy for many practical engineering applications regarding moderately thick to thin functionally graded plates.

8 Recommendations

The following recommendations have been made for consideration and further research:

- Develop a set of non-dimensional curves and/or equations (similar to affinity/similarity laws) for engineering design purposes. This theory may be applied to simply calculate the natural frequency or buckling load for a given volume index λ, aspect ratio a/h and span ratio a/b.
- Develop the present theory to accommodate various plate boundary conditions using other approximation methods such as a polynomial series for trial functions as developed by Baharlou and Leissa [40].

References

[1] M. S. El-Wazery and A. R. El-Desouky. 'A review on functionally graded ceramic-metal materials'. In: *Journal of Materials and Environmental Science* 6.5 (2015), pp. 1369–1376. ISSN: 20282508.

[2] R. M. Mahamood et al. 'Functionally Graded Material: An Overview'. In: III (2012), pp. 2–6. ISSN: 9881925223.

[3] I. Bharti, N. Gupta and K. M. Gupta. 'Novel applications of functionally graded nano, optoelectronic and thermoelectric materials.' In: *International Journal of Materials, Mechanics and Manufacturing* 1.3 (2013), pp. 221–224. ISSN: 1793-8198. DOI: 10.7763/IJMMM.2013.V1.47.

[4] G. Udupa, S. S. Rao and K. Gangadharan. 'Functionally Graded Composite Materials: An Overview'. In: *Procedia Materials Science* 5 (2014), pp. 1291–1299. ISSN: 22118128. DOI: 10.1016/j.mspro.2014.07.442.

[5] K. Swaminathan et al. 'Stress, vibration and buckling analyses of FGM plates-A state-of-the-art review'. In: *Composite Structures* 120 (2015), pp. 10–31. ISSN: 0263-8223. DOI: 10.1016/j.compstruct.2014.09.070.

[6] L. W. Byrd. 'Modeling and Analysis of Functionally Graded Materials'. In: 60.September (2007), pp. 195–216. DOI: 10.1115/1.2777164.

[7] S. S. Vel and R. Batra. 'Three-dimensional exact solution for the vibration of functionally graded rectangular plates'. In: *Journal of Sound and Vibration* 272.3-5 (2004), pp. 703–730. ISSN: 0022460X. DOI: 10.1016/S0022-460X(03)00412-7.

[8] T. Mori and K. Tanaka. 'Average stress in matrix and average elastic energy of materials with misfitting inclusions'. In: *Acta Metallurgica* 21.5 (1973), pp. 571–574. ISSN: 00016160. DOI: 10.1016/0001-6160(73)90064-3.

[9] A. M. A. Neves et al. 'Static, free vibration and buckling analysis of isotropic and sandwich functionally graded plates using a quasi-3D higher-order shear deformation theory and a meshless technique'. In: *Composites Part B: Engineering* 44.1 (2013), pp. 657–674. ISSN: 13598368. DOI: 10.1016/j.compositesb.2012.01.089.

[10] S. S. Akavci and A. H. Tanrikulu. 'Static and free vibration analysis of functionally graded plates based on a new quasi-3D and 2D shear deformation theories'. In: *Composites Part B: Engineering* 83 (2015), pp. 203–215. ISSN: 13598368. DOI: 10.1016/j.compositesb.2015.08.043.

[11] A. M. A. Neves et al. 'A quasi-3D sinusoidal shear deformation theory for the static and free vibration analysis of functionally graded plates'. In: *Composites Part B: Engineering* 43.2 (2012), pp. 711–725. ISSN: 13598368. DOI: 10.1016/j.compositesb.2011.08.009.

[12] M. Rashidi Moghaddam and G. H. Baradaran. 'Three-dimensional free vibrations analysis of functionally graded rectangular plates by the meshless local Petrov-Galerkin (MLPG) method'. In: *Applied Mathematics and Computation* 304 (2017), pp. 153–163. ISSN: 00963003. DOI: 10.1016/j.amc.2017.01.049.

[13] H. Matsunaga. 'Free vibration and stability of functionally graded plates according to a 2-D higher-order deformation theory'. In: *Composite Structures* 82.4 (2008), pp. 499–512. ISSN: 0263-8223. DOI: https://doi.org/10.1016/j.compstruct.2007.01.030.

[14] Z. Belabed et al. 'An efficient and simple higher order shear and normal deformation theory for functionally graded material (FGM) plates'. In: *Composites Part B: Engineering* 60 (2014), pp. 274–283. ISSN: 1359-8368. DOI: https://doi.org/10.1016/j.compositesb.2013.12.057.

[15] S. A. Sheikholeslami and A. R. Saidi. 'Vibration analysis of functionally graded rectangular plates resting on elastic foundation using higher-order shear and normal deformable plate theory'. In: *Composite Structures* 106 (2013), pp. 350–361. ISSN: 0263-8223. DOI: https://doi.org/10.1016/j.compstruct.2013.06.016.

[16] L. F. Qian, R. C. Batra and L. M. Chen. 'Static and dynamic deformations of thick functionally graded elastic plates by using higher-order shear and normal deformable plate theory and meshless local Petrov-Galerkin method'. In: *Composites Part B: Engineering* 35.6-8 (2004), pp. 685–697. ISSN: 13598368. DOI: 10.1016/j.compositesb.2004.02.004.

[17] S. Hosseini-Hashemi, M. Fadaee and S. R. Atashipour. 'Study on the free vibration of thick functionally graded rectangular plates according to a new exact closed-form procedure'. In: *Composite Structures* 93.2 (2011), pp. 722–735. ISSN: 0263-8223. DOI: https://doi.org/10.1016/j.compstruct.2010.08.007.

[18] P. Zhu and K. Liew. 'Free vibration analysis of moderately thick functionally graded plates by local Kriging meshless method'. In: *Composite Structures* 93.11 (2011), pp. 2925–2944. ISSN: 02638223. DOI: 10.1016/j.compstruct.2011.05.011.

[19] A. Benachour et al. 'A four variable refined plate theory for free vibrations of functionally graded plates with arbitrary gradient'. In: *Composites Part B: Engineering* 42.6 (2011), pp. 1386–1394. ISSN: 1359-8368. DOI: https://doi.org/10.1016/j.compositesb.2011.05.032.

[20] A. H. Baferani, A. R. Saidi and E. Jomehzadeh. 'An exact solution for free vibration of thin functionally graded rectangular plates'. In: *Proceedings of the Institution of Mechanical Engineers, Part C: Journal of Mechanical Engineering Science* 225.3 (2011), pp. 526–536. ISSN: 0954-4062. DOI: 10.1243/09544062JMES2171.

[21] Y. Kumar. *The Rayleigh–Ritz method for linear dynamic, static and buckling behavior of beams, shells and plates: A literature review*. 2018. DOI: 10.1177/1077546317694724.

[22] S.-R. Li, X. Wang and R. C. Batra. 'Correspondence Relations Between Deflection, Buckling Load, and Frequencies of Thin Functionally Graded Material Plates and Those of Corresponding Homogeneous Plates'. In: *Journal of Applied Mechanics* 82.11 (2015), p. 111006. ISSN: 0021-8936. DOI: 10.1115/1.4031186.

[23] K. Asemi et al. 'A full compatible three-dimensional elasticity element for buckling analysis of FGM rectangular plates subjected to various combinations of biaxial normal and shear loads'. In: *Finite Elements in Analysis and Design* 74 (2013), pp. 9–21. ISSN: 0168874X. DOI: 10.1016/j.finel.2013.05.011.

[24] S. Liu et al. 'Analysis of functionally graded plates by a simple locking-free quasi-3D hyperbolic plate isogeometric method'. In: *Composites Part B: Engineering* 120 (2017), pp. 182–196. ISSN: 13598368. DOI: 10.1016/j.compositesb.2017.03.061.

[25] H. T. Thai and D. H. Choi. 'An efficient and simple refined theory for buckling analysis of functionally graded plates'. In: *Applied Mathematical Modelling* 36.3 (2012), pp. 1008–1022. ISSN: 0307904X. DOI: 10.1016/j.apm.2011.07.062.

[26] B. Uymaz and M. Aydogdu. 'Three dimensional shear buckling of FG plates with various boundary conditions'. In: *Composite Structures* 96 (2013), pp. 670–682. ISSN: 02638223. DOI: 10.1016/j.compstruct.2012.08.031.

[27] B. Uymaz and M. Aydogdu. 'Three dimensional mechanical buckling of FG plates with general boundary conditions'. In: *Composite Structures* 96 (2013), pp. 174–193. ISSN: 02638223. DOI: 10.1016/j.compstruct.2012.07.033.

[28] B. A. Shariat and M. R. Eslami. 'Buckling of thick functionally graded plates under mechanical and thermal loads'. In: *Composite Structures* 78.3 (2007), pp. 433–439. ISSN: 02638223. DOI: 10.1016/j.compstruct.2005.11.001.

[29] R. Javaheri and M. R. Eslami. 'Buckling of functionally graded plates under in-plane compressive loading'. In: *ZAMM Zeitschrift fur Angewandte Mathematik und Mechanik* 82.4 (2002), pp. 277–283. ISSN: 00442267. DOI: 10.1002/1521-4001(200204)82:4<277::AID-ZAMM277>3.0.CO;2-Y.

[30] M. Bodaghi and A. R. Saidi. 'Levy-type solution for bending-stretching of thick functionally graded rectangular plates based on higer-order shear deformation theory'. In: *Applied Mathematical Modelling* 34.11 (2010), pp. 3659–3673. ISSN: 15376494. DOI: 10.1080/15376494.2011.563409.

[31] M. Mohammadi, A. R. Saidi and E. Jomehzadeh. 'Levy Solution for Buckling Analysis of Functionally Graded Rectangular Plates'. In: *Applied Composite Materials* 17.2 (2010), pp. 81–93. ISSN: 0929-189X. DOI: 10.1007/s10443-009-9100-z.

[32] K. Kulkarni, B. N. Singh and D. K. Maiti. 'Analytical solution for bending and buckling analysis of functionally graded plates using inverse trigonometric shear deformation theory'. In: *Composite Structures* 134 (2015), pp. 147–157. ISSN: 02638223. DOI: 10.1016/j.compstruct.2015.08.060.

[33] T.-K. Nguyen. 'A higher-order hyperbolic shear deformation plate model for analysis of functionally graded materials'. In: *International Journal of Mechanics and Materials in Design* 11.2 (2015), pp. 203–219. ISSN: 1569-1713. DOI: 10.1007/s10999-014-9260-3.

[34] S. Yin et al. 'Isogeometric locking-free plate element: A simple first order shear deformation theory for functionally graded plates'. In: *Composite Structures* 118.1 (2014), pp. 121–138. ISSN: 02638223. DOI: 10.1016/j.compstruct.2014.07.028.

[35] R. G. Reid and R. Paskaramoorthy. 'An extension to classical lamination theory for use with functionally graded plates'. In: *Composite Structures* 93.2 (2011), pp. 639–648. ISSN: 02638223. DOI: 10.1016/j.compstruct.2010.08.015.

[36] Y. Benveniste. 'A new approach to the application of Mori-Tanaka's theory in composite materials'. In: *Mechanics of Materials* 6.2 (1987), pp. 147–157. ISSN: 01676636. DOI: 10.1016/0167-6636(87)90005-6.

[37] A. T. Nettles. *Basic Mechanics of Laminated Composite Plates*. Alabama, 1994.

[38] J. R. Barber. *Intermediate mechanics of materials*. Vol. 175. 2011, pp. 1–633. ISBN: 9789400702943. DOI: 10.1007/978-94-007-0295-0_1.

[39] A. Collop. *Structural vibration*. Vol. 19. 4. Elsevier Ltd., 2002, pp. 338–339. DOI: 10.1016/s0141-0296(97)83369-x.

[40] B. Baharlou and A. Leissa. 'Vibration and buckling of generally laminated composite plates with arbitrary edge conditions.' In: *International Journal of Mechanical Sciences* 29.8 (1987), pp. 545–555.

A Input Parameters and Constituent Properties

The standard input parameters used in the software code for the analysis are listed in Table 22.

Table 22: Standard input parameters.

Parameter	Software Code Variable	Value
Number of Linearly Spaced Vectors for Polynomial Fit	NumPts	1000 [-]
Polynomial Fit Error Percentage	ErrorPercentage	0.1 [%]
Location of Mid-Plane	zBar	0 [mm]
First Mode Parameter	m	1 [-]
Second Mode Parameter	p	1 [-]

The material property values used in the analysis are listed in Table 23.

Table 23: Material properties of plate constituents.

Ceramic	E [GPa]	ν	ρ [kg/m^3]	E/ρ [10^6m^{2}s^{-2}]
Aluminium Oxide, Al_2O_3	380.00	0.30	3800	100
Zirconium Dioxide, ZrO_2	200.00	0.30	5700	35.08
Silicon Nitride, Si_3N_4	348.43	0.24	2370	147.01
Silicon Carbide, SiC	420.00	0.30	3100	135.48
Metal	E [GPa]	ν	ρ [kg/m^3]	E/ρ [10^6m^{2}s^{-2}]
Aluminium, Al	70.00	0.30	2702	25.90
Stainless Steel, SUS304	201.04	0.3262	8166	24.61

Note : Material property values taken from appropriate literature used in the results comparison.

The values listed in Table 22 and 23 may be found in the software code displayed in Appendix C and users are prompted to specify the relevant material for the appropriate load case.

B Bending Stiffness Matrix Investigation

The following section illustrates the effect on the bending stiffness matrix, $\overline{D}$ matrix, due to the shifting neutral axis from the mid-plane. The D matrix terms are calculated about the plate mid-plane. However, since the plate's neutral axis moves away from the mid-plane when there is a difference in stiffness between the top and bottom surfaces of the plate, there is a need to reformulate and calculate the D matrix terms about the neutral axis. This reformulated D matrix is referred to as $\overline{D}$. Figure 13 illustrates how Young's modulus, E, the $D(1,1)$ and the $\overline{D}(1,1)$ terms vary with λ. The Young's modulus, E, varies throughout the thickness so an average value has been used.

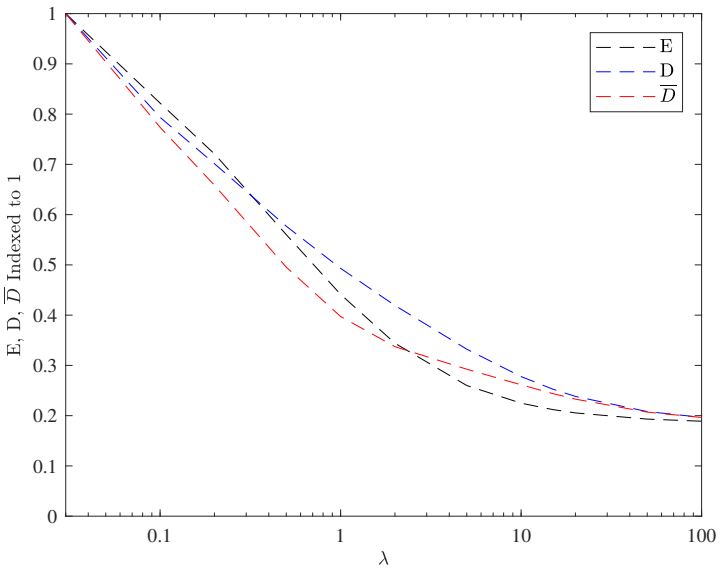


Figure 13: Variation of E, D matrix, $\overline{D}$ matrix with λ

Analysis of the figure illustrates that at and around $\lambda = 1$, the difference between $D(1,1)$ and $\overline{D}(1,1)$ is greatest. This is confirmed by Figure 14, which illustrates the displacement between the mid-plane and the neutral axis, $\widehat{z}_n$. It can be seen that the displacement of the neutral axis peaks at around $\lambda = 1$ and $\lambda = 2$, following which, it approaches zero again. The negative displacement as indicated confirms that the neutral axis moves upwards toward the top surface which is the ceramic surface as illustrated in Figure 4 in Section 4.1.

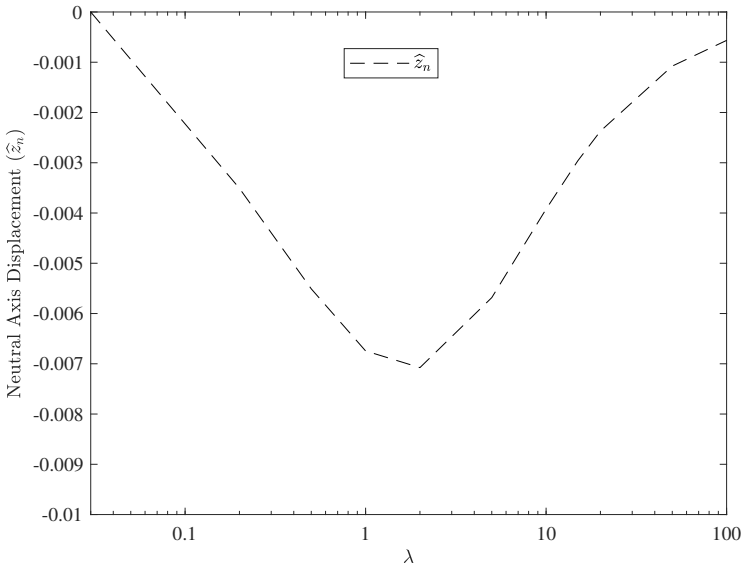


Figure 14: Displacement of the neutral axis from mid-plane with λ

The implications of the neutral axis being displaced from the mid-plane is that $\overline{D}$ matrix has lower values at around $\lambda = 1$ and $\lambda = 2$. A lower bending stiffness matrix results in a greater curvature in the plate. This would therefore, imply that the plate would experience a greater bending strain and as a result, the bending strain will be a significantly greater proportion of the total internal strain energy in the plate, while the through-thickness strains diminish in significance.

The software code used to establish the figures in this section follows.

D Matrix Investigation

General descritpion of each section:

- ANALYSIS - Calculates the values of E, D(1,1) and DBar (1,1) for a range of through-thickness variations.
- PLOTS - Specifies the plot properties used to generate the plots.

Contents

- ANALYSIS
- PLOTS

ANALYSIS

Calculates the values of E, D(1,1) and DBar (1,1) for a range of through-thickness variations.

```
clear all % Clears the Workspace of all variables.
clc % Clears the Command Window.

load('InvestigationInputNF') % Loads the standard load case parameters

ErrorPercentage = 1; % Specifies the error percetage (greater error percentage accepted, analysis is purely visual).
LambdaArray = [0,0.1,0.2,0.5,1,2,5,10,15,20,50,100]; % Array for the variation of material properties.
CountLambda = numel(LambdaArray); % Counts the number of elements in the array.
EMax = zeros(1,CountLambda); % Defines size of matrix to save time and memory.
DArray = zeros(1,CountLambda); % Defines size of matrix to save time and memory.
DBarArray = zeros(1,CountLambda); % Defines size of matrix to save time and memory.
zbarxArray = zeros(1,CountLambda);

%For Loop For Volume Indices%
for y = 1:CountLambda % For loop for the variation of material properties.

        k = LambdaArray(1,y);
        PolynomialFit % Run script Polynomial Fit.
        ABDMatrices % Run script ABDMatrices.
        RayleighRitz % Run script RayleighRitz.
        zbarxArray(1,y) = zbarx; % Defines array to store values for zbarx.
        EMax(1,y) = mean(E)/Ec; % Finds th emean value of the Young's modulus array.
        if y == 1 % First value.
            DMax = D(1,1); % Specifies the largest value of D(1,1)
            DArray(1,y) = 1; % Indexed value starts at 1.
        else
            DArray(1,y) = D(1,1)/DMax; % Indexes all D values after the first.
        end
        if y == 1 % First value.
            DBarMax = DBar(1,1); % Specifies the largest value of DBar(1,1)
            DBarArray(1,y) = 1; % Indexed value starts at 1.
        else
            DBarArray(1,y) = DBar(1,1)/DBarMax; % Indexes all DBar values after the first.
        end
end

LambdaArray(1,1) = 3*10^-2; % Allows for plotting a log plot with a value of zero at the x axis.
```

PLOTS

Specifies the plot properties used to generate the plots.

```
%Present Study Plot Properties%
figure (5) % Opens plot in a sepearate window.
box on %Applies plot border.
semilogx(LambdaArray,EMax,'--k'); % Plots the polynomial density at each point within the plate.
hold on
semilogx(LambdaArray,DArray,'--b'); % Plots the polynomial density at each point within the plate.
hold on
semilogx(LambdaArray,DBarArray,'--r'); % Plots the polynomial density at each point within the plate.
axis([0 100 0 1]) %sets the limits for the x- and y-axis of the current axes
set(gca, 'FontName', 'Times New Roman') % Sets plot font type.
ylabel('E, D, $\overline{D}$ Indexed to 1','Interpreter','Latex','FontSize',10); % Inserts a y-axis label.
xlabel('$\lambda$','Interpreter','Latex','FontSize',10); % Inserts a x-axis label.
legend({'E','D','$\overline{D}$'},'Interpreter','latex','FontSize',10); % Adds a legend to the plot.
set(gca,'XTickLabel',{'0.1','1','10','100'}) % Sets x label ticks.

figure (6) % Opens plot in a sepearate window.
box on %Applies plot border.
semilogx(LambdaArray,zbarxArray,'--k'); % Plots the polynomial density at each point within the plate.
axis([0 100 -0.01 0]) %sets the limits for the x- and y-axis of the current axes
set(gca, 'FontName', 'Times New Roman') % Sets plot font type.
ylabel('Neutral Axis Displacement ($\widehat{z}_n$)','Interpreter','Latex','FontSize',10); % Inserts a y-axis label.
xlabel('$\lambda$','Interpreter','Latex','FontSize',10); % Inserts a x-axis label.
legend({'$\widehat{z}_n$'},'Interpreter','latex','FontSize',10); % Adds a legend to the plot.
set(gca,'XTickLabel',{'0.1','1','10','100'}) % Sets x label ticks.
```

Published with MATLAB® R2017a

C Input Code

The following section provides the software code used to prompt the user for the parameters related to a specific load case for analysis. Material properties and standard input parameters are listed in Section A.

Input

General description of each section:

- STANDARD PARAMETERS - This section has the standard input parameters.
- PROMPTED INPUTS - Prompts the user for various inputs used for the modelling.
- RUN CODES - Runs other scripts to perform the modelling.

Contents

- STANDARD PARAMETERS
- PROMPTED INPUTS
- RUN CODES

STANDARD PARAMETERS

Contains the standard parameters used to perform the modelling. These values may be adjusted as required.

```
clear all % Clears the Workspace of all variables.
clc % Clears the Command Window.

NumPts = 1000; % Number of points used to fit the polynomial.
ErrorPercentage = 0.1; % The allowable absolute error percentage at each point of the polynomial fit.
zBar = 0; % Non-dimensional midplane of the laminate.

m=1; % The number of half wave length in the x-direction which determines the mode shape.
p=1; % The number of half wave length in the y-direction which determines the mode shape.
```

PROMPTED INPUTS

Prompts user for various parameters required to perform the modelling

```
LoadingType = menu('Please Select The Type Of Loading:','Natural Frequency','Buckling Load'); % Prompt for type of loading.

    if(LoadingType == 1) % Natural Frequency loading.
        MaterialVariationMethod = menu('Please Select The Material Variation:','Mori-Tanaka Homogenization Method','Law Of Mixtures'); % Method of calculating the effective material properties.
        NondimensionalEquation = menu('Please Select The Correct Non-Dimensional Equation:','Dimensional Natural Frequency','Omega*h*sqrt(Rhom/Em)','Omega*h*sqrt(Rhoc/Ec)','Omega*(a^2)*(1/h)*sqrt(Rhoc/Ec)', 'Omega

    else % Buckling Load
        MaterialVariationMethod = 2; % Law of mixtures is the only method used to calculate the effective material properties.
        NondimensionalEquation = menu('Please Select The Correct Output:','Dimensional Buckling Load','(N*a^2)/((h^3)*Em)','(N*a^2*12(1-vc^2)/(pi^2*h^3*Ec)','(N*a^2*12(1-vc^2)/(h^3*Ec)'); % Select whether the resu
        LoadDirections = menu('Please Select The Load Directions:','Uniaxial','Biaxial','Tension/Compression');
    end

aDimensionType = menu('Please Select The Dimensions of "a":','0.5','1','1.5','2'); % Prompt for dimensions of length of plate in x-direcion

    if(aDimensionType == 1)
        a = 0.5; % Length of the plate in the x-direction.
    elseif (aDimensionType == 2)
        a = 1; % Length of the plate in the x-direction.
    elseif (aDimensionType == 3)
        a = 1.5; % Length of the plate in the x-direction.
    elseif (aDimensionType == 4)
        a = 2; % Length of the plate in the x-direction.
    end

bDimensionType = menu('Please Select The Dimensions of "b":','0.5','1','1.5','2'); % Prompt for dimensions of length of plate in y-direcion

    if(bDimensionType == 1)
        b = 0.5; % Length of the plate in the y-direction.
    elseif (bDimensionType == 2)
        b = 1; % Length of the plate in the y-direction.
    elseif (bDimensionType == 3)
        b = 1.5; % Length of the plate in the y-direction.
     elseif (bDimensionType == 4)
        b = 2; % Length of the plate in the y-direction.
    end

CeramicType = menu('Please Select The Type Of Ceramic:','Aluminium Oxide','Zirconium Dioxide','Silicon Nitride','Silicon Carbide'); % Prompt for type of ceramic used in the modelling.

%Ceramic Properties%
    if(CeramicType == 1)
        Ec = 380*10^9; % Aluminium Oxide (Al2O3) Bulk modulus.
        Rhoc = 3800; % Aluminium Oxide (Al2O3) density.
        PoissonsRatioC = 0.3; %% Aluminium Oxide (Al2O3) Poissons ratio.
    elseif (CeramicType == 2)
        Ec = 200*10^9; % Zirconium Dioxide (ZrO2) Bulk modulus.
        Rhoc = 5700; % Zirconium Dioxide (ZrO2) density.
        PoissonsRatioC = 0.3; % Zirconium Dioxide (ZrO2) Poissons ratio.
    elseif (CeramicType == 3)
        Ec = 348.43*10^9; % Silicon Nitride (Si3N4) Bulk modulus.
        Rhoc = 2370; % Silicon Nitride (Si3N4) density.
        PoissonsRatioC = 0.24; % Silicon Nitride (Si3N4) Poissons ratio.
    elseif (CeramicType == 4)
        Ec = 420*10^9; % Silicon Carbide (SiC) Bulk modulus.
        PoissonsRatioC = 0.3; % Silicon Carbide (SiC) Poissons ratio.
    end

MetalType = menu('Please Select The Type Of Metal:','Aluminium','Stainless Steel'); % Prompt for type of ceramic used in the modelling.

%Metal Properties%
    if(MetalType == 1)
        Em = 70*10^9; % Aluminium (Al) Bulk modulus.
        Rhom = 2702; % Aluminium (Al) density.
        PoissonsRatioM = 0.3; % Aluminium (Al) Poissons ratio.
    elseif (MetalType == 2)
        Em = 201.04*10^9; % Stainless Steel (SUS304) Bulk modulus.
        Rhom = 8166; % Stainless Steel (SUS304) density.
        PoissonsRatioM = 0.3262; % Stainless Steel (SUS304) Poissons ratio.
    end

CeramicVolumeIndex = menu('Please Select The Ceramic Volume Index:','0','0.5','1','2','3','4','5','10'); % Prompt for the extent of the metal variation for the Power Law.

%Ceramic Index Volume Ratio%
    if(CeramicVolumeIndex == 1)
        k = 0; % The extent of the metal variation for the Power Law.
    elseif (CeramicVolumeIndex == 2)
        k = 0.5; % The extent of the metal variation for the Power Law.
    elseif (CeramicVolumeIndex == 3)
        k = 1; % The extent of the metal variation for the Power Law.
    elseif (CeramicVolumeIndex == 4)
        k = 2; % The extent of the metal variation for the Power Law.
    elseif (CeramicVolumeIndex == 5)
        k = 3; % The extent of the metal variation for the Power Law.
    elseif (CeramicVolumeIndex == 6)
        k = 4; % The extent of the metal variation for the Power Law.
    elseif (CeramicVolumeIndex == 7)
        k = 5; % The extent of the metal variation for the Power Law.
    else
        k = 10; % The extent of the metal variation for the Power Law.
```

```
    end

AspectRatio = menu('Please Select The Aspect Ratio:','5','10','20','30','40','50','60','80','100'); % Aspect ratio ie; a/h.
    %Aspect Ratio%
    if(AspectRatio == 1)
        AR = 5; % Determine the correct aspect ratio based on the users selection.
    elseif (AspectRatio == 2)
        AR = 10; % Determine the correct aspect ratio based on the users selection.
    elseif (AspectRatio == 3)
        AR = 20; % Determine the correct aspect ratio based on the users selection.
    elseif (AspectRatio == 4)
        AR = 30; % Determine the correct aspect ratio based on the users selection.
    elseif (AspectRatio == 5)
        AR = 40; % Determine the correct aspect ratio based on the users selection.
    elseif (AspectRatio == 6)
        AR = 50; % Determine the correct aspect ratio based on the users selection.
    elseif (AspectRatio == 7)
        AR = 60; % Determine the correct aspect ratio based on the users selection.
    elseif (AspectRatio == 8)
        AR = 80; % Determine the correct aspect ratio based on the users selection.
    elseif (AspectRatio == 9)
        AR = 100; % Determine the correct aspect ratio based on the users selection.
    end

    h = a/AR; % Calculating the thickness based on the aspect ratio.
```

RUN CODES

Runs the remaining three (3) scripts required to complete the modelling. The three remaining scrpits include the fitting a curve to teh power law and retrieving a polynomial, establishing the ABD matrices and using the Rayleigh Ritz method to perform the required modelling.

```
PolynomialFit % Run script Polynomial Fit.
ABDMatrices % Run script ABDMatrices.
RayleighRitz % Run script RayleighRitz.
```

```
Omega =

    0.0155
```

Published with MATLAB® R2017a

D Polynomial Fit Code

The following section provides the software code used to establish the curve fit of the polynomial for the elastic constants as described in Section 4.1.

Polynomial Fit For Stiffness Matrix and Density

General descritpion of each section:

- VOLUME FRACTION USING POWER LAW - Discretize the volume fraction into a fixed number of non-dimensional points through the thickness of the plate.
- MORI-TANAKA HOMOGENIZATION METHOD - Applies Mori-Tanaka Homogenization method to calculate the effective material properties and elastic constants at each non-dimensional point within the plate thickness.
- LAW OF MIXTURES METHOD - % The Law of Mixtures Method is used to establish the effective material properties and consequently the elastic constants.
- ELASTIC CONSTANT POLYNOMIAL FIT - Fits a curve with polynomial of order zero to the elastic constants at each non-dimensional point within the plate thickness.
- ELASTIC CONSTANT ERROR CALCULATION - Calculates the absolute error percentage at each point within the plate, increases the order of the polynomial until the absolute error is within predefined limits and a visual plot of the error is then displayed.
- ELASTIC CONSTANT VISUAL COMPARISON - A visual plot of the polynomial fit is then displayed for elastic constant Q11.
- DENSITY USING POWER LAW - Discretize the density into a fixed number of non-dimensional points through the thickness of the plate.
- DENSITY POLYNOMIAL FIT - Fits a curve with polynomial of order zero to the density at each non-dimensional point. within the plate thickness.
- DENSITY ERROR CALCULATION - Calculates the absolute error percentage at each point within the plate, increases the order of the polynomial until the absolute error is within predefined limits and a visual plot of the error is then displayed.
- DENSITY VISUAL COMPARISON - A visual plot of the polynomial fit is then displayed for the density.

Contents

- VOLUME FRACTION USING POWER LAW
- MORI-TANAKA HOMOGENIZATION METHOD
- LAW OF MIXTURES METHOD
- ELASTIC CONSTANT POLYNOMIAL FIT
- ELASTIC CONSTANT ERROR CALCULATION
- ELASTIC CONSTANT VISUAL COMPARISON
- DENSITY USING POWER LAW
- DENSITY POLYNOMIAL FIT
- DENSITY ERROR CALCULATION
- DENSITY VISUAL COMPARISON

VOLUME FRACTION USING POWER LAW

Creates a predefined number of points through the thickness of the laminate and evaluates the volume fraction at each point.

```
PtsVector = linspace(-1,1,NumPts+1); % Returns a row vector, PtsVector, of evenly spaced points between non-dimensional values of -1 and 1.
Vc = ((1-PtsVector)/2).^k; % Converted non-dimensional Power Law equation for volume fraction in terms of predefined points between -1 and 1.
```

MORI-TANAKA HOMOGENIZATION METHOD

The Mori-Tanaka Homogenization Method is used to establish the effective material properties and consequently the elastic constants.

```
if(MaterialVariationMethod == 1)

% Converts two known homogenous isotropic elastic properties (Youngs
% modulus and Poisson's ratio) to the bulk and shear modulus for each
% material.
    Km = Em./(3*(1-2*PoissonsRatioM)); % Bulk modulus of metal.
    Kc = Ec./(3*(1-2*PoissonsRatioC)); % Bulk modulus of ceramic.
    Gm = Em./(2*(1+PoissonsRatioM)); % Shear modulus of metal.
    Gc = Ec./(2*(1+PoissonsRatioC)); % Shear modulus of ceramic.

%The Mori-Tanaka Homogenization Method%
    Fm = (Gm.*((9.*Km)+(8.*Gm)))/(6.*(Km+(2.*Gm)));

    K = zeros(1,NumPts+1); % Defines size of matrix to save time and memory.
    G = zeros(1,NumPts+1); % Defines size of matrix to save time and memory.
    v = zeros(1,NumPts+1); % Defines size of matrix to save time and memory.
    E = zeros(1,NumPts+1); % Defines size of matrix to save time and memory.
    PowerLawQ11 = zeros(1,NumPts+1); % Defines size of matrix to save time and memory.
    PowerLawQ12 = zeros(1,NumPts+1); % Defines size of matrix to save time and memory.
    PowerLawQ66 = zeros(1,NumPts+1); % Defines size of matrix to save time and memory.

%Calculation of Elastic Constants at Each Point Using Power Law%
    for j = 1:NumPts+1
        K(:,j) = (((Vc(:,j)).*(Kc-Km))./(1+((1-(Vc(:,j))).*((Kc-Km)./(Km+((4/3)*Gm))))))+Km; %Mori-Tanaka effective Bulk modulus.
        G(:,j) = (((Vc(:,j)).*(Gc-Gm))./(1+((1-(Vc(:,j))).*((Gc-Gm)./(Gm+Fm)))))+Gm; % Mori-Tanaka effective Shear modulus.

        v(:,j) = (3.*K(:,j)-2.*G(:,j))./(2.*(3.*K(:,j)+G(:,j))); %Mori-Tanaka effective Poisson's ratio.
        E(:,j) = (9.*K(:,j).*G(:,j))./((3.*K(:,j))+G(:,j)); %Mori-Tanaka effective Youngs modulus.

        PowerLawQ11(:,j) = E(:,j)./(1-(v(:,j).^2)); %Elastic constant Q11 for power law using effective material properties.
        PowerLawQ12(:,j) = (v(:,j).*E(:,j))./(1-(v(:,j).^2)); %Elastic constant Q12 for power law using effective material properties.
        PowerLawQ66(:,j) = G(:,j); %Elastic constant Q66 for power law using effective material properties.
    end
end
```

LAW OF MIXTURES METHOD

The Law of Mixtures Method is used to establish the effective material properties and consequently the elastic constants.

```
if(MaterialVariationMethod == 2)

PoissonsRatio = zeros(1,NumPts+1); % Defines size of matrix to save time and memory.
%Law of Mixtures Method%
    for j = 1:NumPts+1 %j is a count variable

        E(:,j) = Em+(Ec-Em).*Vc(:,j);
        PoissonsRatio(:,j) = PoissonsRatioM+(PoissonsRatioC-PoissonsRatioM).*Vc(:,j);

        PowerLawQ11(:,j) = E(:,j)./(1-(PoissonsRatio(:,j).^2)); %Q11 Elastic Constant using Effective Material Properties
        PowerLawQ12(:,j) = (PoissonsRatio(:,j).*E(:,j))./(1-(PoissonsRatio(:,j).^2)); %Q12 Elastic Constant using Effective Material Properties
        PowerLawQ66(:,j) = E(:,j)./(2.*(1+PoissonsRatio(:,j))); %Q66 Elastic Constant using Effective Material Properties
    end
end
```

ELASTIC CONSTANT POLYNOMIAL FIT

Fits a curve to the predefined number of points and establishes the coefficients of a polynomial, starting with a zero order polynomial for each elastic constant. The elastic constant is then evaluted using the polynomial. This is repeated for the remaining two elastic constants.

```
PolyOrderElasticConstants = 0; % Polynomial order starting at zero, ie; straight line curve fit.

%Polynomial Fit Trendline To Order of "PolyOrderElasticConstants = 0"%
PolyCoeffQ11 = polyfit(PtsVector,PowerLawQ11,PolyOrderElasticConstants); % Returns the coefficients for the polynomial fit based on the power law points.
PolyCoeffQ12 = polyfit(PtsVector,PowerLawQ12,PolyOrderElasticConstants); % Returns the coefficients for the polynomial fit based on the power law points.
PolyCoeffQ66 = polyfit(PtsVector,PowerLawQ66,PolyOrderElasticConstants); % Returns the coefficients for the polynomial fit based on the power law points.
```

```
PolynomialQ11 = polyval(PolyCoeffQ11,PtsVector); % Returns the Q11 values of the new polynomial at each point for comparison with the power law function.
PolynomialQ12 = polyval(PolyCoeffQ12,PtsVector); % Returns the Q12 values of the new polynomial at each point for comparison with the power law function.
PolynomialQ66 = polyval(PolyCoeffQ66,PtsVector); % Returns the Q66 values of the new polynomial at each point for comparison with the power law function.
```

ELASTIC CONSTANT ERROR CALCULATION

Calculates the percentage error between the value of the elastic constant evaluted using the power law and the polynomial. A while loop is run which increases the order of the polynomial until such time that all the errors at each of the points of the elastic constant fall below a predetermined absolute percentage.

```
%Calculation of Error Percentage Between Polynomial and Power Law%
ErrorQ11 = zeros(1,NumPts+1); % Defines size of matrix to save time and memory.
ErrorQ12 = zeros(1,NumPts+1); % Defines size of matrix to save time and memory.
ErrorQ66 = zeros(1,NumPts+1); % Defines size of matrix to save time and memory.
for j = 1:NumPts+1
    ErrorQ11(:,j) = 100*abs((PowerLawQ11(:,j)-PolynomialQ11(:,j))/PowerLawQ11(:,j)); % Error calculation at each point as a percentage.
    ErrorQ12(:,j) = 100*abs((PowerLawQ12(:,j)-PolynomialQ12(:,j))/PowerLawQ12(:,j)); % Error calculation at each point as a percentage.
    ErrorQ66(:,j) = 100*abs((PowerLawQ66(:,j)-PolynomialQ66(:,j))/PowerLawQ66(:,j)); % Error calculation at each point as a percentage.
end

%Increasing of Polynomial Degree to Decrease Error Percentage%
while (any(~((abs(ErrorQ11)) <= ErrorPercentage)) && any(~((abs(ErrorQ12)) <= ErrorPercentage)) && any(~((abs(ErrorQ66)) <= ErrorPercentage))) %Loop runs while any elastic constant is outside error limits.

    PolyOrderElasticConstants = PolyOrderElasticConstants + 1;% Increasing Order of Polynomial To Reduce Error Percentage.

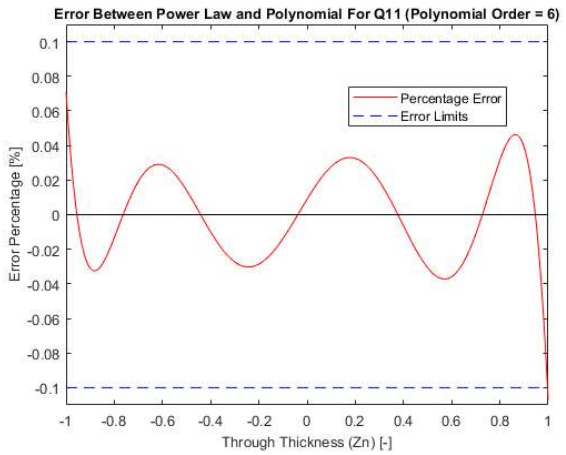
    %Fitting of Polynomial Trendline%
    PolyCoeffQ11 = polyfit(PtsVector,PowerLawQ11,PolyOrderElasticConstants); % Returns the coefficients for the polynomial fit based on the power law points.
    PolyCoeffQ12 = polyfit(PtsVector,PowerLawQ12,PolyOrderElasticConstants); % Returns the coefficients for the polynomial fit based on the power law points.
    PolyCoeffQ66 = polyfit(PtsVector,PowerLawQ66,PolyOrderElasticConstants); % Returns the coefficients for the polynomial fit based on the power law points.

    PolynomialQ11 = polyval(PolyCoeffQ11,PtsVector); % Returns the Q11 values of the new polynomial for comparison with the power law function.
    PolynomialQ12 = polyval(PolyCoeffQ12,PtsVector); % Returns the Q12 values of the new polynomial for comparison with the power law function.
    PolynomialQ66 = polyval(PolyCoeffQ66,PtsVector); % Returns the Q66 values of the new polynomial for comparison with the power law function.

    %Calculation of Error Percentage Between Polynomial and Power Law%
    for j = 1:NumPts+1
        ErrorQ11(:,j) = 100*((PowerLawQ11(:,j)-PolynomialQ11(:,j))/PowerLawQ11(:,j)); % Error calculation at each point as a percentage.
        ErrorQ12(:,j) = 100*((PowerLawQ12(:,j)-PolynomialQ12(:,j))/PowerLawQ12(:,j)); % Error calculation at each point as a percentage.
        ErrorQ66(:,j) = 100*((PowerLawQ66(:,j)-PolynomialQ66(:,j))/PowerLawQ66(:,j)); % Error calculation at each point as a percentage.
    end

end

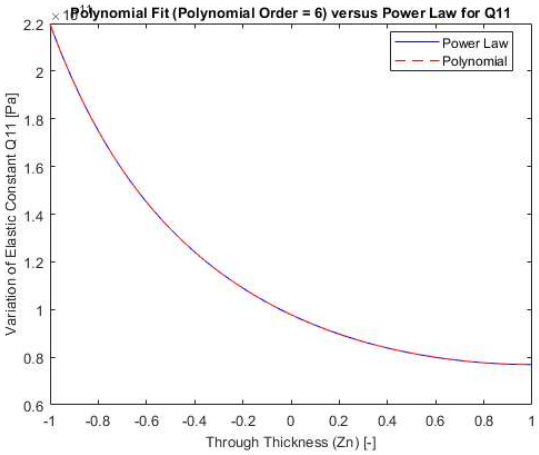
%Plotting of Error Between Polynomial and Power Law Elastic Constant for Comparison%
    figure (1) %Opens plot in a seperate window
    PloterrorQ11 = plot(PtsVector,ErrorQ11,'Color', 'r','LineWidth', 0.5); % Plots the polynomial elastic constant error at each point within the plate.
    title(['Error Between Power Law and Polynomial For Q11 (Polynomial Order = ' num2str(PolyOrderElasticConstants) ')'],'FontSize',10); % Inserts a title.
    xlabel('Through Thickness (Zn) [-]','FontSize',10); % Inserts an x-axis label.
    ylabel('Error Percentage [%]','FontSize',10); % Inserts a y-axis label.
    hline = refline(0,ErrorPercentage); % Inserts the upper error reference line.
        set(hline,'color','b');
        set(hline,'LineStyle','--');
    hline = refline(0,-ErrorPercentage); % Inserts the lower error reference line.
        set(hline,'color','b');
        set(hline,'LineStyle','--');
    hline = refline(0,0.); % Inserts the zero reference line.
        set(hline,'color','k');
        set(hline,'LineStyle','-');
    ylim([-ErrorPercentage*1.1 ErrorPercentage*1.1]) % Sets the y-axis value limits.
    legend('Percentage Error', 'Error Limits','Location','Best') % Adds a legend to the plot.
```



ELASTIC CONSTANT VISUAL COMPARISON

Plots a visual comparison of the variation through the thickness of elastic constant Q11 for both the polynomial function as well as the power law.

```
%Plotting of Elastic Constant Polynomial and Power Law for Comparison%
    figure (2) % Opens plot in seperate window.
    PlotQ11 = plot(PtsVector,PowerLawQ11,'Color', 'b','LineWidth', 0.5); % Plots the power law elastic constant at each point within the plate.
    title(['Polynomial Fit (Polynomial Order = ', num2str(PolyOrderElasticConstants), ') versus Power Law for Q11'],'FontSize',10); % Inserts a title.
    xlabel('Through Thickness (Zn) [-]','FontSize',10); % Inserts an x-axis label.
    ylabel('Variation of Elastic Constant Q11 [Pa]','FontSize',10); % Inserts a y-axis label.
    hold on % Retains current plot when adding a new plot.
    PlotPolynomialQ11 = plot(PtsVector,PolynomialQ11,'--', 'Color','r'); % Plots the polynomial elastic constants at each point within the plate.
    legend([PlotQ11 PlotPolynomialQ11],{'Power Law','Polynomial'},'Location','Best') % Adds a legend to the plot.
```



DENSITY USING POWER LAW

Calculation of density at each point using the Power Law.

```
if(LoadingType == 1)

%Calculation of Density Using Power Law Over Predefined Number of Points%
    PowerLawRho = zeros(1,NumPts+1); % Defines size of matrix to save time and memory.
    for j = 1:NumPts+1 % j is a count variable
        PowerLawRho(:,j) = Rhom + Vc(j)*(Rhoc-Rhom); % Average density calculation equation.
    end
end
```

DENSITY POLYNOMIAL FIT

Fits a curve to the predefined number of points and establishes the coefficients of a polynomial, starting with a zero order polynomial for density. The density is then evaluted using the polynomial.

```
if(LoadingType == 1)

    PolyOrderRho = 0; % Polynomial order starting at zero, ie; straight line curve fit.

%Polynomial Fit Trendline To Order of "PolyOrderRho = 0"%
    PolyCoeffRho = polyfit(PtsVector,PowerLawRho,PolyOrderRho); % Returns the coefficients for the polynomial fit based on the power law points.
    PolynomialRho = polyval(PolyCoeffRho,PtsVector); % Returns the density values of the new polynomial for comparison with the power law function.

end
```

DENSITY ERROR CALCULATION

Calculates the percentage error between the value of the density evaluted using the power law and the polynomial. A while loop is run which increases the order of the polynomial until such time that all the errors at each of the points of the density fall below a predetermined absolute percentage.

```
if(LoadingType == 1)

%Calculation of Error Percentage Between Polynomial and Power Law%
    ErrorRho = zeros(1,NumPts+1); % Defines size of matrix to save time and memory.
    for j = 1:NumPts+1 % For loop runs for each of the predetermined points within the through thickness.
        ErrorRho(:,j) = 100*abs((PowerLawRho(:,j)-PolynomialRho(:,j))/PowerLawRho(:,j)); % Error calculation at each point as a percentage.
    end

%Increasing Order of Polynomial to Decrease Error Percentage%
    while any(~((abs(ErrorRho)) <= ErrorPercentage)) % Loop runs while the density at any point is outside error limits.
        PolyOrderRho = PolyOrderRho + 1;% Increasing order of polynomial in order to reduce error percentage.

    %Fitting of Polynomial Trendline%
        PolyCoeffRho = polyfit(PtsVector,PowerLawRho,PolyOrderRho); % Returns the coefficients for the polynomial fit based on the power law points.

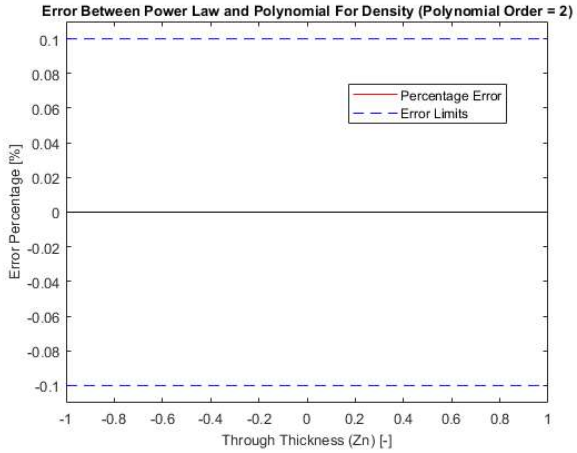
        PolynomialRho = polyval(PolyCoeffRho,PtsVector); % Returns the density values of the new polynomial for comparison with the power law function.

    %Calculation of Error Percentage Between Polynomial and Power Law%
        for j = 1:NumPts+1
            ErrorRho(:,j) = 100*((PowerLawRho(:,j)-PolynomialRho(:,j))/PowerLawRho(:,j)); % Error calculation at each point as a percentage.
        end

    end

%Plotting of Error Between Polynomial and Power Law Densities for Comparison%
    figure (3) % Opens plot in seperate window.
    PlotErrorRho = plot(PtsVector,ErrorRho,'Color', 'r','LineWidth', 0.5); % Plots the polynomial density error at each point within the plate.
    title(['Error Between Power Law and Polynomial For Density (Polynomial Order = ' num2str(PolyOrderRho) ')'],'FontSize',10); % Inserts a title.
    xlabel('Through Thickness (Zn) [-]','FontSize',10); % Inserts an x-axis label.
    ylabel('Error Percentage [%]','FontSize',10); % Inserts a y-axis label.
    hline = refline(0,ErrorPercentage); % Inserts the upper error reference line.
        set(hline,'color','b');
        set(hline,'LineStyle','--');
    hline = refline(0,-ErrorPercentage); % Inserts the lower error reference line.
        set(hline,'color','b');
        set(hline,'LineStyle','--');
    hline = refline(0,0.); % Inserts the zero reference line.
        set(hline,'color','k');
        set(hline,'LineStyle','-');
    ylim([-ErrorPercentage*1.1 ErrorPercentage*1.1]) % Sets the y-axis value limits.
    legend('Percentage Error', 'Error Limits','Location','Best') % Adds a legend to the plot.

end
```



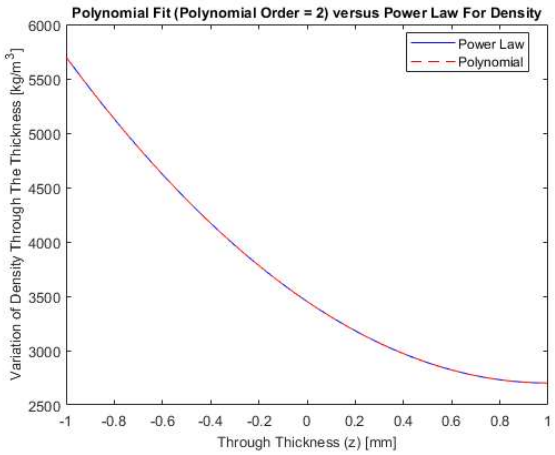
DENSITY VISUAL COMPARISON

Plots a visual comparison of the density variation through the thickness of the plate for both the polynomial as well as the power law.

```
if(LoadingType == 1)

%Plotting of Polynomial and Power Law Densities for Comparison%
    figure (4) % Opens plot in a sepearate window.
    Plotrho = plot(PtsVector,PowerLawRho,'Color', 'b','LineWidth', 0.5); % Plots the power law density at each point within the plate.
    title(['Polynomial Fit (Polynomial Order = ', num2str(PolyOrderRho), ') versus Power Law For Density'],'FontSize',10); % Inserts a title.
    xlabel('Through Thickness (z) [mm]','FontSize',10); % Inserts an x-axis label.
    ylabel('Variation of Density Through The Thickness [kg/m^3]','FontSize',10); % Inserts a y-axis label.
    hold on % Retains current plot when adding a new plot.
    PlotPolynomialRho = plot(PtsVector,PolynomialRho,'--', 'Color','r'); % Plots the polynomial density at each point within the plate.
    legend([Plotrho PlotPolynomialRho],{'Power Law','Polynomial'},'Location','Best') % Adds a legend to the plot.

end
```



Published with MATLAB® R2017a

E ABD Matrices Code

The following section provides the software code used to establish the stiffness matrix as described in Section 4.1.

Establishment of ABD Matrix

General descritpion of each section:

- CALCULATION OF A MATRIX - Performs the summation of matrix A
- CALCULATION OF B MATRIX - Performs the summation of matrix B
- CALCULATION OF D MATRIX - Performs the summation of matrix D
- DISPLAY MATRIX A - Displays the values of matrix A.
- DISPLAY MATRIX B - Displays the values of matrix B.
- DISPLAY MATRIX D - Displays the values of matrix D.

Contents

- CALCULATION OF A MATRIX
- CALCULATION OF B MATRIX
- CALCULATION OF D MATRIX
- DISPLAY MATRIX A
- DISPLAY MATRIX B
- DISPLAY MATRIX D

CALCULATION OF A MATRIX

Calculates the A Matrix.

```
Q11A = 0;
for j = 0:PolyOrderElasticConstants
    TempMatrix = ((1-((-1)^(j+1)))/(j+1))*PolyCoeffQ11(PolyOrderElasticConstants+1-j); % A matrix summation for Q11
    Q11A = TempMatrix + Q11A;
end

Q12A = 0;
for j = 0:PolyOrderElasticConstants
    TempMatrix = ((1-((-1)^(j+1)))/(j+1))*PolyCoeffQ12(PolyOrderElasticConstants+1-j);% A matrix summation for Q12
    Q12A = TempMatrix + Q12A;
end

Q66A = 0;
for j = 0:PolyOrderElasticConstants
    TempMatrix = ((1-((-1)^(j+1)))/(j+1))*PolyCoeffQ66(PolyOrderElasticConstants+1-j);% A matrix summation for Q66
    Q66A = TempMatrix + Q66A;
end

A = (h/2)*[Q11A Q12A 0;Q12A Q11A 0;0 0 Q66A]; % A Matrix
```

CALCULATION OF B MATRIX

Calculates the B Matrix.

```
Q11B = 0;
for j = 0:PolyOrderElasticConstants
    TempMatrix = (((zBar*(1-((-1)^(j+1))))/(j+1))*PolyCoeffQ11(PolyOrderElasticConstants+1-j)) + ((h*(1-((-1)^(j+2))))/(2*(j+2)))*PolyCoeffQ11(PolyOrderElasticConstants+1-j);
    Q11B = TempMatrix + Q11B;
end

Q12B = 0;
for j = 0:PolyOrderElasticConstants
    TempMatrix = (((zBar*(1-((-1)^(j+1))))/(j+1))*PolyCoeffQ12(PolyOrderElasticConstants+1-j)) + ((h*(1-((-1)^(j+2))))/(2*(j+2)))*PolyCoeffQ12(PolyOrderElasticConstants+1-j);
    Q12B = TempMatrix + Q12B;
end

Q66B = 0;
for j = 0:PolyOrderElasticConstants
    TempMatrix = (((zBar*(1-((-1)^(j+1))))/(j+1))*PolyCoeffQ66(PolyOrderElasticConstants+1-j)) + ((h*(1-((-1)^(j+2))))/(2*(j+2)))*PolyCoeffQ66(PolyOrderElasticConstants+1-j);
    Q66B = TempMatrix + Q66B;
end

B = (h/2)*[Q11B Q12B 0;Q12B Q11B 0;0 0 Q66B]; % B Matrix
```

CALCULATION OF D MATRIX

Calculates the D Matrix.

```
Q11D = 0;
for j = 0:PolyOrderElasticConstants
    TempMatrix = ((((zBar^2)*(1-((-1)^(j+1))))/(j+1))*PolyCoeffQ11(PolyOrderElasticConstants+1-j)) + ((h*zBar*(1-((-1)^(j+2))))/((j+2)))*PolyCoeffQ11(PolyOrderElasticConstant
    Q11D = TempMatrix + Q11D;
end

Q12D = 0;
for j = 0:PolyOrderElasticConstants
    TempMatrix = ((((zBar^2)*(1-((-1)^(j+1))))/(j+1))*PolyCoeffQ12(PolyOrderElasticConstants+1-j)) + ((h*zBar*(1-((-1)^(j+2))))/((j+2)))*PolyCoeffQ12(PolyOrderElasticConstant
    Q12D = TempMatrix + Q12D;
end

Q66D = 0;
for j = 0:PolyOrderElasticConstants
    TempMatrix = ((((zBar^2)*(1-((-1)^(j+1))))/(j+1))*PolyCoeffQ66(PolyOrderElasticConstants+1-j)) + ((h*zBar*(1-((-1)^(j+2))))/((j+2)))*PolyCoeffQ66(PolyOrderElasticConstant
    Q66D = TempMatrix + Q66D;
end
```

```
D = (h/2)*[Q11D Q12D 0;Q12D Q11D 0;0 0 Q66D]; % D Matrix
```

DISPLAY MATRIX A

Displays matrix A.

```
disp (A)
```

```
    1.0e+09 *

     7.1427    2.0867         0
     2.0867    7.1427         0
          0         0    2.5280
```

DISPLAY MATRIX B

Displays matrix B.

```
disp (B)
```

```
    1.0e+07 *

     5.0390    1.4483         0
     1.4483    5.0390         0
          0         0    1.7953
```

DISPLAY MATRIX D

Displays matrix D.

```
disp (D)
```

```
    1.0e+06 *

     1.8235    0.5353         0
     0.5353    1.8235         0
          0         0    0.6441
```

Published with MATLAB® R2017a

F Rayleigh Ritz Code

The following section provides the software code used to establish the natural frequency and critical buckling load as described in Section 4.2, 4.3 and 4.4.

Rayleigh Ritz Energy Method

General descritpion of each section:

- ESTABLISHMENT OF NEUTRAL AXIS - Obtains the non-dimensional locations of the neutral axes and amends the D matrix accordingly.
- OUT OF PLANE STRAIN ENERGY - Calculates the strain energy associated with the out-of-plane displacements.
- IN PLANE STRAIN ENERGY - Calculates the strain energy associated with the in plane displacements in the x and y directions.
- EQUILIBRIUM - Equates the strain energy to the potential energy and solves equation for the natural frequency or buckling load.

Contents

- ESTABLISHMENT OF NEUTRAL AXIS
- OUT OF PLANE STRAIN ENERGY
- IN PLANE STRAIN ENERGY
- EQUILIBRIUM

ESTABLISHMENT OF NEUTRAL AXIS

Performs the inverse of the ABD matrices in order to establish the non-dimensional location of th eneutral axis. Lastly, amends the D matrix accordingly.

```
ABDMatrix = [A B;B D]; % Generates the combined ABD matrix.

InvABDMatrix = inv(ABDMatrix); % Inverse function to obtain the inverse of the ABD matrix.

b11 = InvABDMatrix(1,4); % Defines a specific element in the combined matrix.
d11 = InvABDMatrix(4,4); % Defines a specific element in the combined matrix.
b12 = InvABDMatrix(1,5); % Defines a specific element in the combined matrix.
d12 = InvABDMatrix(4,5); % Defines a specific element in the combined matrix.
b13 = InvABDMatrix(3,6); % Defines a specific element in the combined matrix.
d13 = InvABDMatrix(6,6); % Defines a specific element in the combined matrix.

zbarx = -b11/d11; % Non-dimensional location of the neutral axis in the x-direction.
zbary = -b12/d12; % Non-dimensional location of the neutral axis in the y-direction.
zbarz = -b13/d13; % Non-dimensional location of the neutral axis in the z-direction.

DBar = D - zbarx*B; % Modification to the D matrix to account for the location in the neutral axis.
```

OUT OF PLANE STRAIN ENERGY

Calculates the strain energy associated with the out-of-plane displacements.

```
if(LoadingType == 1)

%Strain Energy Due To Accelerations in the Z-Direction%
    VW = (1/((1)-(-1)))*diff(polyval(polyint(PolyCoeffRho), [(-1) (1)])); % Out of plane energy integration and evaluation.
end
```

IN PLANE STRAIN ENERGY

Calculates the strain energy associated with the in plane displacements in the x and y directions.

```
if(LoadingType == 1)

%Strain Energy Due To Accelerations in the X-Direction%
    Vu1 = [0 0 ((1/2)*(-b11/d11)^2)]; % Term 1 of energy equation.
    Vu2 = [0 (b11/d11) 0]; % Term 2 of energy equation.
    Vu3 = [(1/2) 0 0]; % Term 3 of energy equation.
    VU1 = (1/((1)-(-1)))*diff(polyval(polyint(conv(PolyCoeffRho,Vu1)), [(-1) (1)])); % Term 1 in plane energy integration and evaluation.
    VU2 = (1/((1)-(-1)))*diff(polyval(polyint(conv(PolyCoeffRho,Vu2)), [(-1) (1)])); % Term 2 in plane energy integration and evaluation.
    VU3 = (1/((1)-(-1)))*diff(polyval(polyint(conv(PolyCoeffRho,Vu3)), [(-1) (1)])); % Term 3 in plane energy integration and evaluation.
    VU = VU1 + VU2 + VU3; % Summation of all the energy terms.

%Strain Energy Due To Accelerations in the Y-Direction%
    Vv1 = [0 0 ((1/2)*(-b12/d12)^2)]; % Term 1 of energy equation.
    Vv2 = [0 (b12/d12) 0]; % Term 2 of energy equation.
    Vv3 = [(1/2) 0 0]; % Term 3 of energy equation.
    VV1 = (1/((1)-(-1)))*diff(polyval(polyint(conv(PolyCoeffRho,Vv1)), [(-1) (1)])); % Term 1 in plane energy integration and evaluation.
    VV2 = (1/((1)-(-1)))*diff(polyval(polyint(conv(PolyCoeffRho,Vv2)), [(-1) (1)])); % Term 2 in plane energy integration and evaluation.
    VV3 = (1/((1)-(-1)))*diff(polyval(polyint(conv(PolyCoeffRho,Vv3)), [(-1) (1)])); % Term 3 in plane energy integration and evaluation.
    VV = VV1 + VV2 + VV3;% Summation of all the energy terms.

end
```

EQUILIBRIUM

Equates the strain energy to the potential energy and solves equation for the natural frequency or buckling load.

```
%Definition of Parameters%
alpham = (m*pi)/a; % Defines alpham.
betap = (p*pi)/b; % Defines betap.

%Establishment of Stiffness Matrix%
Kmp = (DBar(1,1)*(alpham)^4)+((2*DBar(1,2)+4*DBar(3,3))*((alpham)^2)*((betap)^2))+(DBar(2,2)*((betap)^4)); % Equation for the stiffness matrix.

%Establishment of Mass Matrix and Calculation%
if(LoadingType == 1) % Natural frequency load.
    MmpNF = (h*(VW+(VU)*((h^2)/2)*(alpham^2)+(VV)*((h^2)/2)*(betap^2))); % Equation for the mass matrix.
    %MmpNF = (h*(VW)); % Exclude in-plane accelerations.

    if(NondimensionalEquation == 1) % Non-dimensional output type 1 selected.
        Omega = sqrt(Kmp/MmpNF); % Equation for natural frequency.

    elseif (NondimensionalEquation == 2) % Non-dimensional output type 2 selected.
        Omega = sqrt(Kmp/MmpNF)*h*sqrt(Rhom/Em); % Equation for natural frequency.

    elseif (NondimensionalEquation == 3) % Non-dimensional output type 3 selected.
        Omega = sqrt(Kmp/MmpNF)*h*sqrt(Rhoc/Ec); % Equation for natural frequency.

    elseif (NondimensionalEquation == 4) % Non-dimensional output type 4 selected.
        Omega = sqrt(Kmp/MmpNF)*(a^2)*(1/h)*sqrt(Rhoc/Ec); % Equation for natural frequency.

    else % Non-dimensional output type 5 selected.
        Omega = sqrt(Kmp/MmpNF)*(a^2)*sqrt((12*(1-PoissonsRatioC^2)*Rhoc*h)/(Ec*(h^3))); % Equation for natural frequency.

    end

    display (Omega) % Displays result.
end

if(LoadingType == 2) % Buckling load.

    if(LoadDirections == 1) % Uniaxial buckling load.
        Gamma = 0;
    elseif(LoadDirections == 2) % Biaxial buckling load.
        Gamma = 1;
    elseif(LoadDirections == 3) % Tension/compression buckling load.
        Gamma = -1;
    end

    MmpBL = (alpham^2+Gamma*betap^2); % Equation for the mass matrix.

    if(NondimensionalEquation == 1) % Dimensional output 1 selected.
        N = Kmp/MmpBL; % Equation for buckling load.

    elseif (NondimensionalEquation == 2) % Non-dimensional output type 2 selected.
        N =((Kmp/MmpBL)*a^2)/((h^3)*Em); % Equation for buckling load.

    elseif (NondimensionalEquation == 3) % Non-dimensional output type 2 selected.
        N =(Kmp/MmpBL*(a^2)*12*(1-PoissonsRatioC.^2))/((pi^2)*Ec*(h^3)); % Equation for buckling load.

    elseif (NondimensionalEquation == 4) % Non-dimensional output type 2 selected.
        N =(Kmp/MmpBL*(a^2)*12*(1-PoissonsRatioC.^2))/(Ec*(h^3)); % Equation for buckling load.

    end

    display (N) % Displays result.

end
```

```
Omega =

    0.0155
```

Published with MATLAB® R2017a

G Natural Frequency with Buckling Load Code

The following section provides the software code used to establish the variation of natural frequency with end load as described in Section 4.5.

Natural Frequency with Buckling Load

General description of the section:

- CALCULATION & PLOTTING - This section performs the calculation and plots various load cases on a single plot for comparison.

Contents

- CALCULATION & PLOTTING

CALCULATION & PLOTTING

This section performs the calculation and plots various load cases on a single plot for comparison.

```
Input % Run code for a specific buckling load case.

LoadDirectionSelector = [1,2,1,2,1,2]; % Defines an array specifying uniaxial or biaxial load.
CeramicVolumeIndexSelector = [0,0,1,1,10,10]; % Defines an array for the volume index for the variation of material properties.
PlotMarkerType = ['o','d','o','d','o','d']; % Defines an array for the marker type for the plot.
PlotMarkerColour = ([228, 26, 28;228, 26, 28;0.13*256 0.98*256 0.53*256;0.13*256 0.98*256 0.53*256; 253, 180, 98; 253, 180, 98]/256); % Defines an array for the colour of the markers.
NNumPts = 40; % Defines the number of vectors points plotted for each load case.
MarkerSize = linspace(45,5,40); % Defines a vector for the variation of sizes of the markers being plotted.

Omega = zeros(6,NNumPts); % Defines size of matrix to save time and memory.
Ncr = zeros(6,NNumPts); % Defines size of matrix to save time and memory.

for LCCount = 1:6 % Count variable for the number of load cases bring plotted.

    LoadingType = 2; % Change load type to natural frequency for calculation.
    k = CeramicVolumeIndexSelector(1,LCCount); % Selects the volume index from array CeramicVolumeIndexSelector for the load case.
    LoadDirections = LoadDirectionSelector(1,LCCount); % Selects the buckling type from array LoadDirectionSelector for the load case.

    PolynomialFit % Re-run code to calculate buckling load the specific load case.
    ABDMatrices % Re-run code to calculate buckling load the specific load case.
    RayleighRitz % Re-run code to calculate buckling load the specific load case.
    NVector = linspace(N,0,NNumPts); % Generates NNumPts linearly spaced vectors for buckling load.
    Ncr(LCCount,:) = NVector; % Array with the linearly spaced vectors of buckling load for plotting on the x-axis.

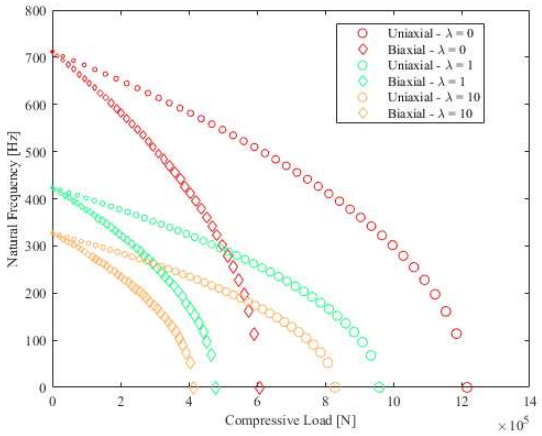
    LoadingType = 1; % Change load type to natural frequency for calculation.
    MaterialVariationMethod = 2; % Change material variation method for natural frequency calculation (Law of Mixtures).
    NondimensionalEquation = 1; % Change output of natural frequency for natural frequency calculation (Hz).

    PolynomialFit; % Re-run code to calculate the specific load case for natural frequency.
    ABDMatrices; % Re-run code to calculate the specific load case for natural frequency.
    RayleighRitz; % Re-run code to calculate the specific load case for natural frequency.

    for NCount = 1:NNumPts % Count for each vector point per load case.
        Omega(LCCount,NCount) = sqrt((Kmp-NVector(:,NCount)*MmpBL)/(h*(VW+(VU)*((h^2)/2)*(alpham^2)+(VV)*((h^2)/2)*(betap^2)))); % Natural frequency calculated for each buckling load vector.
    end

    figure (5) % Opens plot in a sepearate window.
    PlotOmegavsN = scatter(Ncr(LCCount,:),Omega(LCCount,:),MarkerSize,PlotMarkerColour(LCCount,:),PlotMarkerType(1,LCCount)); % Plots the the natural frequency and corresponding buckling load vector.
    hold on % Retains current plot when adding a new plot.
end

box on % Applies plot border.
set(gca, 'FontName', 'Times New Roman') % Sets plot font.
xlabel('Compressive Load [N]','FontSize',10); % Inserts an x-axis label.
ylabel('Natural Frequency [Hz]','FontSize',10); % Inserts a y-axis label.
legend({'Uniaxial - \lambda = 0','Biaxial - \lambda = 0', 'Uniaxial - \lambda = 1', 'Biaxial - \lambda = 1','Uniaxial - \lambda = 10','Biaxial - \lambda = 10'},'Location','Best') % Adds a legend to the plot.
```



Published with MATLAB® R2017a

H Curve Fit Accuracy and Convergence Code

The following section provides the software code used to establish the results for the curve fit accuracy and convergence in Section 5.4.

Convergence and Curve Fit Accuracy

General descritpion of each section:

- CLT ANALYSIS - Calculates the natural frequency or critical buckling load for a particular load case for various volume indices and discretzation layers using CLT.
- VOLUME FRACTION USING POWER LAW - Creates a predefined number of points through the thickness of the laminate and evaluates the volume fraction at each point.
- MORI-TANAKA HOMOGENIZATION METHOD - The Mori-Tanaka Homogenization Method is used to establish the effective material properties and consequently the elastic constants.
- LAW OF MIXTURES METHOD - The Law of Mixtures Method is used to establish the effective material properties and consequently the elastic constants.
- DENSITY USING POWER LAW - Calculation of density at each point using the Power Law and CLT.
- ABD MATRICES - Establishment of the ABD matrix using CLT.
- ESTABLISHMENT OF NEUTRAL AXIS - Performs the inverse of the ABD matrices in order to establish the non-dimensional location of th eneutral axis. Lastly, amends the D matrix accordingly.
- OUT OF PLANE STRAIN ENERGY - Calculates the strain energy associated with the out-of-plane displacements.
- IN PLANE STRAIN ENERGY - Calculates the strain energy associated with the in plane displacements in the x and y directions.
- EQUILIBRIUM - Equates the strain energy to the potential energy and solves equation for the natural frequency or buckling load.
- CLT PLOT - Specifies the plot properties used to generate the plot.
- PRESENT STUDY ANALYSIS - Calculates the natural frequency or critical buckling load for a particular load case for various volume indices and polynomial fit error percentage limits using the present study.
- PRESENT STUDY PLOT - Specifies the plot properties used to generate the plot.

Contents

- CLT ANALYSIS
- VOLUME FRACTION USING POWER LAW
- MORI-TANAKA HOMOGENIZATION METHOD
- LAW OF MIXTURES METHOD
- DENSITY USING POWER LAW
- ABD MATRICES
- ESTABLISHMENT OF NEUTRAL AXIS
- OUT OF PLANE STRAIN ENERGY
- IN PLANE STRAIN ENERGY
- EQUILIBRIUM
- CLT PLOT
- PRESENT STUDY ANALYSIS
- PRESENT STUDY PLOT

CLT ANALYSIS

Calculates the natural frequency or critical buckling load for a particular load case for various volume indices and discretzation layers using CLT.

```
clear all % Clears the Workspace of all variables.
clc % Clears the Command Window.

load('ConvergeInputBL') % Loads the standard load case parameters

DiscretizationLayersCLT = [50,100,200,500,1000,2000,5000,10000,20000,50000,100000]; % Array for the discretization layers.
LambdaArrayCLT = [0,0.1,0.2,0.5,1,2,5,10,12,15,20,50,100]; % Array for the variation of material properties.
CountLambda = numel(LambdaArrayCLT); % Counts the number of elements in the array.
CountIterations = numel(DiscretizationLayersCLT); % Counts the number of elements in the array.
OmegaCLT = zeros(CountLambda,CountIterations); % Defines size of matrix to save time and memory.
NCLT = zeros(CountLambda,CountIterations); % Defines size of matrix to save time and memory.
figure (1) % Opens plot in a sepearate window.
MarkerColour1 = colormap(autumn); % Defines a standard colour set for makers in plots.
MarkerColour2 = colormap(winter); % Defines a standard colour set for makers in plots.
ColourPos = round(linspace(1, 64, CountLambda),0); % Defines a number of positions within the color map vector, used to plot various shades of colour for markers.

for g = 1:CountLambda % For loop for the variation of material properties.

    k = LambdaArrayCLT(1,g); % Variable to define the value of Lambda within the array.

    for f = 1: CountIterations
```

VOLUME FRACTION USING POWER LAW

Creates a predefined number of points through the thickness of the laminate and evaluates the volume fraction at each point.

```
        PtsVector = linspace(-1,1,DiscretizationLayersCLT(f)+1); % Returns a row vector, PtsVector, of evenly spaced points between non-dimensional values of -1 and 1.
        Vc = ((1-PtsVector)/2).^k; % Converted non-dimensional Power Law equation for volume fraction in terms of predefined points between -1 and 1.
```

MORI-TANAKA HOMOGENIZATION METHOD

The Mori-Tanaka Homogenization Method is used to establish the effective material properties and consequently the elastic constants.

```
    if(MaterialVariationMethod == 1)

       % Converts two known homogenous isotropic elastic properties (Youngs
       % modulus and Poisson's ratio) to the bulk and shear modulus for each
       % material.
       Km = Em./(3*(1-2*PoissonsRatioM)); % Bulk modulus of metal.
       Kc = Ec./(3*(1-2*PoissonsRatioC)); % Bulk modulus of ceramic.
       Gm = Em./(2*(1+PoissonsRatioM)); % Shear modulus of metal.
       Gc = Ec./(2*(1+PoissonsRatioC)); % Shear modulus of ceramic.

       %The Mori-Tanaka Homogenization Method%
       Fm = (Gm.*((9.*Km)+(8.*Gm)))/(6.*(Km+(2.*Gm)));

       K = zeros(1,DiscretizationLayersCLT(f)); % Defines size of matrix to save time and memory.
       G = zeros(1,DiscretizationLayersCLT(f)); % Defines size of matrix to save time and memory.
       v = zeros(1,DiscretizationLayersCLT(f)); % Defines size of matrix to save time and memory.
       E = zeros(1,DiscretizationLayersCLT(f)); % Defines size of matrix to save time and memory.
       PowerLawQ11 = zeros(1,DiscretizationLayersCLT(f)); % Defines size of matrix to save time and memory.
       PowerLawQ12 = zeros(1,DiscretizationLayersCLT(f)); % Defines size of matrix to save time and memory.
       PowerLawQ66 = zeros(1,DiscretizationLayersCLT(f)); % Defines size of matrix to save time and memory.

       %Calculation of Elastic Constants at Each Point Using Power Law%
       for j = 1:DiscretizationLayersCLT(f)
           K(:,j) = (((Vc(:,j)).*(Kc-Km))./(1+((1-(Vc(:,j))).*((Kc-Km)./(Km+((4/3)*Gm))))))+Km; %Mori-Tanaka effective Bulk modulus.
           G(:,j) = (((Vc(:,j)).*(Gc-Gm))./(1+((1-(Vc(:,j))).*((Gc-Gm)./(Gm+Fm)))))+Gm; % Mori-Tanaka effective Shear modulus.

           v(:,j) = (3.*K(:,j)-2.*G(:,j))./(2.*(3.*K(:,j)+G(:,j))); %Mori-Tanaka effective Poisson's ratio.
           E(:,j) = (9.*K(:,j).*G(:,j))./((3.*K(:,j))+G(:,j)); %Mori-Tanaka effective Youngs modulus.

           PowerLawQ11(:,j) = E(:,j)./(1-(v(:,j).^2)); %Elastic constant Q11 for power law using effective material properties.
           PowerLawQ12(:,j) = (v(:,j).*E(:,j))./(1-(v(:,j).^2)); %Elastic constant Q12 for power law using effective material properties.
           PowerLawQ66(:,j) = G(:,j); %Elastic constant Q66 for power law using effective material properties.
       end

    end
```

LAW OF MIXTURES METHOD

The Law of Mixtures Method is used to establish the effective material properties and consequently the elastic constants.

```
if(MaterialVariationMethod == 2) % Law of mixtures.

    PoissonsRatio = zeros(1,DiscretizationLayersCLT(f)); % Defines size of matrix to save time and memory.
    %Law of Mixtures Method%
    for j = 1:DiscretizationLayersCLT(f) %j is a count variable

        E(:,j) = Em+(Ec-Em).*Vc(:,j);
        PoissonsRatio(:,j) = PoissonsRatioM+(PoissonsRatioC-PoissonsRatioM).*Vc(:,j);

        PowerLawQ11(:,j) = E(:,j)./(1-(PoissonsRatio(:,j).^2)); %Q11 Elastic Constant using Effective Material Properties
        PowerLawQ12(:,j) = (PoissonsRatio(:,j).*E(:,j))./(1-(PoissonsRatio(:,j).^2)); %Q12 Elastic Constant using Effective Material Properties
        PowerLawQ66(:,j) = E(:,j)./(2.*(1+PoissonsRatio(:,j))); %Q66 Elastic Constant using Effective Material Properties
    end
end
```

DENSITY USING POWER LAW

Calculation of density at each point using the Power Law and CLT.

```
if(LoadingType == 1)

%Calculation of Density Using Power Law Over Predefined Number of Points%
    PowerLawRho = zeros(1,DiscretizationLayersCLT(f)); % Defines size of matrix to save time and memory.
    for j = 1:DiscretizationLayersCLT(f) % j is a count variable.
        PowerLawRho(:,j) = Rhom + Vc(j)*(Rhoc-Rhom); % Average density calculation equation.
    end

    Rho = 0;
    TempRho = zeros(1,DiscretizationLayersCLT(f)); % Defines size of matrix to save time and memory.

    for e = 1:DiscretizationLayersCLT(f) % For loop for the number of discretization layers considered.
    TempRho(1,e) = (PowerLawRho(1,e))*(((h/2)*(PtsVector(1,e+1)))^1 - ((h/2)*(PtsVector(1,e+1)))^1); % Temporary storage of density.
    Rho = Rho + TempRho(1,e); % Density matrix summation.
    end

    Rho = Rho/h; % Average density in plate.
end
```

ABD MATRICES

Establishment of the ABD matrix using CLT.

```
Q11A = 0; % Clears previous value used for calculation.
Q12A = 0; % Clears previous value used for calculation.
Q66A = 0; % Clears previous value used for calculation.
TempQ11A = zeros(1,DiscretizationLayersCLT(f)); % Defines size of matrix to save time and memory.
TempQ12A = zeros(1,DiscretizationLayersCLT(f)); % Defines size of matrix to save time and memory.
TempQ66A = zeros(1,DiscretizationLayersCLT(f)); % Defines size of matrix to save time and memory.

for e = 1:DiscretizationLayersCLT(f)
    TempQ11A(1,e) = (PowerLawQ11(1,e))*(((PtsVector(1,e+1)))^1 - ((PtsVector(1,e)))^1); % Temporary storage of A matrix summation for Q11
    Q11A = Q11A + TempQ11A(1,e); % A matrix summation for Q11
    TempQ12A(1,e) = (PowerLawQ12(1,e))*(((PtsVector(1,e+1)))^1 - ((PtsVector(1,e)))^1); % Temporary storage of A matrix summation for Q12
    Q12A = Q12A + TempQ12A(1,e); % A matrix summation for Q12
    TempQ66A(1,e) = (PowerLawQ66(1,e))*(((PtsVector(1,e+1)))^1 - ((PtsVector(1,e)))^1); % Temporary storage of A matrix summation for Q66
    Q66A = Q66A + TempQ66A(1,e); % A matrix summation for Q66
end
A = (h/2)*[Q11A Q12A 0;Q12A Q11A 0;0 0 Q66A]; %Defines the A matrix.

Q11B = 0; % Clears previous value used for calculation.
Q12B = 0; % Clears previous value used for calculation.
Q66B = 0; % Clears previous value used for calculation.
TempQ11B = zeros(1,DiscretizationLayersCLT(f)+1); % Defines size of matrix to save time and memory.
TempQ12B = zeros(1,DiscretizationLayersCLT(f)+1); % Defines size of matrix to save time and memory.
TempQ66B = zeros(1,DiscretizationLayersCLT(f)+1); % Defines size of matrix to save time and memory.

for e = 1:DiscretizationLayersCLT(f)
    TempQ11B(1,e) = (PowerLawQ11(1,e))*(((h/2)*(PtsVector(1,e+1)))^2 - ((h/2)*(PtsVector(1,e)))^2); % Temporary storage of B matrix summation for Q11
    Q11B = Q11B + TempQ11B(1,e); % B matrix summation for Q11
    TempQ12B(1,e) = (PowerLawQ12(1,e))*(((h/2)*(PtsVector(1,e+1)))^2 - ((h/2)*(PtsVector(1,e)))^2); % Temporary storage of B matrix summation for Q12
    Q12B = Q12B + TempQ12B(1,e); % B matrix summation for Q12
    TempQ66B(1,e) = (PowerLawQ66(1,e))*(((h/2)*(PtsVector(1,e+1)))^2 - ((h/2)*(PtsVector(1,e)))^2); % Temporary storage of B matrix summation for Q66
    Q66B = Q66B + TempQ66B(1,e); % B matrix summation for Q66
end
B = (1/2)*[Q11B Q12B 0;Q12B Q11B 0;0 0 Q66B]; %Defines the B matrix.

Q11D = 0; % Clears previous value used for calculation.
Q12D = 0; % Clears previous value used for calculation.
Q66D = 0; % Clears previous value used for calculation.
TempQ11D = zeros(1,DiscretizationLayersCLT(f)+1); % Defines size of matrix to save time and memory.
TempQ12D = zeros(1,DiscretizationLayersCLT(f)+1); % Defines size of matrix to save time and memory.
TempQ66D = zeros(1,DiscretizationLayersCLT(f)+1); % Defines size of matrix to save time and memory.

for e = 1:DiscretizationLayersCLT(f)
    TempQ11D(1,e) = (PowerLawQ11(1,e))*(((h/2)*(PtsVector(1,e+1)))^3 - ((h/2)*(PtsVector(1,e)))^3); % Temporary storage of D matrix summation for Q11
    Q11D = Q11D + TempQ11D(1,e); % D matrix summation for Q11
    TempQ12D(1,e) = (PowerLawQ12(1,e))*(((h/2)*(PtsVector(1,e+1)))^3 - ((h/2)*(PtsVector(1,e)))^3); % Temporary storage of D matrix summation for Q12
    Q12D = Q12D + TempQ12D(1,e); % D matrix summation for Q12
    TempQ66D(1,e) = (PowerLawQ66(1,e))*(((h/2)*(PtsVector(1,e+1)))^3 - ((h/2)*(PtsVector(1,e)))^3); % Temporary storage of D matrix summation for Q66
    Q66D = Q66D + TempQ66D(1,e); % D matrix summation for Q66
end
D = (1/3)*[Q11D Q12D 0;Q12D Q11D 0;0 0 Q66D]; % Defines the D matrix.
```

ESTABLISHMENT OF NEUTRAL AXIS

Performs the inverse of the ABD matrices in order to establish the non-dimensional location of th eneutral axis. Lastly, amends the D matrix accordingly.

```
ABDMatrix = [A B;B D]; % Generates the combined ABD matrix.

InvABDMatrix = inv(ABDMatrix); % Inverse function to obtain the inverse of the ABD matrix.

b11 = InvABDMatrix(1,4); % Defines a specific element in the combined matrix.
d11 = InvABDMatrix(4,4); % Defines a specific element in the combined matrix.
b12 = InvABDMatrix(1,5); % Defines a specific element in the combined matrix.
d12 = InvABDMatrix(4,5); % Defines a specific element in the combined matrix.
b13 = InvABDMatrix(3,6); % Defines a specific element in the combined matrix.
d13 = InvABDMatrix(6,6); % Defines a specific element in the combined matrix.

zbarx = -b11/d11; % Non-dimensional location of the neutral axis in the x-direction.
zbary = -b12/d12; % Non-dimensional location of the neutral axis in the y-direction.
zbarz = -b13/d13; % Non-dimensional location of the neutral axis in the z-direction.

DBar = D - zbarx*B; % Modification to the D matrix to account for the location in the neutral axis.
```

OUT OF PLANE STRAIN ENERGY

Calculates the strain energy associated with the out-of-plane displacements.

```
    if(LoadingType == 1) % Natural frequency case.

    %Strain Energy Due To Accelerations in the Z-Direction%
        VW = (Rho); % Out of plane energy integration and evaluation.
    end
```

IN PLANE STRAIN ENERGY

Calculates the strain energy associated with the in plane displacements in the x and y directions.

```
    if(LoadingType == 1) % Natural frequency case.

    %Strain Energy Due To Accelerations in the X-Direction%
         Vu1 = [0 0 ((1/2)*(-b11/d11)^2)]; % Term 1 of energy equation.
         Vu2 = [0 (b11/d11) 0]; % Term 2 of energy equation.
         Vu3 = [(1/2) 0 0]; % Term 3 of energy equation.
         VU1 = Rho*(1/((1)-(-1)))*diff(polyval(polyint(Vu1),[(-1) (1)])); % Term 1 in plane energy integration and evaluation.
         VU2 = Rho*(1/((1)-(-1)))*diff(polyval(polyint(Vu2),[(-1) (1)])); % Term 2 in plane energy integration and evaluation.
         VU3 = Rho*(1/((1)-(-1)))*diff(polyval(polyint(Vu3),[(-1) (1)])); % Term 3 in plane energy integration and evaluation.
         VU = (VU1 + VU2 + VU3); % Summation of all the energy terms.

    %Strain Energy Due To Accelerations in the Y-Direction%
         Vv1 = [0 0 ((1/2)*(-b12/d12)^2)]; % Term 1 of energy equation.
         Vv2 = [0 (b12/d12) 0]; % Term 2 of energy equation.
         Vv3 = [(1/2) 0 0]; % Term 3 of energy equation.
         VV1 = Rho*(1/((1)-(-1)))*diff(polyval(polyint(Vv1), [(-1) (1)])); % Term 1 in plane energy integration and evaluation.
         VV2 = Rho*(1/((1)-(-1)))*diff(polyval(polyint(Vv2), [(-1) (1)])); % Term 2 in plane energy integration and evaluation.
         VV3 = Rho*(1/((1)-(-1)))*diff(polyval(polyint(Vv3), [(-1) (1)])); % Term 3 in plane energy integration and evaluation.
         VV = (VV1 + VV2 + VV3);% Summation of all the energy terms.

    end
```

EQUILIBRIUM

Equates the strain energy to the potential energy and solves equation for the natural frequency or buckling load.

```
    %Definition of Parameters%
    alpham = (m*pi)/a; % Defines alpham.
    betap = (p*pi)/b; % Defines betap.

    %Establishment of Stiffness Matrix%
    Kmp = (DBar(1,1)*(alpham)^4)+((2*DBar(1,2)+4*DBar(3,3))*((alpham)^2)*((betap)^2))+(DBar(2,2)*((betap)^4)); % Equation for the stiffness matrix.

    %Establishment of Mass Matrix and Calculation%
    if(LoadingType == 1) % Natural frequency load.
         MmpNF = (h*(VW+(VU)*((h^2)/2)*(alpham^2)+(VV)*((h^2)/2)*(betap^2))); % Equation for the mass matrix.

        if(NondimensionalEquation == 1) % Non-dimensional output type 1 selected.
            OmegaCLT(g,f) = sqrt(Kmp/MmpNF); % Equation for natural frequency.
        end

    end

    if(LoadingType == 2) % Buckling load.

        if(LoadDirections == 1) % Uniaxial buckling load.
            Gamma = 0;
        elseif(LoadDirections == 2) % Biaxial buckling load.
            Gamma = 1;
        elseif(LoadDirections == 3) % Tension/compression buckling load.
            Gamma = -1;
        end

        MmpBL = (alpham^2+Gamma*betap^2); % Equation for the mass matrix.

        if(NondimensionalEquation == 1) % Dimensional output 1 selected.
            NCLT(g,f) = (Kmp/MmpBL)/(1*10^3); % Equation for buckling load.

        end
    end
```

```
    end

    if(LoadingType == 1) % Natural frequency
        loglog(DiscretizationLayersCLT,OmegaCLT(g,:),'o','MarkerEdge',MarkerColour1(ColourPos(g),:),'MarkerSize',5); %Plots the natural frequency for each degree of discretization layer.
        hold on % Keeps the data on the plot graph
    end
    if(LoadingType == 2) % Critical buckling load
        loglog(DiscretizationLayersCLT,NCLT(g,:),'o','MarkerEdge',MarkerColour1(ColourPos(g),:),'MarkerSize',5); %Plots the critical buckling load for each degree of discretization layer.
        hold on % Keeps the data on the plot graph
    end
end
```

CLT PLOT

Specifies the plot properties used to generate the plot.

```
% Classic Lamination Theory Plot Properties%
box on % Applies plot border.
set(gca, 'FontName', 'Times New Roman') % Sets plot font.
xlabel('Number of Discretized Layers','FontSize',10); % Inserts an x-axis label.
set(gca,'xLim',[2 150000]); % Sets the x axis limits.

if(LoadingType == 1) % Natural frequency case.
ylabel('Natural Frequency [Hz]','FontSize',10); % Inserts a y-axis label.
set(gca,'yLim',[1500 3200]); % Sets the y axis limits.
end

if(LoadingType == 2) % Critical buckling load case.
ylabel('Critical Buckling Load [kN]','FontSize',10); % Inserts a y-axis label.
set(gca,'yLim',[1500 9000]);% Sets the y axis limits.
end
legend('\lambda = 0', '\lambda = 0.1','\lambda = 0.2','\lambda = 0.5','\lambda = 1', '\lambda = 2', '\lambda = 5', '\lambda = 5', '\lambda = 10', '\lambda = 12', '\lambda = 20', '\lambda = 50', '\lambda = 100') %
```

PRESENT STUDY ANALYSIS

Calculates the natural frequency or critical buckling load for a particular load case for various volume indices and polynomial fit error percentage limits using the present study.

```
%Parameters%
AccuracyArrayECLT = [100, 50,20,10,5,2,1,0.5,0.2,0.1,0.05]; % Polynomial fit error percentage limit array.
CountAccuracy = numel(AccuracyArrayECLT); % Counts the number of elements in the array.
OmegaECLT = zeros(CountLambda,CountAccuracy); % Defines size of matrix to save time and memory.
NECLT = zeros(CountLambda,CountAccuracy); % Defines size of matrix to save time and memory.
Diff = zeros(13,1); % Defines size of matrix to save time and memory.
clear PowerLawQ11 PowerLawQ12 PowerLawQ66 % Clears these variable for new values using the present study.
figure (2) % Opens plot in a sepearate window.
aH = axes;
```

```
%For Loop For Volume Indices%
for y = 1:CountLambda % For loop for the variation of material properties.

    %For Loop For Polynomial Fit Error Percentage Limits%

    for r = 1:CountAccuracy % For loop for the various polynomial fit error percentage limits.

        k = LambdaArrayCLT(1,y);
        ErrorPercentage = AccuracyArrayECLT(r); % Updates the polynomial error percentage limit for particular load case.
        PolynomialFit % Run script Polynomial Fit.
        ABDMatrices % Run script ABDMatrices.
        RayleighRitz % Run script RayleighRitz.

        if(LoadingType == 1) % Natural frequency case.
            OmegaECLT(y,r) = (Omega); % Creates array with all the natural frequencies calculated.
        end

        if(LoadingType == 2) % Critical buckling load case.
            NECLT(y,r) = (N)/(1*10^3); % % Creates array with all the critical buckling loads calculated and converts critical buckling load to MN.
        end
    end

    if(LoadingType == 1) % Natural frequency case.
        Diff(1,y) = 100*((OmegaECLT(y,11)-OmegaCLT(y,11))/OmegaCLT(y,11)); % Calculates the error percentage difference between CLT and present study.
        loglog(AccuracyArrayECLT,OmegaECLT(y,:),'o','MarkerEdge',MarkerColour2(ColourPos(y),:),'MarkerSize',5); %Plots the natural frequency for each polynomial error percentage fit limit.
        hold on % Keeps the data on the plot graph.
    end

     if(LoadingType == 2) % Critical buckling load case.
        Diff(1,y) = 100*((NECLT(y,11)-NCLT(y,11))/NCLT(y,11)); % Calculates the error percentage difference between CLT and present study.
        loglog(AccuracyArrayECLT,NECLT(y,:),'o','MarkerEdge',MarkerColour2(ColourPos(y),:),'MarkerSize',5); %Plots the critical buckling load for each polynomial error percentage fit limit.
        hold on % Keeps the data on the plot graph.
    end
end
```

PRESENT STUDY PLOT

Specifies the plot properties used to generate the plot.

```
% Present Study Plot Properties%
box on % Applies plot border.
set(gca, 'FontName', 'Times New Roman') % Sets plot font.
xlabel('Polynomial Fit Error Percentage Limit','FontSize',10); % Inserts an x-axis label.
if(LoadingType == 1) %Natural frequency case.
    ylabel('Natural Frequency [Hz]','FontSize',10); % Inserts a y-axis label.
    set(gca,'yLim',[1500 3200]); % Sets y axis limits.
end
if(LoadingType == 2) % Critical buckling load case.
    ylabel('Critical Buckling Load [kN]','FontSize',10); % Inserts a y-axis label.
    set(gca,'yLim',[1500 9000]); % Sets y axis limits
end
set(gca,'xLim',[0.02 4000]); % Sets x axis limits.
aH.XDir = 'reverse'; % Sets x axis to reverse.
legend('\lambda = 0', '\lambda = 0.1','\lambda = 0.2','\lambda = 0.5','\lambda = 1', '\lambda = 2', '\lambda = 5', '\lambda = 5', '\lambda = 10', '\lambda = 12', '\lambda = 20', '\lambda = 50', '\lambda = 100') %
```

Published with MATLAB® R2017a